CARBON MONOXIDE AND DIOXYGEN PHOTO-RELEASE, BINDING KINETICS, AND THERMODYNAMICS IN 1:1 MONONUCLEAR AND 2:1 DINUCLEAR COPPER/DIOXYGEN COMPLEXES

by

Claudio Saracini

A dissertation submitted to Johns Hopkins University in conformity with the requirements for the degree of Doctor of Philosophy

Baltimore, Maryland

January, 2014

Abstract

Enzymes where the active site contains one or more copper ions catalyze a wide range of organic substrate transformations in Nature. The structures and function of such active sites have been finely tuned by evolution to reach the point where dioxygen binding, activation, and utilization for oxidative chemistry have become finely modulated. As is overviewed in Chapter 1, it is useful to categorize the enzymes supported by two copper centers in their active sites as 'uncoupled' (i.e. in peptidylglycine α-hydroxylating monooxygenase (PHM) and in dopamine β-monooxygenase (DβM)) or 'coupled' (i.e. in tyrosinase (Tyr) and in catechol oxidase (Co)) on the basis of the spatial proximity of the two metals in the three-dimensional matrix of the protein. This proximity has profound effects on the chemistry displayed by these two classes of enzymes. Importantly, dioxygen binding to the copper centers is the first step of the catalytic cycle in all of these systems. However, both mononuclear 1:1 and dinuclear 2:1 copper/O_2 adducts forming in the enzymes have been shown to be unstable and their detection and their study has been difficult. As it is also discussed in Chapter 1, low temperature spectroscopic techniques together with synthetic model chemistry have come into play and greatly improved our understanding of the mechanistic details involved in such kinds of reactivity. In this work, laser flash-photolysis techniques in combination with copper-synthetic model chemistry have been employed to help the elucidation of fundamental physical and chemical properties of copper/O_2 coordination and dynamics.

One of the methods that has been successfully employed to study labile copper/dioxygen adducts is laser flash-photolysis of synthetic (L)copper(I)-CO compounds (L =ligand) in the presence of O_2 in organic solvents. In Chapter 2, a flash-photolysis study of tridentate N-donor ligand-copper(I)-CO complexes is presented using such techniques. The implications

of tricoordination vs. tetracoordination of copper ion on the dynamics of CO and O_2 binding to the metal are discussed for these metal complexes. Tricoordinate environments are more similar in their coordination sphere with those present in the enzymes, as compared to their tetracoordinated synthetic counterparts.

In Chapter 3, a new method to study copper/dioxygen binding for mononuclear copper complexes is presented. The previously employed carbon monoxide utilization to start from stable (L)copper(I)-CO complexes is bypassed, in this work, by affording direct O_2 photo-release from relatively stable mononuclear copper(II)-superoxide complexes. Interestingly, a different quantum yield for O_2 release was found depending on the excitation wavelength used and in collaborative efforts, this effect has been investigated by means of Time-Dependent Density Functional Theory (TD-DFT) studies.

This work was further extended and presented in Chapter 4, where the same technique was employed for dinuclear 2:1 Cu/O_2 synthetic adducts with a peroxo fragment bound in a side-on mode to the two copper centers. These peroxo moieties not only displayed photo-activity upon irradiation with visible light whereas analogue trans-peroxo dicopper(II) complexes did not, but they also undergone a remarkable one-photon two-electron oxidation of the peroxo fragment to molecular oxygen which, then, reversibly re-binds the two metal centers. The implications and comparison with the binding dynamics of O_2 in hemocyanin (Hc) and Tyr are also discussed.

Advisor: Professor Kenneth D. Karlin
Ira Remsen Chair in Chemistry

Thesis Committee:

Professor David P. Goldberg
Professor Gerald J. Meyer

Acknowledgements

I would like to thank Prof. Kenneth D. Karlin for his guidance during the 5 years of my graduate research. He has been a great mentor not only concerning research itself but also because of his ability of teaching his students his philosophy of approaching problems in general. Attention to details, integrity, and the ability of being reasonable in terms of the way of pursuing goals are only a few of the principles he teaches his students. I like to make a joke about him saying that he reminds me of the ancient philosopher Socrates for his ability to go to the bottom of the problems and to question everything. It is also thanks to this philosophy and to his great qualities as a mentor that I was able to grow as a researcher in the past few years. I feel fortunate to have joined Karlin's group. That gave me the chance to learn from Prof. Karlin's outstanding teaching skills.

I would like to thank Prof. Gerald J. Meyer for his precious guidance during our collaboration for laser studies. He has been very kind with me and I have learned a lot thanks to his very insightful suggestions. He was always able to find time to talk with me about research, even in a very busy time. Meyer group members also gave a great contribution to my pleasant stay in the Department of Chemistry and also to my research. Shane Ardo, John Rowley, Darren Achey, and Byron Farnum are only a few of the people who helped me during my graduate studies. I am thankful to them and to the whole Meyer's group.

My thanks go to Prof. David P. Goldberg for helping during my PhD, also through his research group, and I would like to thank both Prof. Meyer and Prof. Goldberg to be part of my thesis committee.

It is my pleasure to thank Prof. Barbara Floris and all the Professors of the Physical Chemistry group in University of Rome ' Tor Vergata ' (Italy) who greatly contributed to my formation as scientist and introduced me to the fascinating world of Sciences.

All the work I have done in the past few years wouldn't have been possible without the help of our collaborators. First of all, I would like to thank Prof. Shunichi Fukuzumi and his research group for their great contribution to my research and to make my stay in Japan be very pleasant. In particular, discussions with Prof. Fukuzumi really sparked my interest in the research we accomplished together, and I would like to thank both Dr. Tomoyoshi Suenobu and Dr. Kei Ohkubo for their mentorship and guidance. I would also like to thank Prof. Frank Neese for his collaboration on theoretical studies and Dr. Dimitrios Liakos for his great support and help. My thanks go also to Prof. Lin X. Chen and to her research group for their help and support in our collaboration. I am thankful for the help I received from Harry Christopher Fry, Megan Shelby, and Michael Mara during and after our experiments at the Argonne National Laboratory (USA).

It is my great pleasure to have had the opportunity to work with such great laboratory colleagues who, each, gave their contribution to my research and to my pleasant stay in Karlin group in the past 5 years. In particular, I would like to thank Zakaria Halime, Ga Young Park, Clarence Rolle III, and Savita Sharma for their help with the research and in the laboratory. I would also like to thank Jean Goodwin for her great help with the technical and bureaucratic aspects of my graduate studies.

Finally, a special thank to my parents, to my brother, and to my sister. Moving to the USA from Italy and accomplishing all I did would not have been possible without their support, understanding, and love. I would also like to thank my close friends of a life time for their endless support throughout all my graduate studies.

Table of Contents

Chapter 1: Copper/CO and Copper/O_2 Interactions in Copper-Containing Proteins and in Model Compounds

1 Introduction **3**

2 CO and O_2 Interactions in Non-Coupled Dinuclear Copper Enzymes and in Model Compounds **4**

2.1 Static Structure of the Catalytic Core of Peptidylglycine α-Hydroxylating Monooxygenase as Determined by X-Ray Crystallography **5**

2.2 Active Site Probing of the Catalytic Core of Peptidylglycine α-Hydroxylating Monooxygenase and Dopamine b-Monooxygenase through Carbon Monoxide Coordination **9**

3 Copper/O_2 Interactions in Coupled Dicopper Enzymes and in Model Compounds **16**

3.1 Structure of Cu^{II}_2–O_2 Adducts **20**

3.2 Formation of Cu^{II}_2-O_2^{2-} Adducts **27**

4 Conclusions **30**

5 Acknowledgments **31**

6 References **32**

Chapter 2: Light-Induced Copper-CO and Copper-O_2 Reactivity

1 Introduction **41**

2 Experimental **44**

2.1 Materials **44**

2.2 O_2-Free Techniques and Cryogenics **45**

2.3 NMR Measurements **45**

2.4 CO and O_2 Solubility in acetone **45**

2.5 Gas Mixing **46**

2.6 Laser Flash Photolysis **46**

2.7 Ligand and Complex Syntheses **47**

3 Results and Discussion **53**

3.1 X-Ray Crystallography of $[(nQ_2)Cu^{I}(CH_3CN)]PF_6$, $[(nQ_2)Cu^{I}(CO)]PF_6$, $[(BzDMM)Cu^{I}(CO)]BArF$, $[\{(BzDMM)Cu^{II}(OH)\}_2](PF_6)_2$, $[\{(BzDMM)Cu^{II}(Cl)\}_2](PF_6)_2$, and $[\{(nQ_2)Cu^{II}(OH)\}_2](ClO_4)_2$ **54**

3.2 Infrared Spectroscopy (ν_{CO} in MeTHF and THF Solvents) **63**

3.3 CO Binding to Copper(I) in Acetone Solvent: Laser Experiments **65**

3.4 Dioxygen Binding to Copper(I) in Acetone Solvent: Benchtop Experiments **72**

3.5 Dioxygen Binding to Copper(I) in Acetone Solvent: Laser Experiments **78**

4 Conclusions **84**

5 Acknowledgments **85**

6 References **85**

Chapter 3: Wavelength-Dependent O_2 Photo Release from Mononuclear $LCuO_2$ Compounds

1 Introduction **91**

2 Experimental **93**

2.1 Materials and Methods **93**

2.2 Determination of O_2 solubility in 2-MeTHF **93**

2.3 Gas Mixing **94**

2.4 Transient Absorption Experimental Details **95**

2.5 Data Treatment for Benchtop Titration Measurements **95**

2.6 Model Used for Kinetic Studies **97**

2.7 Quantum Efficiency Measurements **99**

2.8 DFT Calculations **101**

3 Results and Discussion **101**

3.1 Flash-Photolysis Experiments **101**

3.2 DFT and TD-DFT Calculations **114**

4 Conclusions **118**

5 Acknowledgments **119**

6 References **119**

Chapter 4: One-Photon Two-Electron Oxidation of Peroxide to O_2 from Dicopper(II) Compounds

1 Introduction **125**

2 Experimental **126**

2.1 Materials **126**

2.2 Synthetic Procedures **126**

2.3 Determination of O_2 solubility in Acetone **129**

2.4 Gas Mixing **129**

2.5 Transient Absorption Experimental Details **130**

2.6 Determination of k_{O2} and Eyring Plots for the reactions of O_2 with N3 and N5 Ligand-Copper Compounds **130**

2.7 Quantum Efficiency Measurements **131**

3 Results and Discussion **132**

4 Conclusions **146**

5 Acknowledgments **147**

6 References **147**

List of Figures and Tables

Chapter 1: Copper/CO and Copper/O_2 Interactions in Copper-Containing Proteins and in Model Compounds

Page Number

Figure 1. X-ray crystal structure of PHM displaying a peptidyl substrate near the Cu_M site. Adapted from Lucas HR, Karlin KD *Met. Ions Life Sci.* 2009, 6, 295. 6

Figure 2. Schematic of two synthetic copper(II) η^1-superoxide complexes for comparison to the analogous precatalytic O_2-species crystallized for PHMcc. Figure modified from Lucas HR, Karlin KD *Met. Ions Life Sci.* 2009, 6, 295. 8

Figure 3. Summary of the reactions of CO at the active sites of PHM and DβM and the changes occurring upon addition of peptidyl substrate to carbonylated PHMcc and tyramine to carbonylated DβM. Figure adapted from Lucas HR, Karlin KD *Met. Ions Life Sci.* 2009, 6, 295. 10

Figure 4. Copper(I)-carbonyl synthetic models with different ligand donor atoms from (A) Sorrell and coworkers[52] and (B) Karlin and coworkers.[53,54] Figure adapted from Lucas HR, Karlin KD *Met. Ions Life Sci.* 2009, 6, 295. 11

Figure 5. Two-coordinate copper(I)-carbonyl adducts derived from two- or three-coordinate copper(I) complexes. Figure adapted from Lucas HR, Karlin KD *Met. Ions Life Sci.* 2009, 6, 295. 14

Figure 6. Reaction overview in Hc, involving Deoxy and Oxy-Hc. 17

Figure 7. Diagram from the X-ray structure of Oxy-Hc from *octopus dofleini* showing (i) the side-on binding mode of dioxygen (as peroxide) to the dicopper site and (ii) the C2His/S-Cys crosslink. 17

Figure 8. Biological active site of Tyr and Co and their functions. 18

Figure 9. Crystal structure of the Kitajima/Fujisawa side-on peroxo complex $[\{Cu^{II}[HB(3,5\text{–}i\text{–}Pr_2pz)_3]\}_2(O_2^{2-})]$. 22

Figure 10. Crystal structure of $[\{Cu^{II}(TMPA)\}_2(O_2^{2-})]^{2+}$ resulting from the reaction of $[Cu^{I}(TMPA)(MeCN)]^{+}$ and dioxygen at low temperature. 24

Figure 11. Aliphatically tethered Cu^{II}_2-peroxo complexes **a** and **b**. Figure 11c depicts the distortion, or butterflying, of the $Cu_2O_2^{2-}$ core facilitated by the ligand constraints that the aliphatic tether imposes on the copper complex. Figure 11d depicts the structure of Oxy-Hc from *Limulus polyphemus*, which shows some degree of butterflying of the $Cu_2O_2^{2-}$ core. 24

Figure 12. Equilibrium between $Cu^{II}_2(O_2^{2-})$ and Cu^{III}_2-bis-μ-oxo moieties. 26

Figure 13. Formation of side-on peroxo intermediate $[Cu^{II}_2(R\text{–}XYL)(O_2^{2-})]^{2+}$ from O_2-reaction with $[Cu^{I}_2(R\text{-}XYL)]^{2+}$, followed by oxygenation of the arene bridge. 27

Figure 14. Formation of an initial superoxo-species has been long suspected in the formation of Cu^{II}_2-peroxo species. For example the formation of $[Cu^{I}_2(Nn)(O_2^{2-})]^{2+}$ from $[Cu^{I}_2(Nn)]^{2+}$ proceeds with a very low (and sometimes negative) activation enthalpy, suggestive of the formation of an initial species $Cu^{II}\text{-}O_2^{-}\ldots Cu^{I}$ (a). Direct observation of such an intermediate came from dioxygen reactivity studies with $[Cu^{I}(TMPA)]^{+}$ complexes (b). 29

Figure 15. Oxygenation of $[Cu^{I}(i\text{-}Pr_3TACN)(MeCN)]^{+}$ in acetone leads to both the corresponding peroxo and oxo-species, apparently in concert, suggesting that a rapid equilibrium exists between bis-μ-oxo and μ–η^2:η^2-peroxo complexes. 30

Scheme 1. Reactivity of DβM and PHM. Adapted from Lucas HR, Karlin KD *Met. Ions Life Sci.* 2009, 6, 295. 5

Scheme 2. The difference in *o*-aminophenol reaction of Tyr vs. NspF. 19

Chapter 2: Light-Induced Copper-CO and Copper-O_2 Reactivity

Page Number

Figure 1. ORTEP diagrams of (A) $[(nQ_2)Cu^{I}(CH_3CN)]PF_6$, (B) $[(nQ_2)Cu^{I}(CO)]PF_6$, and (C) $[\{(nQ_2)Cu^{II}(OH)\}_2](ClO_4)_2$. Both hydrogen atoms and the counterions have been omitted for clarity. 56

Figure 2. ORTEP diagrams of (A) $[(BzDMM)Cu^{I}(CO)]BArF$, (B) $[\{(BzDMM)Cu^{II}(OH)\}_2](PF_6)_2$, and (C) $[\{(BzDMM)Cu^{II}(Cl)\}_2](PF_6)_2$. Both hydrogen atoms (except for the OH groups in Figure 2B) and the counterions have been omitted for clarity. 57

Figure 3. Super-molecular structure found for $[\{(nQ_2)Cu^{II}(OH)\}_2](ClO_4)_2$ crystals. 63

Figure 4. Transient absorption difference spectra collected at the indicated 65

delay times after 355 nm laser excitation (8 mJ/pulse, 8-10 ns fwhm) of $[(BzDMM)Cu^{I}(CO)]^{+}$ in MeTHF.

Figure 5. (A) Absorption spectrum collected before (black line) and after (red line) CO bubbling into a solution of $[(nQ_2)Cu^{I}]BArF$ in acetone (150 μM) at room temperature. (B) Absorption difference spectrum (Abs($[(nQ_2)Cu^{I}]BArF$) - Abs(**1**)). 66

Figure 6. (A) Absorption spectrum collected before (black line) and after (red line) CO bubbling into a solution of $[(BzQ_2)Cu^{I}]BArF$ in acetone (10 μM) at room temperature. (B) Absorption difference spectrum (Abs($[(BzQ_2)Cu^{I}]BArF$) - Abs(**2**)). 67

Figure 7. (A) Transient absorption difference spectra collected at the indicated delay times after 355 nm laser excitation (8 mJ/pulse, 8-10 ns fwhm) of **1** in acetone (B) Representative absorption changes monitored at 370 nm after photo-excitation of **1** at various ratios of $O_{2(g)}/N_{2(g)}$ at -94 ^{0}C in acetone. The inset shows the plots for the determination of k_{CO}. (C) Eyring plot for the determination of the activation parameters associated with the rate constants k_{CO}. 68

Figure 8. Transient absorption difference spectra collected at the indicated delay times after 355 nm laser excitation (8 mJ/pulse, 8-10 ns fwhm) of $[(BzQ_2)Cu^{I}(CO)]^{+}$ (**2**) in acetone at -94 ^{0}C. 68

Figure 9. (A) Representative absorption changes monitored at 370 nm after photo-excitation of **2** at various ratios of $O_{2(g)}/N_{2(g)}$ at -74^{0}C in acetone. The inset shows the plots for the determination of k_{CO}. (B) Eyring plot for the determination of the activation parameters associated with the rate constants k_{CO}. 69

Figure 10. Magnitude of the absorption change as a function of the incident irradiance for **1**. Measurements collected at 370 nm, 0.5 μs delay time, -94^{0}C in MeTHF. 72

Figure 11. Absorption spectral change after introduction of O_2 into a MeTHF solution of [(BzDMM)$Cu^I(CH_3CN)$]BArF (209 μM) at -80 ^{0}C, to give a dioxygen adduct (bis-μ-oxo-dicopper(III) or side-on peroxo-dicopper(II) species) with $\varepsilon_{390\ nm}$ = 9700 M^{-1} cm^{-1}. 73

Figure 12. Addition of O_2 into a acetone solutions of [(nQ_2)$Cu^I(CH_3CN)$]BArF and [(BzQ_2)$Cu^I(CH_3CN)$]BArF at -80 ^{0}C resulted in no reaction. 74

Figure 13. (A) Absorption spectral change after introduction of O_2 into a 2 mM acetone solution of [(nQ_2)Cu^I]$^+$ at -94 ^{0}C (in red). (B) Same experiment performed using a higher concentration of [(nQ_2)Cu^I]$^+$ (5 mM). 75

Figure 14. Comparison between the spectrum from the oxygenation experiment (in magenta) and that from the authentic [{(nQ_2)Cu^{II} $(OH)_2$]$^{2+}$ compound prepared at two different concentrations (green and black spectra). 77

Figure 15. (A) Transient absorption difference spectra collected at the indicated delay times after 355 nm laser excitation (8 mJ/pulse, 8-10 ns fwhm) of **1** in acetone at -94 ^{0}C in the presence of O_2 (B) Representative absorption changes monitored in the experiment shown in A (C) First-order mono-exponential fit of the growth observed at 410 nm in A (D) Confirmation of the absorption increase in the range 405-440 nm in a separate experiment. 80

Figure 16. (A) Representative absorption changes monitored at 418 nm after photo-excitation of **1** at various ratios of $O_{2(g)}/CO_{2(g)}$ at -94^{0}C in acetone (B) Determination of the activation parameters for the rate constants k_{O2}. 82

Table 1. Selected bond lengths and bond angles for the copper(I)-acetonitrile species [(nQ_2)$Cu^I(CH_3CN)$]$^+$ and [($BzPY_1$)$Cu^I(CH_3CN)$]$^+$. 58

Table 2. Selected bond lengths and bond angles for the copper(I)-CO species $[(nQ_2)Cu^{I}(CO)]^{+}$, $[(BzQ_2)Cu^{I}(CO)]^{+}$, $[(BzDMM)Cu^{I}(CO)]^{+}$, and $[(BzPY_1)Cu^{I}(CO)]^{+}$. 59

Table 3. Comparison of selected bond lengths and bond angles between the bis-μ-hydroxo dicopper(II) compounds $[\{(nQ_2)Cu^{II}(OH)\}_2](ClO_4)_2$, $[\{(BzDMM)Cu^{II}(OH)\}_2](PF_6)_2$, $[\{(BzQ_2)Cu^{II}(OH)\}_2](ClO_4)_2$, and the bis-$\mu$-chloride dicopper(II) complex $[\{(BzDMM)Cu^{II}(Cl)\}_2](PF_6)_2$. 62

Table 4. CO stretching frequences (ν_{CO}) for 1 and 2 in MeTHF, and for $[(BzDMM)Cu^{I}(CO)]^{+}$ and $[(BzPY_1)Cu^{I}(CO)]^{+}$ in THF. 64

Table 5. Comparison of second-order rate constants and activation parameters for the binding of O_2 to $[(nQ_2)Cu^{I}(acetone)]^{+}$ in acetone with $[(TMPA)Cu^{I}]^{+}$ in THF and in EtCN. 70

Table 6. Comparison of spectroscopic features of $[\{(nQ_2)Cu^{II}\}_2(O_2)]^{2+}$ with those of previously characterized compounds. 76

Table 7. Comparison of second-order rate constants and activation parameters for the binding of O_2 to $[(nQ_2)Cu^{I}]^{+}$ or $[(nQ_2)Cu^{I}(acetone)]^{+}$ in acetone with $[(TMPA)Cu^{I}]^{+}$ in THF and in EtCN. 83

Scheme 1. Proposed mechanism for the CO photochemstry in acetone. 69

Scheme 2. Proposed mechanism for $[(nQ_2)Cu^{I}]^{+}/O_2$ reactivity in acetone. 78

Scheme 3. Possible O_2 reactive species. 79

Scheme 4. Flash-and-trap kinetic model. 81

Chart 1. Ligands systems examined in this study (middle) and those from previous works (top) and complex formulas examined in this study (bottom). 44

Chart 2. Ligand-copper(I) carbonyl complexes examined in this work for photolysis experiments. 54

Chapter 3: Wavelength-Dependent O_2 Photo Release from Mononuclear $LCuO_2$ Compounds

Page Number

Figure 1. (A) Absorption spectrum of $[(TMG_3tren)Cu^{II}(O_2)]^+$ (**1**) (red line) obtained from oxygenation of $[(TMG_3tren)Cu^{I}]^+$ (**3**) (black line) at 218 K in MeTHF. (B) Transient absorption difference spectra collected at the indicated delay times after 436 nm laser excitation (15 mJ/pulse, 8-10 ns fwhm) of **1** in MeTHF at 218 K. Overlaid in red on the experimental data is a simulated spectrum (Abs(**3**) - Abs(**1**)). 102

Figure 2. (A) Absorption spectrum of $[(PV\text{-}TMPA)Cu^{II}(O_2)]^+$ (**2**) (red line) obtained from oxygenation of $[(PV\text{-}TMPA)Cu^{I}]^+$ (**4**) (black line) at 143 K in MeTHF. (B) Transient absorption difference spectra collected at the indicated delay times after 436 nm and 683 nm laser excitation of **2** in MeTHF at 143 K. Overlaid in red on the experimental data is a simulated spectrum (Abs(**4**)- Abs(**2**)). 103

Figure 3. Transient absorption difference spectra collected at the indicated 104

delay times after 436 nm and 683 nm laser excitation of $[(TMG_3tren)Cu^{II}(O_2)]^+$ (**1**) in MeTHF at 218 K. Overlaid in red on the experimental data is a simulated spectrum (Abs($[(TMG_3tren)Cu^{I}]^+$ (**3**))-Abs(**1**)).

Figure 4. Left: Representative absorption changes monitored at 460 nm at various ratios of $O_{2(g)}/N_{2(g)}$ at -40 ^{0}C in 2-MeTHF for $[(TMG_3tren)Cu^{I}]^+$ (**3**) + O_2. Right: determination of k_{O2} and k_{-O2} fitting data with equation **(10)**. 105

Figure 5. Determination of the equilibrium constant for the binding of $[(TMG_3tren)Cu^{I}]$BArF to O_2 at -65^{0}C in 2-MeTHF solvent. 106

Figure 6. Van't Hoff plot for the variable temperature K_{O2} data for the binding of $[(TMG_3tren)Cu^{I}]$BArF to O_2 in 2-MeTHF solvent. 108

Figure 7. Van't Hoff plot for the equilibrium constants K_{O2} determined through transient absorption spectroscopy. 109

Figure 8. K_{O2} values determined at -60^{0}C in different solvents as follows: a) K_{O2}(DMF) = 3030 ± 4340 from Lanci et al. *J. Am. Chem. Soc.* 2007**,** 129, 14697; b) K_{O2}(MeTHF) = 467 ± 26 determined in this work; c) K_{O2}(chlorobenzene) = (K_{O2}(DMF) / 14) = 216 estimated from Lanci et al. *J. Am. Chem. Soc.* 2007, 129, 14697 and Lide, D. R. CRC Handbook of Chemistry and Physics, 74th ed.; CRC Press: Boca Raton, 1993. Dielectric constants for DMF, MeTHF, and chlorobenzene were taken as 37, 7, and 2.7, respectively. 110

Figure 9. Determination of the activation parameters from the rate constants k_{O2} and k_{-O2} for $[(TMG_3tren)Cu^{I}]^+$ (**3**) and $[(TMG_3tren)Cu^{II}(O_2)]^+$ (**1**). 111

Figure 10. Determination of the activation parameters for the reaction 111

between $[(PV\text{-}TMPA)Cu^{I}]^{+}$ (**4**) and O_2 following laser excitation (λ_{exc} = 436 nm) of $[(PV\text{-}TMPA)Cu^{II}(O_2)]^{+}$ (**2**) in the temperature range 138 K to 148 K in MeTHF and comparison with the rate constant for the reaction between **4** and O_2 extrapolated at 143 K.

Figure 11. Localized orbital description for $[(TMG_3tren)Cu(O_2)]^{+}$ (**1**). 115

Figure 12. TD-DFT calculated excited state potential energy surfaces (PESs) as a function of copper-oxygen bond distance. 116

Figure 13. TD-DFT calculated energy and shape of the beta HOMO and beta LUMO orbitals as a function of copper-oxygen bond distance. 117

Table 1. Comparison of kinetic and thermodynamic parameters for O_2 binding and dissociation for [(L)Cu] adducts. 107

Table 2. Comparison of thermodynamic parameters for O_2 binding to $[(TMG_3tren)Cu^{I}]^{+}$ determined with two different methods in 2-MeTHF solvent. 108

Scheme 1. Flash-photolysis studies of **1** and **2**. 92

Chart 1. Structure of ligands for this work compared to the 'parent' TMPA ligand. 112

Chapter 4: One-Photon Two-Electron Oxidation of Peroxide to O_2 from Dicopper(II) Compounds

Page Number

Figure 1. ^{1}H NMR (CD_3NO_2) of $[(N3)Cu^I_2(CH_3CN)_2](BArF)_2$. 127

Figure 2. ^{1}H NMR (CD_3NO_2) of $[(N5)Cu^I_2(CH_3CN)_2](BArF)_2$. 128

Figure 3. Benchtop and laser absorption spectra of $[(N3)Cu^I_2(CH_3CN)_2]^{2+}$ and $[(N3)Cu^{II}_2(O_2)]^{2+}$ (**1**). (a) Absorption spectrum of **1** (red line) obtained from oxygenation of $[(N3)Cu^I_2]^{2+}$ (black line) at 193 K in acetone. (b) Transient absorption difference spectra collected at the indicated delay times after 532 nm laser excitation (10 mJ/pulse, 8-10 ns fwhm) of **1** in acetone at 193 K. Overlaid in blue is a simulated spectrum based on subtraction of the red spectrum from the black in 1a. The inset shows the magnitude of the absorption change as a function of the incident irradiance. 133

Figure 4. Absorption spectrum of **2** (red line) obtained from oxygenation of $[(N5)Cu^I_2(CH_3CN)_2]^{2+}$ (black line) at 193 K in acetone. 134

Figure 5. Transient absorption difference spectra collected at the indicated delay times after 532 nm laser excitation (10 mJ/pulse, 8-10 ns fwhm) of **2** in acetone at 193 K. Overlaid in red on the experimental data is a simulated spectrum (Abs($[(N5)Cu^I_2(CH_3CN)_2]^{2+}$)- Abs(**2**)). 135

Figure 6. Difference in absorbance observed at 360 nm as a function of the applied laser energy for **2**. 136

Figure 7. Representative kinetic traces observed at 365 nm obtained upon 143

varying O_2 concentration at 193 K. The first-order exponential fit for the trace relative to $[O_2]$ = 8 mM is overlaid in yellow. The inset shows the pseudo-first-order plot for O_2 binding to $[(N3)Cu^{I}_2(CH_3CN)_2]^{2+}$ yielding a second-order rate constant of $(5.0 \pm 0.6)\cdot 10^3$ M^{-1} s^{-1}.

Figure 8. Eyring plots obtained for the determination of the activation parameters for the rate constants k_{O2} for (A) $[(N3)Cu^{I}_2(CH_3CN)_2](BArF)_2$ and for (B) $[(N5)Cu^{I}_2(CH_3CN)_2](BArF)_2$. 143

Table 1. Comparison of reduction potentials for some copper complexes. ΔG is the estimated free Gibbs energy variation for the dissociation reaction of O_2 from the relative copper(II)-superoxide species. 139

Table 2. Comparison of kinetic parameters for O_2 binding to $[(N3)Cu^{I}_2(CH_3CN)_2]^{2+}$ and $[(N5)Cu^{I}_2(CH_3CN)_2]^{2+}$. 144

Table 3. Comparison of second order rate constants for O_2 binding to copper(I): 'dTy' is 'deoxy tyrosinase' and 'dHc' is 'deoxy hemocyanin'. 145

Scheme 1. One-photon two-electron oxidation of peroxide to dioxygen. 136

Scheme 2. Reaction schemes for the photochemistry of side-on vs. end-on dicopper(II) compounds. 138

Chart 1. Structure of the compounds studied in this work. 132

Chart 2. Structure of dicopper(II) μ-1,2-(end-on) compounds studied in this work. 137

Chapter 1:

Copper/CO and Copper/O_2 Interactions in Copper-Containing Proteins and in Model Compounds

Abstract

Copper-containing enzymes catalyze a wide variety of chemical reactions involving O_2 activation and transport. Among the active sites responsible for these processes, those containing dicopper centers play a central role. These include the enzymes peptidylglycine α-hydroxylating monooxygenase (PHM) and dopamine β-monooxygenase (DβM). Here, one of the coppers facilitates dioxygen binding and activation towards substrate oxidation and the other one functions as electron source/carrier. In enzymes such as tyrosinase (Tyr) and catechol oxidase (Co) the copper ions, instead, bridge the bound dioxygen moiety as a μ–η^2:η^2 peroxo fragment to catalyze *o*-phenol aromatic hydroxylations and dehydrogenation of *o*-catechols, respectively. Dicopper centers also perform O_2 transport in the enzyme hemocyanin (Hc) found in mollusks and arthropods. The binding of dioxygen to the copper centers in the active site of such enzymes constitutes the first event of the catalytic cycle in all cases (except for Hc where no catalysis occurs) and this process has been studied extensively. The labile nature of the intermediates forming upon the copper/O_2 reaction, on the other hand, has represented a great challenge for chemists interested in elucidating their

nature. Utilization of carbon monoxide (CO) as a non-redox surrogate of molecular oxygen has greatly aided the understanding of O_2 binding to copper ions as CO forms more stable (copper(I)-CO) intermediates. In addition, infrared spectroscopy (IR) studies allowed determination of copper ligation and environmental changes within the active site of both coupled (PHM and DβM) and non-coupled (Tyr and Co) copper-containing enzymes, by using CO stretching frequencies as a labeling tool. The kinetics and thermodynamics of CO binding to copper(I) have also been determined in many cases. Furthermore, studies on synthetic model compounds have improved our understanding of structure, coordination, stability, reactivity, and spectroscopic properties of the biological active sites present in these enzymes. This chapter is meant to provide an introduction on carbon monoxide utilization as a tool to gain more insights into copper/O_2 binding in non-coupled enzymes (PHM and DβM) using synthetic compounds and as general overview for copper/dioxygen chemistry occurring in coupled dicopper-containing enzymes such as Tyr and Co.

1. Introduction

Copper(I)-carbon monoxide binding and ligation does not occur naturally in copper enzymes, as CO is not the natural substrate for proteins like the O_2-carrier hemocyanins, coupled (Tyr and Co)[1-3] or uncoupled (PHM and DβM)[4-6] dicopper monoxygenases and copper oxidases. It would be not intuitive, then, to think about CO as a valuable tool to gain more insights into copper/O_2 binding and reactivity in such systems. On the other hand, utilization of this non-redox active molecule to probe the active site of many of the enzymes mentioned above has been key to understand properties like coordination, binding dynamics, kinetics, and thermodynamics of copper/dioxygen interactions in biological systems. It is the purpose of section 2 of this chapter to give an overview of the incidence of carbon monoxide-based copper ligands in the bioinorganic chemistry of dinuclear uncoupled copper enzymes as background for the chemistry presented in Chapter 2. Coupled dicopper centers present in enzymes such as Hc,[1,2] Tyr[1,2] and Co[3] have also been extensively studied. Hcs are proteins that are responsible for dioxygen transport and their dinuclear copper-peroxo center is not reactive towards organic substrates. The reason why this occurs is thought to be caused by the fact that the copper^{II}-O_2-copper^{II} moiety is deeply buried into the protein three dimensional structure in Hc, making substrate approach to the dicopper center not possible. This has been confirmed by both X-ray crystallographic studies[7-12] and by experiments where phenol oxidase reactivity was 'artificially' induced upon treating the protein with detergents.[13,14] The dicopper(II) peroxo moieties present in Tyr and Co, instead, are well-known to give hydroxylations and dehydrogenation chemistry towards organic substrates *via* an electrophilic aromatic substitution pathway (in the former case).[3,15,16] The scope of section 3 of this chapter is to give a general overview on the copper/O_2 chemistry occurring in such enzymes.

2. CO and O_2 Interactions in Non-Coupled Dinuclear Copper Enzymes and in Model Compounds

The first studies where carbon monoxide was utilized as a tool to probe chemical and spectroscopic properties of copper protein active sites were reported by Craifaleanu (1919) who observed that solutions of the oxygenated form of Hc (Oxy-Hc) changed from intensely colored to colorless upon bubbling with CO[17] and by Dhere and Schneider (1922) who showed that exposure of the latter solutions to air would reinstate the original intense color. More detailed studies from Root (1934)[17] revealed that both O_2 and CO bind to Hc with a 2:1 copper:small molecule stoichiometry and that O_2 binds about 20 times stronger than CO to the copper, in sharp contrast to the behavior of the two small molecules in hemoglobin. Thus, the use of the CO ligand for the interrogation of metallo-protein centers has been adopted extensively for both iron and copper sites. In particular, new information on dioxygen binding to copper was inferred from CO binding to copper(I) as it is well known that the carbon monoxide ligand is a good π electron-acceptor, thus excellent ligand for low-valent copper(I). Since the cuprous ion has a closed-shell electronic configuration (d^{10}), realtively few spectroscopic techniques allow the extraction of information from its complexes. For example, EPR spectroscopy does not apply. On the other hand, it is well known that IR spectroscopy for CO is very sensitive to the copper coordination sphere.

DβM and PHM are dinuclear copper enzymes with uncoupled, well separated, mononuclear active sites.[18,19] Both enzymes bind and activate molecular oxygen at a single copper site (Cu_B in DβM and Cu_M in PHM) and catalyze the hydroxylation of prohormone peptides (Scheme 1).

Scheme 1. Reactivity of DβM and PHM. Adapted from Lucas HR, Karlin KD *Met. Ions Life Sci.* 2009, 6, 295.

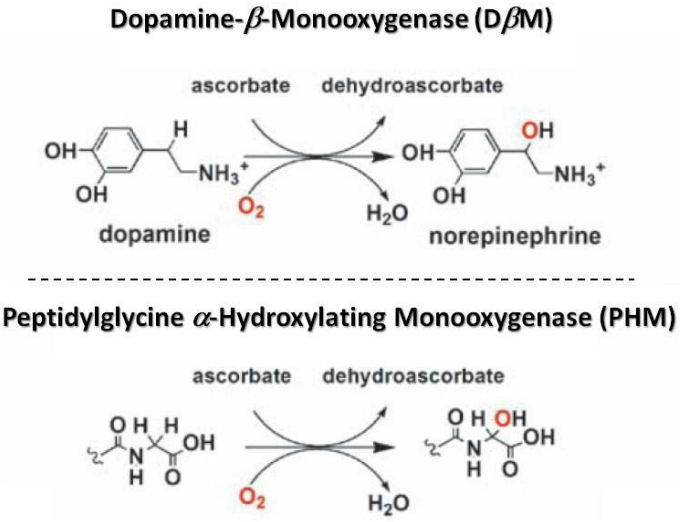

In particular, while DβM catalyzes a benzylic hydroxylation in phenylethylamines (i.e. dopamine hydroxylation to form norepinephrine), PHM catalyzes the first step of the C-terminus peptide amidation by hydroxylating peptidylglycine residues, which is essential in control of cellular function. These enzymes share a high sequence homology and display similar catalytic activity.[18,19]

2.1 Structure of the Catalytic Core of Peptidylglycine α-Hydroxylating Monooxygenase as Determined by X-Ray Crystallography

Amzel and coworkers showed the first crystal structure for both the oxidized and reduced forms of PHMcc, a form of PHM containing only the protein domains responsible for its catalytic activity.[20] Figure 1 shows the arrangement of the active site where the two copper ions, Cu_M and Cu_H, are separated by ~ 11 Å. In its resting state, the catalytic domain Cu_M is constituted by a copper(II) core with a distorted tetrahedral geometry and it coordinates two

histidines (His242 and His244, both bound through their ε-nitrogens), a methionine (Met314), and a water molecule. This domain is responsible for both O_2 and substrate binding. The second copper present in the active site, Cu_H, is coordinated to three histidines, all bound through their δ-nitrogens giving a T-shaped geometry. This center is involved in electron storage and also in outer-sphere electron transfer with the Cu_M site.

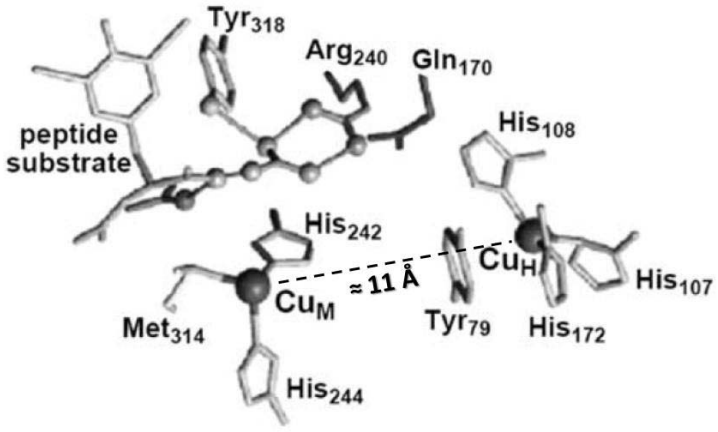

Figure 1. X-ray crystal structure of PHM displaying a peptidyl substrate near the Cu_M site. Adapted from Lucas HR, Karlin KD *Met. Ions Life Sci.* 2009, 6, 295.

The identity of the active species responsible for hydrogen atom transfer towards the organic substrate has been object of intense investigations for many years. Species featuring a copper(II)-superoxo,[18,21-27] a copper(II)-hydroperoxo,[28,29] and also a copper(III)-oxo[24,30-34] moieties have all been proposed as candidates for substrate hydroxylation. An intermediate having a hydroperoxo Cu(II) Cu_M structure (i.e. $Cu_M^{II}OOH$) was early on proposed by Klinman and coworkers to be the species responsible for hydrogen atom abstraction from the substrate. On the other hand, Amzel and coworkers reported the crystal structure of a

precatalytic PHMcc analogue that has a superoxide fragment bound in an end-on fashion to the copper(II) present in the catalytic site (Figure 2)[35] favoring the hypothesis of a copper(II)-superoxide intermediate as active species in the catalytic cycle of PHM, instead.[18,21]

Theoretical studies (DFT) performed by Chen and Solomon also support this hypothesis.[25] Other possibilities for the identity of the hydrogen atom abstractor in PHM and DβM are, however, still open. For example, Jaron and Blackburn proposed a debated mechanism where a 'superoxide tunneling'[36] mechanism was hypothesized to occur on the basis of an unexpected reactivity of the Cu_H site with carbon monoxide in PHMcc.

Stabilization of copper(II)-superoxide species has proven to be challenging both in synthetic and in natural systems. A huge effort made by synthetic chemists in order to stabilize such species has been focused on using organic ligands that can provide sufficient electron density to stabilize cupric species and that, at the same time, posses relatively bulky moieties that can avoid the reaction of copper(II)-superoxide species with a second equivalent of copper(I). Figure 2 shows two cases where stabilization of such copper(II)-superoxide species was achieved;[37-39] in Chapter 3 it will be mentioned an even more recent case where an intramolecular hydrogen bond contributes to the stabilization of the superoxo complex $[(PV\text{-}TMPA)Cu^{II}(O_2)]^{+}$.[40]

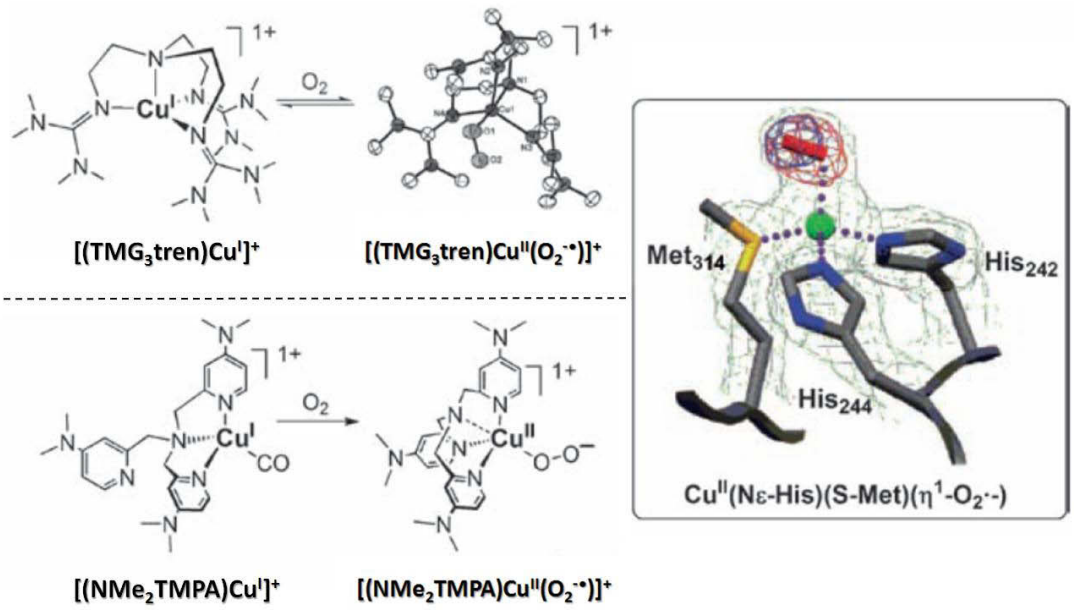

Figure 2. Schematic of two synthetic copper(II) η^1-superoxide complexes for comparison to the analogous precatalytic O_2-species crystallized for PHMcc. Figure modified from Lucas HR, Karlin KD *Met. Ions Life Sci.* 2009, 6, 295.

The complex $[(TMG_3tren)Cu^{II}(O_2^{-\bullet})]^+$ (TMG_3tren = tris(2-(N-tetramethylguanidyl)ethyl)-amine) was crystallographically characterized by Schindler and coworkers and it is also capable of abstracting an H atom from a donor facilitating the insertion of O-atoms into C-H bonds.[28,37] The mononuclear 1:1 Cu/O_2 adduct $[(NMe_2TMPA)Cu^{II}(O_2^{-\bullet})]^+$ (NMe_2-tmpa = tris(4-dimethylaminopyrid-2-ylmethyl)amine), instead, was spectroscopically characterized by Karlin and coworkers. The complex was formed adding dioxygen to the carbonyl form of its copper(I) counterpart ($[(NMe_2TMPA)Cu^{I}(CO)]^+$) thus, preventing the reaction of $[(NMe_2TMPA)Cu^{II}(O_2^{-\bullet})]^+$ with a second molecule of non-carbonylated copper(I).[41] Kinetic studies of the O_2 binding to copper(I) were also possible to be made irradiating

$[(TMPA)Cu^{I}(CO)]^{+}$ with light in the presence of dioxygen.[42] A similar work will be presented in Chapter 2, carried out on two tridentate tripodal N-donor ligand-copper complexes while in Chapter 3 a study where dioxygen was photo-released directly from the complexes $[(TMG_3tren)Cu^{II}(O_2^{-\bullet})]^{+}$ and $[(PV\text{-}TMPA)Cu^{II}(O_2^{-\bullet})]^{+}$ by irradiation with either blue or red light will be presented.

2.2 Active Site Probing of the Catalytic Core of Peptidylglycine α-Hydroxylating Monooxygenase and Dopamine β-Monooxygenase through Carbon Monoxide Coordination

Investigation of the binding of carbon monoxide to both DβM and PHMcc have been performed by Blackburn and coworkers[36,43-48] and their findings showed that CO binds only to the catalytic site (Cu_M) for both the enzymes. Infrared and X-ray absorption studies also confirmed this evidence with C-O stretching frequencies of ν_{CO} = 2089 cm^{-1} found for DβM and ν_{CO} = 2092 cm^{-1} found for PHM (Figure 3).

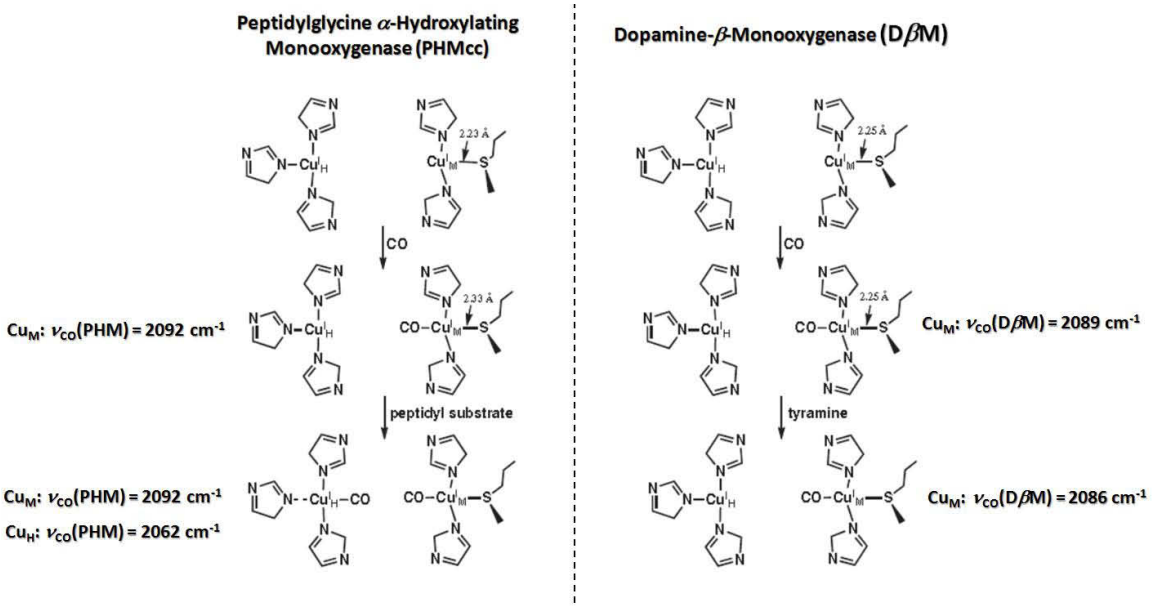

Figure 3. Summary of the reactions of CO at the active sites of PHM and DβM and the changes occurring upon addition of peptidyl substrate to carbonylated PHMcc and tyramine to carbonylated DβM. Figure adapted from Lucas HR, Karlin KD *Met. Ions Life Sci.* 2009, 6, 295.

As illustrated by several studies, among which, the one performed by Sorrell and coworkers[49-52] for copper ion complexes, the C-O stretching frequency of a CO bound to the metal is proportional to the electron-donating capability of the other ligands binding the metal ion. Of course, this is well known in general for metal-carbonyl compounds in inorganic chemistry. Figure 4 shows an interesting example where the change of one of the donor atoms in the pyrazole-based ligand (X) features a change in the C-O stretching frequency of the CO ligand due to the effect mentioned above: X = N-amino (ν_{CO} = 2082 cm^{-1}); X = O-ether (ν_{CO} = 2106 cm^{-1}); and X = S-thioether (ν_{CO} = 2123 cm^{-1}).[52]

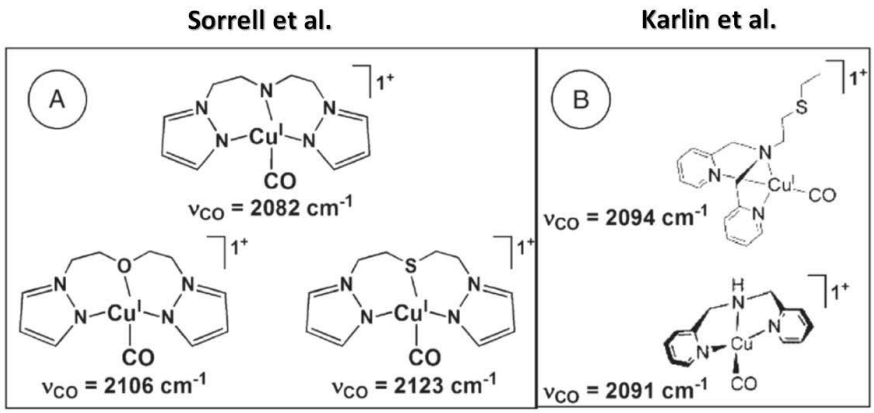

Figure 4. Copper(I)-carbonyl synthetic models with different ligand donor atoms from (A) Sorrell and coworkers[52] and (B) Karlin and coworkers.[53,54] Figure adapted from Lucas HR, Karlin KD *Met. Ions Life Sci.* 2009, 6, 295.

Since the ν_{CO} values found for the Cu(I)-CO forms of DβM and PHMcc were higher than the values established for hemocyanin (ν_{CO} = 2040–2060 cm^{-1}), CO was thus assumed to coordinate to the Cu_M site in DβM and PHMcc which has a soft sulfur donor relative to that of Cu_H site. In the case of Hc, instead, the higher CO stretching frequencies would be explained by the absence of S-atom donors in both the copper ion moieties present in the protein. Unlike what was found by crystallographic studies of DβM and PHMcc that showed no detectable changes in the coordination geometry of the coppers between the reduced and oxidized forms of the enzymes, XAS analysis conducted by Blackburn and coworkers on the oxidized and reduced forms of PHMcc indicated significant changes occurring within the Cu_M and Cu_H coordination environments.[4,47] Strong evidence for these changes were that both Cu_M and Cu_H centers lose their water ligands and that the Met314 sulfur atom binds to Cu_M upon reduction of PHMcc by ascorbate while this residue does not bind the copper when the enzyme is in its oxidized form. The latter evidence came from extensive X-ray

absorption fine structure (EXAFS) studies. EXAFS data further indicated that the Cu_M – SMet314 distance increased from 2.23 Å to 2.33 Å upon CO binding (see Figure 3).[36] Similar ligand loss was also observed by Karlin and coworkers in synthetically derived copper complex systems,[54,55] like for example, the ligand-copper(I) species of the tetradentate N_3S chelator ligand L^{N3S} (L^{N3S} = 2-ethylthio-N,N-bis(pyridin-2yl)methylethanamine) that loses one coordinated donor atom upon addition of CO (Figure 4B).[54] Indirect supporting evidence for the four coordinate (three atom donors + CO) vs. five coordinate (four atom donors + CO) geometry in the $[(L^{N3S})Cu^{I}(CO)]^{+}$ complex was provided by observing a very similar ν_{CO} value with that of the tridentate chelate PY1 ligand (PY1 = bis(2-pyridylmethyl)amine) copper(I) carbonyl species;[53] L^{N3S} possesses the bis(2-pyridylmethyl)amine entity. Surprisingly, further findings consistent with the latter observations were shown upon binding of CO to PHMcc in the presence of the substrate.

In particular, it has been found that the Cu_H site of PHMcc also coordinates carbon monoxide upon addition of peptidylglycine substrates to carbonylated PHMcc [Cu_M-CO···Cu_H] (Figure 3). In this case, a second carbonyl stretch is observed at ν_{CO} = 2062 cm^{-1} due to Cu_H-CO coordination[36] and an only 3 cm^{-1} C-O frequency blue shift was observed when His172 (Cu_H bound) was replaced (by site-directed mutagenesis) by a non-coordinating alanine residue.[43,56] Such a small CO frequency shift suggested that His172 was only weakly bound to the Cu_H ion of the wild-type enzyme and that Cu_H-CO possesses an overall three-coordinate geometry, although the Cu_H-CO frequency of ν_{CO} = 2062 cm^{-1} is lower than would be expected for three-coordinate copper(I)-carbonyls, which are typically in a different frequency range (2090-2110 cm^{-1}).[43,57-59] In analogy with ligand loss upon CO binding observed in both biological and synthetically derived copper systems, EXAFS spectroscopic analysis of wild-type PHMcc also showed that one liganded Cu_H histidine

residue (His172) is lost upon reduction, resulting in a change in the geometry from T-shaped to two coordinate linear.[4,47] Such a dramatic change in the coordination geometry of the Cu_H site is surprising as it is not typical for metal-containing electron transfer proteins that, instead, tend to retain both coordination number and geometry to minimize the reorganization energy involved in the electron transfer process.

Another interesting result from the work of Blackburn et al. concerning the catalytic activity of PHMcc was that its activity dramatically decreased to less than 1% in a mutant where His172 was replaced by an alanine (mutant: H172A).[43] The authors proposed that the decreased or non-existent electron-donating ability of alanine decreases Cu_H reduction potential to the point of favoring a linear two-coordinate geometry for copper(I).[43,58] Another possible explanation according to Blackburn and coworkers for the reduced catalytic activity of the H172A mutant was that changes in the histidine coordination could alter hydrogen bond interactions that are critical for efficient electron transfer.[43]

Furthermore, replacement of the His172 residue by Tyr79 in the first coordination sphere of the copper in the mutant resulted in a lower than expected ν_{CO} value for Cu_H-CO. Decreased activity could also be due to the lack of hydrogen bond interaction between His108 and a glutamine residue, Gln170, that keeps His108 indirectly bound to the peptide substrate, as was shown in the X-ray structure (Figure 1).

A complex showing a linear two-coordinate copper ligation, similarly with that found in Cu_H, was some time ago synthesized and characterized by Karlin and coworkers (Figure 5).[58]

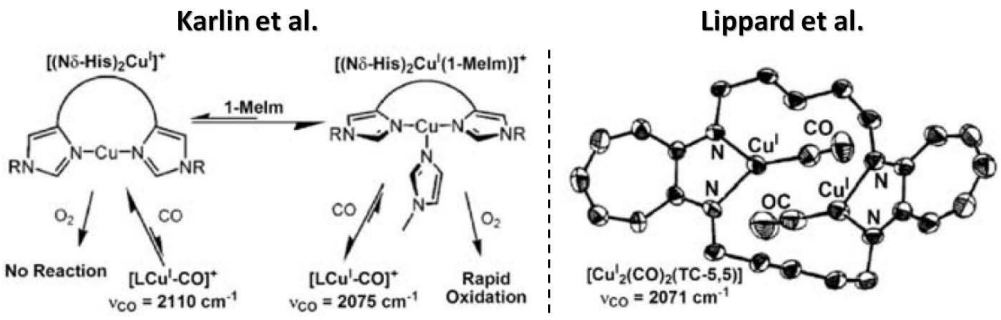

Figure 5. Two-coordinate copper(I)-carbonyl adducts derived from two- or three-coordinate copper(I) complexes. Figure adapted from Lucas HR, Karlin KD *Met. Ions Life Sci.* 2009, 6, 295.

The copper(I)-CO version of the complex showed a C-O stretching frequency of 2110 cm^{-1} which shifted to ν_{CO} = 2075 cm^{-1} upon addition of 1-methylimidazole (1-MeIm). Furthermore, this three-coordinated complex was active towards O_2 activation upon addition of the substrate.[58] Other mononuclear copper(I) complexes displaying two-coordinate linear ligation (although with two imidazole free ligands) that also showed a low C-O stretching frequency (ν_{CO} = 2059–2067 cm^{-1}) are those from Sorrell and Jameson.[60] Similarly with the finding observed for Cu_H, additional CO coordination occurs in these complexes only when an excess of imidazole is present. A three-coordinate dicopper(I) complex showing low C-O stretching frequencies was also characterized by Villacorta and Lippard (ν_{CO} = 2071 cm^{-1}, Figure 5)[61] while other four-coordinate copper(I)-CO complexes based on macrocyclic ligands, like calixarenes (by Reinaud and coworkers), have much higher CO stretching frequencies, of 2092 cm^{-1} and 2102 cm^{-1}, due to the high flexibility of their structures.[59]

An interesting phenomenon observed for the PHCcc where the Cu_H copper is removed is the presence of a low C-O frequency stretch, 2062 cm^{-1}, which was attributed to the copper

ion transferring from the Cu_M to the Cu_H site and to CO binding.[47] As mentioned above, a 'superoxo channeling' involved in the catalytic mechanism of the enzyme was also hypothesized on the basis of this observation, although it was later dismissed. In contrast with PHM, technical challenges still prevent a crystallographic characterization of DβM.[18] The high sequence homology of the two enzymes could suggest a similar catalytic mechanism occurring in the two cases although XAS and FTIR data collected by Blackburn and coworkers for reactions of DβM with CO reveals structural and chemical differences.[46,62,63]

As depicted in Figure 3, the major difference between PHM and DβM is their reactivity pattern with CO in the presence of substrate. While the presence of tyramine induces a 3 cm^{-1} ($\Delta\nu_{CO}$) shift in the Cu_M-CO frequency in DβM, coordination of the substrate close to the Cu_M site in PHM results, instead, in coordination of CO to the Cu_H site and no Cu_M-CO frequency change.[45] In addition, the same frequency shift with that observed for PHM was also found for the H172A mutant.[43] Furthermore, CO binding to Cu_M in DβM resulted in the displacement of an unknown fourth ligand, proposed by Blackburn and coworkers to be a nearby tyrosine residue (Tyr216 or Tyr477) instead of the methionine sulfur ligand present in PHM.[46]

3. Copper/O_2 Interactions in Coupled Dicopper Enzymes and in Model Compounds

In nature, there are many copper proteins that are capable of binding, activating, and incorporating dioxygen that afford a wide range of processes. Within biological systems, the reaction of copper(I) metal centers with molecular oxygen plays an essential role in modulating the oxidative power of molecular oxygen for chemical and biological energy transfer. One of the best characterized and most extensively studied biological motifs for copper is the coupled dinuclear copper center, which is found in enzymes such as Hc,[1,2] Tyr,[1,2] and Co.[3] Hcs are proteins that are responsible for dioxygen transport and are found in the blood of many arthropods and mollusks. These large, multisubunit, highly cooperative proteins bind dioxygen at a dicopper site where each copper ion is ligated by three histidines forming a pseudo-trigonal coordination geometry around the copper ion. In Hc's fully reduced form (Deoxy-Hc), the active site is characterized by an unbridged Cu^I_2 moiety with a $Cu^I \cdots Cu^I$ separation of ~ 4.5 Å (Figure 6).[64] The oxidized form of the dinuclear center, Oxy-Hc, is formed upon exposure to dioxygen. Upon dioxygen binding, each copper ion is oxidized by one electron and dioxygen is reduced by two electrons to form peroxide. The reaction results in formation of an intense purple species: the μ-η^2: η^2-peroxo-dicopper(II) adduct (Figure 7) where the Cu···Cu distance shortens to ~ 3.5 Å. In Hc, the reversible binding and reduction of dioxygen to peroxide is responsible for its blood O_2-transporting activity.

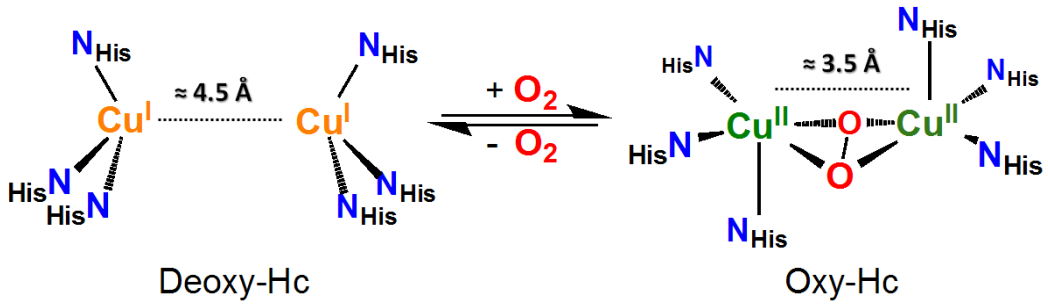

Figure 6. Reaction overview in Hc, involving Deoxy and Oxy-Hc.

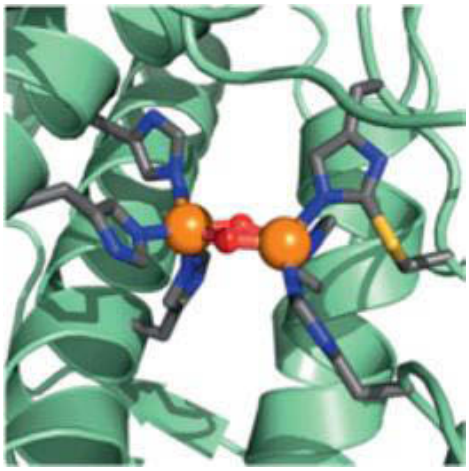

Figure 7. Diagram from the X-ray structure of Oxy-Hc from *octopus dofleini* showing (i) the side-on binding mode of dioxygen (as peroxide) to the dicopper site and (ii) the C2His/S-Cys crosslink.

Tyr and Co are dinuclear copper monooxygenases and oxidases that have active sites structurally related to Hc, but they are capable of performing oxidation reactions. Tyr *ortho*-hydroxylates phenols to give *ortho*-catechols, while Co performs the oxidation of *ortho*-catechols to *ortho*-quinones (Figure 8). The oxygenated form of the dicopper active sites in Tyr and Co (Oxy-Tyr or Oxy-Co) has a peroxo O-O fragment bound to the copper ions in a side-on mode to form a peroxo-dicopper(II) intermediate possessing structural and

spectroscopic properties similar to those found in Oxy-Hc: λ_{max} = 345 nm (ε = 18000 M^{-1} cm^{-1}), the Cu···Cu distance is 3.6 Å, and the O–O bond distance of 1.4 Å.

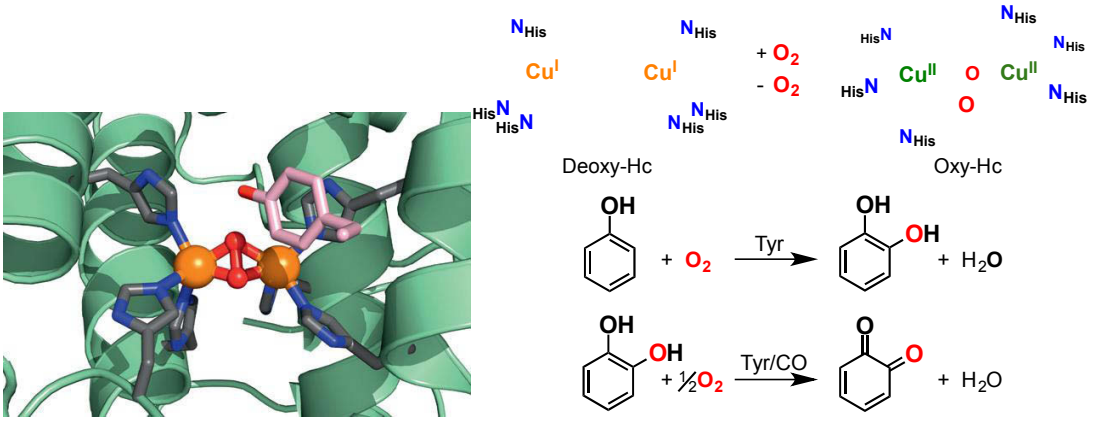

Figure 8. Biological active site of Tyr and Co and their functions.

The Oxy form of these O_2-binding dinuclear copper centers is characterized by a number of distinct spectroscopic signatures. The electronic absorption spectrum contains two intense charge transfer bands at ~ 350 nm (ε ~ 20000 M^{-1} cm^{-1}) and ~ 570 nm (ε ~ 1000 M^{-1} cm^{-1}).[65] A strong magnetic coupling ($-2J$ > 600 cm^{-1}) between the two Cu^{II} centers is also observed, which results in a diamagnetic behavior, and hence no EPR signal. It should be pointed out that the inactive met forms of these enzymes (produced by F^-, N_3^-, and SCN^- coordination to the oxidized copper ions) also display similar characteristics. These met forms were previously the best spectroscopically characterized forms, and represented a major thrust in early synthetic modeling endeavors.[65,66]

In addition to these two (above) physical properties, resonance Raman (rR) studies on Oxy-Hc have shown that the $Cu^{II}_2(O_2^{2-})$ core displays an exceptionally low O-O stretching frequency of ~ 750 cm^{-1}, compared with a $\upsilon_{O\text{-}O}$ of 800 – 900 cm^{-1} normally displayed by

transition metal peroxo complexes. In addition, rR studies have also elucidated a symmetrical binding mode for the peroxo moiety (based on mixed ^{18}O-^{16}O gas experiments to generate the peroxo form) many years before the structure of Oxy-Hc was crystallographically determined.

The ability of Hc, Co, and Tyr to form the same side-on peroxo intermediate while facilitating different chemistry has led to great efforts to better understand the factors dictating this side-on peroxo binding and substrate oxidation capabilities and specificity. Recently, a new Tyr-like enzyme, NspF, was found to effect *o*-aminophenol (OMP) to nitrosophenol oxygenation.[67] This hydroxyanilinase activity contrasts to that observed for Tyr which reacts with OMP substrates to form *o*-iminoquinones (Scheme 2). Spectroscopic evidence indicates that NspF also coordinates O_2 in a μ-η^2: η^2 manner. Thus, NspF, Tyr, and Co perform different types of oxidation chemistry, but all derived from the same Cu_2O_2 species. The reaction specificity noted here may result from that nature of substrate interactions with protein active site pocket residues.

Scheme 2. The difference in *o*-aminophenol reaction of Tyr vs. NspF.

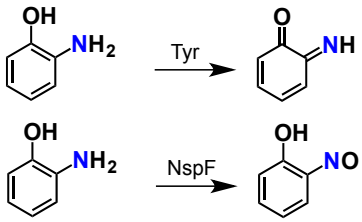

Although no crystal structure has been elucidated for NspF the nearly identical spectroscopic properties of Oxy-Hc, Oxy-Tyr, and Oxy-Co suggest similar active-site structures.[1,2] This new example highlights again that the $Cu^{II}_2(O_2^{2-})$ core is not only a competent oxidant (in Co), but an oxygenating agent (monooxygenase) in Tyr or NspF.

Based on several crystal structures and mutagenesis experiments on Tyr and Co, it has been proposed that solvent (and therefore substrate) accessibility to the dinuclear copper core plays a crucial role in dictating substrate reactivity.[68] Both the catecholase and cresolase activities have been observed in Hc when the dinuclear copper site has been made more accessible to the solution by either proteolytic cleavage or the addition of chemical denaturants including SDS or urea.[13,14,69] Itoh and coworkers[69] have shown that octopus Hc is capable of monooxygenase activity *via* an electrophilic aromatic substitution mechanism with an observed Hammett constant of $\rho = 2.0$, similar to what is observed in mushroom Tyr, suggesting a common reaction pathway.

It is worthwhile to mention that synthetic modeling endeavors have been of fundamental importance in elucidating structural information concerning hemocyanin peroxo coordination (prior to the elucidation of the structure for Oxy-Hc), the mechanism of the hydroxylation of tyrosine by Tyr, and in gaining insights into Co activity. Many detailed reviews have been written on specific aspects of this field.[70-78]

3.1 Structure of Cu^{II}_2–O_2 Adducts

The coordination of O_2 to copper in synthetic systems involves a large degree of electron transfer from the reduced copper center to molecular oxygen in what is most often believed to be an inner-sphere mechanism, i.e., complex formation includes bond formation accompanied by electron transfer. The nature of the copper-dioxygen adduct formed is

highly variable and depends on many factors including the ligand (e.g., S vs. N), resulting coordination number and geometry, the number of copper ions in close proximity, etc...

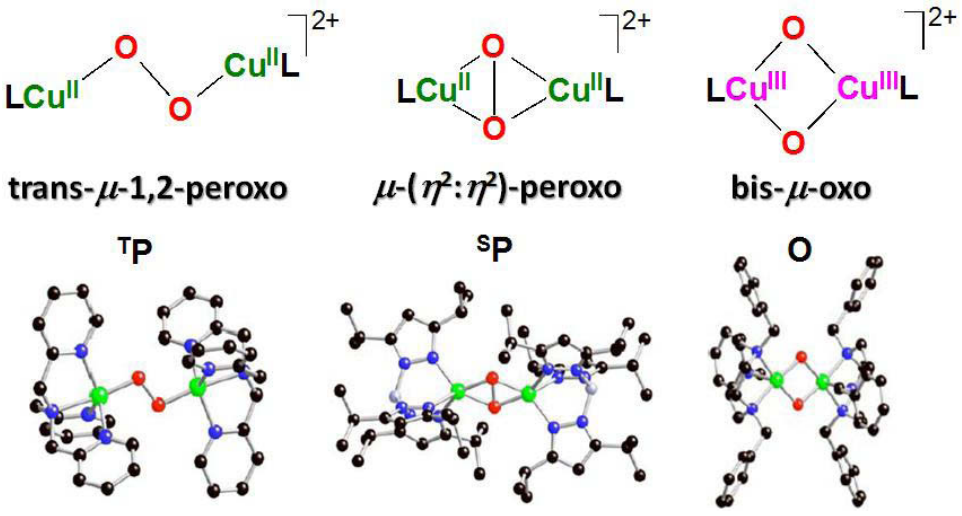

Early endeavors in the late 1970s into modeling Hc's ability to bind dioxygen, and form a μ-peroxo–Cu^{II}_2 species met with little success.[79] Although the formation of such species was indirectly suggested, the extreme thermal sensitivity of these complexes made isolation difficult. Thus, definitive evidence (e.g. vibrational, electronic absorption, and structural data) was lacking. It was only with advances in low–temperature spectroscopic techniques (for example, better laser sources for rR studies, CCD detectors for rR and crystallographic studies, and improved optics for X-ray absorption studies), coupled with a better understanding of how to handle these generally thermally unstable compounds, that has allowed for an explosion in the number of Cu-peroxo species reported. Generation of $Cu_2(O_2)$ species is usually performed at low temperatures (< -40 °C) in weakly coordinating

solvents such as THF and CH_2Cl_2 by exposing solutions of discrete Cu^I complexes to dioxygen.[71]

A major advance in Hc modeling chemistry was made in 1989 from the group of the late N. Kitajima when he reported on the preparation of a Cu^I complex where copper is contained in a tridentate trispyrazolyl-borate ligand environment.[68,80] Dioxygen binds quasireversibly to the Cu^I center at low temperatures, forming a $Cu^{II}_2(O_2^{2-})$ species. The spectroscopic properties of the dioxygen adduct $[\{Cu^{II}[HB(3,5\text{–}i\text{–}Pr_2pz)_3]\}_2(O_2^{2-})]$ (Figure 9) very closely matched that of Oxy-Hc (ν_{OO} = 741 cm^{-1}; λ_{max} = 349 (21000 M^{-1} cm^{-1}) and 551 nm (790 M^{-1} cm^{-1}); $-2J$ > 800 cm^{-1}).

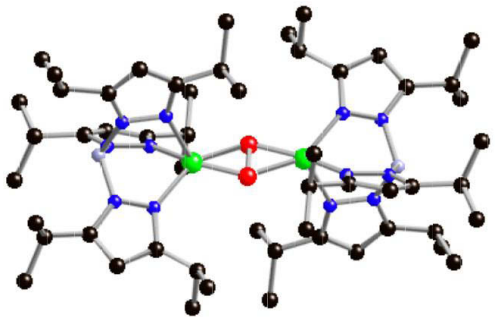

Figure 9. Crystal structure of the Kitajima/Fujisawa side-on peroxo complex $[\{Cu^{II}[HB(3,5\text{–}i\text{–}Pr_2pz)_3]\}_2(O_2^{2-})]$.

Crystallographic studies on $[\{Cu^{II}[HB(3,5\text{–}i\text{–}Pr_2pz)_3]\}_2(O_2^{2-})]$ demonstrated a side-on binding mode for the peroxo-ligand, with a Cu···Cu separation of 3.56 Å, nearly identical to the Cu···Cu distance in the enzyme as determined by EXAFS at that time, and an O-O bond distance of 1.41 Å. All of this evidence strongly suggested a similar coordination geometry for the $Cu^{II}_2(O_2^{2-})$ core with that in the enzyme. This was confirmed when the 2.4 Å resolution crystal structure of Oxy-Hc was solved. The work demonstrates the potential

power of bioinorganic modeling as coordination chemistry studies (employing a non-biologically relevant ligand) yielded a new compound which allowed the (correct) prediction of an important biological structure.

The first crystallographically characterized peroxo containing model for Oxy-Hc was originally reported by Karlin, and resulted from dioxygen binding to the tetradentate Cu^{I} center of $[Cu^{I}(TMPA)]^{+}$, forming the purple $[\{Cu^{II}(TMPA)\}_2(O_2)]^{2+}$ complex (Figure 10); the crystal structure of $[\{Cu^{II}(TMPA)\}_2(O_2)]^{2+}$ was obtained in 1988, and featured a *trans*–μ–1,2 peroxo ligand coordination.[81,82] Although the Cu^{II} centers were strongly magnetically coupled ($-2J > 600$ cm^{-1}), the electronic absorption spectrum (λ_{max} (ε) = 440 (2000), 525 (11500), and 590 nm (7600)) and relatively high-energy $\nu_{O\text{-}O}$ stretching frequency (834 cm^{-1}) were significantly different from the corresponding properties of Oxy-Hc, strongly suggesting the peroxo binding mode was not the same. This dioxygen binding mode (end–on) seems to be the preferred one when Cu is placed in a tetradentate ligand environment, however, recent studies have suggested this is not a steadfast rule.[71,83] Although apparently not a biologically relevant binding mode for O_2^{2-} at dinuclear copper centers, complex $[\{Cu^{II}(TMPA)\}_2(O_2)]^{2+}$ (and derivatives thereof)[77] have been exceptionally important in determining the fundamental dioxygen chemistry of Cu^{I} complexes. A good number of *trans*-μ-1,2 peroxo complexes have since been generated.[71,84]

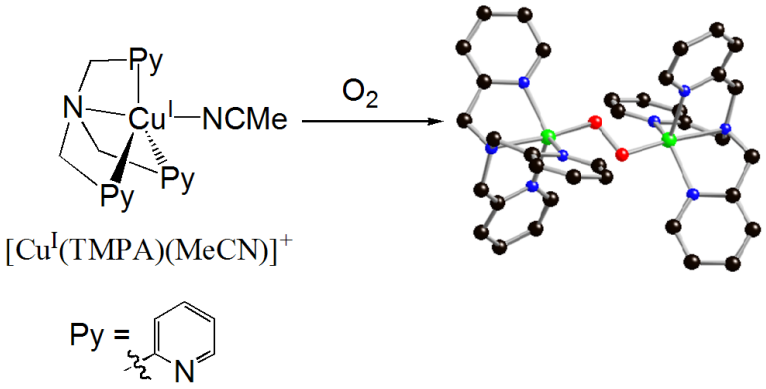

Figure 10. Crystal structure of $[\{Cu^{II}(TMPA)\}_2(O_2^{2-})]^{2+}$ resulting from the reaction of $[Cu^{I}(TMPA)(MeCN)]^{+}$ and dioxygen at low temperature.

Aliphatically tethered dinuclear Cu^{I} complexes, where the metal center was bound to tri- and tetradentate ligands, $[Cu^{I}_2(Nn)]^{2+}$, were prepared by Karlin and coworkers (tridentates; Figure 11a), and demonstrated reversible O_2 binding at low temperatures.[85,86]

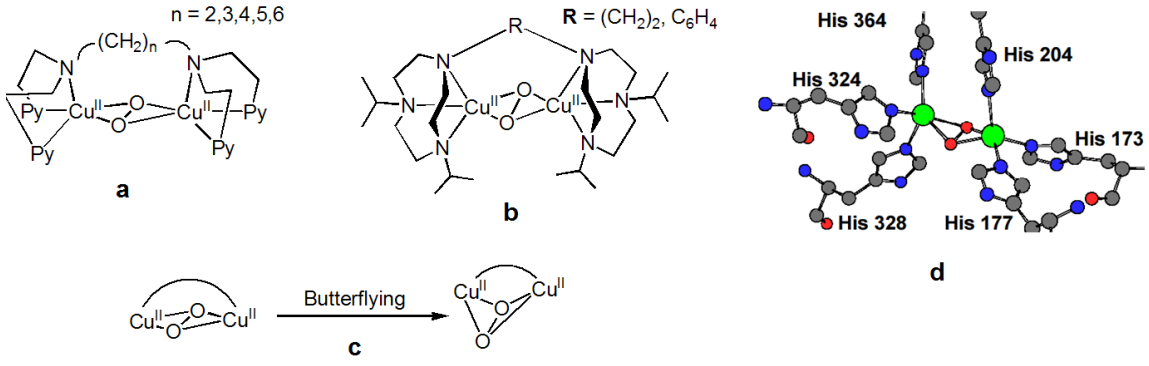

Figure 11. Aliphatically tethered Cu^{II}_2-peroxo complexes **a** and **b**. Figure 11c depicts the distortion, or butterflying, of the $Cu_2O_2^{2-}$ core facilitated by the ligand constraints that the aliphatic tether imposes on the copper complex. Figure 11d depicts the structure of Oxy-Hc from *Limulus polyphemus*, which shows some degree of butterflying of the $Cu_2O_2^{2-}$ core.

Tolman and coworkers reported on the preparation of Cu^{I} complexes contained in tethered TACN ligands (Figure 11b).[78] In the case of the dinuclear complexes with tridentate ligand donors for each copper ion, ($[Cu^{II}_2(Nn)(O_2)]^{2+}$, Figure 11a), it was suggested by low-temperature solution EXAFS that the peroxo ligand bridged the metal centers in a side-on fashion.[86,87] The spectroscopic properties were consistent with those of Oxy-Hc, with an intense charge transfer band in the UV-Vis region at ~ 350 nm ($\varepsilon \sim 20000\ M^{-1}\ cm^{-1}$), and the rR spectroscopy showed a range for $\nu_{O\text{-}O}$ between 760-720 cm^{-1}.[88] The tether was found to impose a structural constraint about the $Cu^{II}_2O_2^{2-}$ core that, according to EXAFS data, causes a distortion, or 'butterflying' so that the peroxo ligand is out of the Cu_2O_2 plane (based on the observed Cu···Cu separations, Figure 11c).[86,88] This butterflying causes a strengthening of the O-O bond (i.e. higher O-O stretching frequencies indicating less O_2 bond activation, meaning potential O-O bond cleavage), and has interesting consequences concerning dioxygen binding and reactivity of the peroxo core, namely that the butterflied Cu_2O_2 core is a poorer oxidant compared to that in a planar arrangement.[88] Available crystallographic data for Oxy-Hc from *Limulus polyphemus* and *Octopus doflenini* suggest that there is some butterflying of the O_2^{2-} ligand from the central core (see Figure 11d).[89] In dinuclear complexes possessing mononucleating tridentate Cu moieties, ligand constraints are less severe, allowing for planar μ-η^2:η^2-peroxo coordination, low $\nu_{O\text{-}O}$ values and resulting exogenous substrate oxidation reactions (see further discussion below). Implications of the polymethylene linker length with consequent distortion of the peroxide binding mode on the copper/dioxygen binding dynamics will be presented in Chapter 4 where a one-photon-two-electron photo-release of O_2 is induced by visible light irradiation in complexes $[Cu^{II}_2(Nn)(O_2)]^{2+}$ with n = 3 and 5.

Independent work by Tolman and Stack in the mid- and late 1990s, using cyclic and linear bi/tridentate amine-based ligands, demonstrated that the side-on peroxo ligand in $Cu^{II}_2(O_2^{2-})$ complexes can be in equilibrium with its Cu^{III}_2-bis-μ-oxo isomer (Figure 12).[71,90]

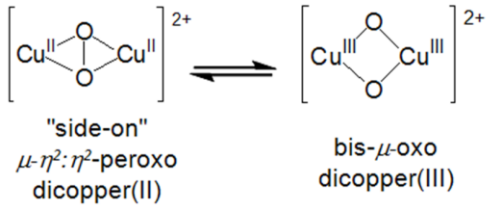

Figure 12. Equilibrium between $Cu^{II}_2(O_2^{2-})$ and Cu^{III}_2-bis-μ-oxo moieties.

This has also been supported by work performed by Karlin and Itoh using bi/tri-dentate pyridyl amine ligands.[91,92] It has been found that copper complex attributes such as ligand electronics, changes in counter ion, ligand steric bulk along with changing solvent, can influence the equilibrium position and interconversion of the Cu^{II}_2 (peroxo) and Cu^{III}_2(bis-μ-oxo) forms. The breadth of work concerning this field is far too great to be done justice here, so we will only briefly touch upon this subject, and point to relevant reviews.[71,73,74,90,93]

Upon interconversion from the side-on peroxo to the bis-μ-oxo form, a change in structure is noted, with a breaking of the O-O bond followed by elongation of the O···O distance to ~ 2.3 Å, and a contraction of the Cu···Cu distance to between 2.7-2.9 Å. The electronic absorption spectrum is also altered with the disappearance of the charge transfer peak at ~ 350 nm and the appearance of two intense peaks at 300 and ~ 400 nm. Breaking of the O-O bond is also evident by rR studies where the characteristic $\nu_{O\text{-}O}$ frequency at ~

750 cm^{-1} is lost, and a Cu-O vibration at ~ 600 cm^{-1} appears. Variations do occur. Core interconversion may also have important consequences concerning subsequent substrate activation-oxidation. It has yet to be determined if the Cu^{III}_2(bis-μ-oxo) core is a biologically relevant O_2-binding mode.

3.2 Formation of Cu^{II}_2-O_2^{2-} Adducts

One of the first model systems to undergo detailed low temperature kinetic studies was the $[Cu^{I}_2(R\text{-}XYL)]^{2+}$ system of Karlin (Figure 13).[85,94]

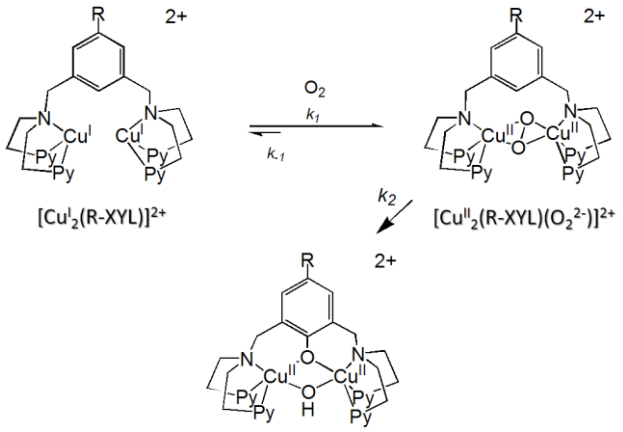

Figure 13. Formation of side-on peroxo intermediate $[Cu^{II}_2(R\text{–}XYL)(O_2^{2-})]^{2+}$ from O_2-reaction with $[Cu^{I}_2(R\text{-}XYL)]^{2+}$, followed by oxygenation of the arene bridge.

$[Cu^{I}_2(R\text{-}XYL)]^{2+}$ (where R = NO_2, H, F, and ^{t}Bu,) will bind O_2 at low-temperatures, forming $[Cu^{II}_2(R\text{-}XYL)(O_2)]^{2+}$, which contains a bridging side-on peroxo ligand. Complexes will then further react with itself performing an oxygenation reaction, similar to Tyr (*vide infra*). Stopped-flow measurements of formation at 183 K demonstrate quasireversible binding of dioxygen with k_{on} values ranging between 470 M^{-1} s^{-1} (R = ^{t}Bu) to 7.2 M^{-1} s^{-1} (R =

F) and k_{off} values varying from 1.5 x 10^{-6} s^{-1} (R = F) to 2.1 x 10^{-5} s^{-1} (R = NO_2).[70,77] The resulting equilibrium constants (K_{eq}) highly favor O_2 binding at low temperatures. This is driven by fairly low activation enthalpies which are partially offset by unfavorable entropy terms at low-temperatures ($\Delta S^{\ddagger} \sim -40$ cal mol^{-1} K^{-1}). At higher temperatures, the activation entropy term precludes the observation of Cu^{I} dioxygen adduct formation. This appears to be a general finding for copper dioxygen chemistry; *$Cu^{II}_2(O_2^{2-})$ formation is driven by highly favorable activation enthalpies, but at high temperature unfavorable activation entropies dominate*.[77]

Another hallmark of $Cu^{II}_2(\mu\text{-}\eta^2\text{:}\eta^2$ peroxo) formation appears to be the fact that a Cu^{II}-superoxo complex is initially formed, which then reacts with another Cu^{I} complex forming the corresponding Cu^{II}_2-peroxo species.[77,86] This was always suspected, however direct observation of a superoxo intermediate during the O_2 binding process was lacking. For example, the oxidation of $[Cu^{I}_2(Nn)]^{2+}$ (Figure 11) and subsequent formation of $[Cu^{II}_2(Nn)(O_2)]^{2+}$ follows an overall quasireversible second order process.[80] However, the enthalpies of activation are very low and in some cases negative, indicative of a pre-equilibrium step involving the formation of Cu^{II}-$O_2^{-}\cdots Cu^{I}$ species followed by a 'closing' step that forms the Cu^{II}_2-peroxo products (Figure 14a).

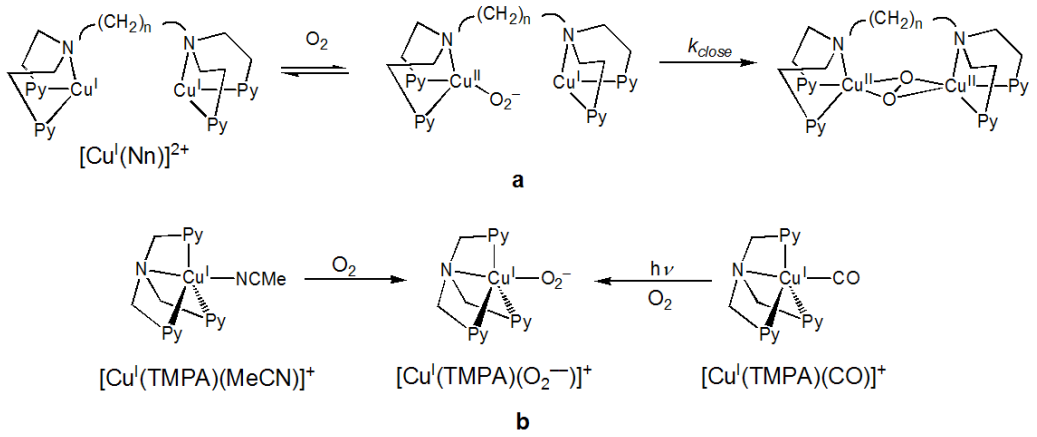

Figure 14. Formation of an initial superoxo-species has been long suspected in the formation of Cu^{II}_2-peroxo species. For example the formation of $[Cu^{I}_2(Nn)(O_2^{2-})]^{2+}$ from $[Cu^{I}_2(Nn)]^{2+}$ proceeds with a very low (and sometimes negative) activation enthalpy, suggestive of the formation of an initial species Cu^{II}-O_2^{-}…Cu^{I} (a). Direct observation of such an intermediate came from dioxygen reactivity studies with $[Cu^{I}(TMPA)]^{+}$ complexes (b).

Cu^{II}-superoxo formation can in fact be directly observed using $[Cu^{I}(TMPA)(L)]^{+}$ (L = RCN or CO; Figure 14b). In a coordinating solvent (such as EtCN) formation of a $[Cu^{II}(TMPA)(O_2^{-})]^{+}$ can be observed by low temperature stopped-flow measurements,[85,95] while a flash photolysis study involving $[Cu^{I}(tmpa)(CO)]^{+}$ in weakly coordinating solvents (THF) demonstrated superoxo formation following photodissociation of the CO ligand.[96]

These results are supported by the work of Kitajima/Fujisawa[97,98] and Tolman[99,100] who have isolated and characterized Cu^{II}-superoxo complexes bound in a side-on fashion. In other ligand systems, particularly tetradentate, there is also ample kinetic and spectroscopic evidence for Cu^{II}-superoxo complexes which are intermediates on the way towards dinuclear peroxo-dicopper(II) formation.[84,85,95,101,102]

The kinetics of $Cu_2(O_2)$ adduct formation was also followed utilizing Tolman's $[Cu^{I}(i\text{-}Pr_3TACN)]^{+}$ systems.[90,93,103] Oxygenation of $[Cu^{I}(i\text{-}Pr_3TACN)]^{+}$ in acetone affords a Cu_2-

dioxygen adduct, which has been identified as being a mixture of peroxo/bis-μ-oxo complexes (Figure 15).

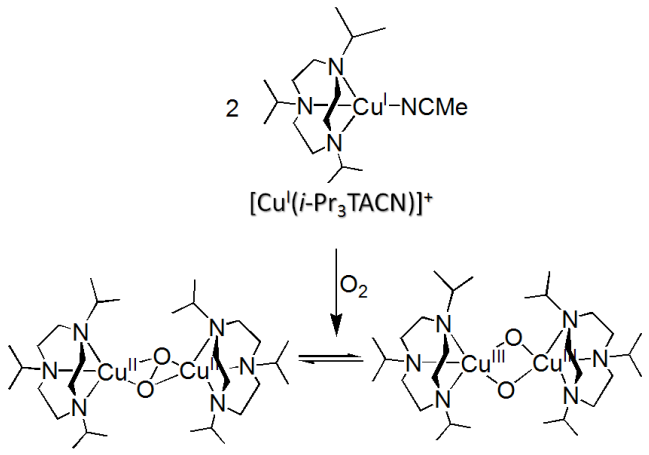

Figure 15. Oxygenation of [Cu^{I}(*i*-Pr$_3$TACN)(MeCN)]$^+$ in acetone leads to both the corresponding peroxo and oxo-species, apparently in concert, suggesting that a rapid equilibrium exists between bis-μ-oxo and μ–η^2:η^2-peroxo complexes.

The formation of the Cu$^{II}_2$-peroxo complex occurs in parallel with Cu$^{III}_2$-bis-μ-oxo formation, implying a rapid equilibrium involving peroxo/oxo core interconversion. It is unknown if one forms prior to the other, but see further discussions in recent reviews.[71,93]

4. Conclusions

Copper-carbon bonds are formed in biological systems in the extensive use of carbon monoxide as spectroscopic and chemical probe ligands for copper ion protein active sites. Observation of copper(I)-carbonyl CO stretching frequencies gives valuable comparative

information about the copper local environment. For example, carbonmonoxy protein derivatives possess revealing spectroscopic IR properties that provide insights about the basic coordination properties of these chemical entities. Fundamental insights into copper/dioxygen binding dynamics and thermodynamics have been obtained using this information as well as the employment of copper(I)-CO synthetic compounds as tools to probe this reactivity which is the topic of the research presented in Chapter 2 of this work.

Regarding dicopper active sites where the two ions are coupled to give side-on peroxo structures, since the structures and spectroscopic correlations for both oxidized and reduced forms of Hc, Co, and Tyr are well understood, much of the future synthetic modeling work will focus on the reactivity of Cu_2O_2 species. Tyr activity, *o*-phenol hydroxylation, seems to occur *via* an electrophilic aromatic substitution, but the broader scope of reaction for side-on μ–η^2:η^2-peroxodicopper(II) complexes should be further explored. Much remains to be accomplished in determining the detailed mechanism of Co catalysis. Since binding of O_2 to copper(I) is the first step involved in the reactivity of all the enzymes mentioned, the studies of this fundamental reactivity for both mononuclear and dinuclear synthetic copper compounds presented here is of fundamental interest.

5. Acknowledgments

The following co-authors contributed to the work presented in this chapter:

Clarence J. Rolle III and Kenneth D. Karlin

6. References

(1) Solomon, E. I.; Chen, P.; Metz, M.; Lee, S. K.; Palmer, A. E. *Angew. Chem. Int. Ed.* **2001**, *40*, 4570.

(2) Solomon, E. I.; Sundaram, U. M.; Machonkin, T. E. *Chem. Rev.* **1996**, *96*, 2563.

(3) Gerdemann, C.; Eicken, C.; Krebs, B. *Acc. Chem. Res.* **2002**, *35*, 183.

(4) Blackburn, N.; Rhames, F.; Ralle, M.; Jaron, S. *J. Biol. Inorg. Chem.* **2000**, *5*, 341.

(5) Prigge, S. T.; Mains, R. E.; Eipper, B. A.; Amzel, L. M. *Cell Mol. Life Sci.* **2000**, *57*, 1236.

(6) Stewart, L. C.; Klinman, J. P. *Annu. Rev. Biochem.* **1988**, *57*, 551.

(7) Matoba, Y.; Kumagai, T.; Yamamoto, A.; Yoshitsu, H.; Sugiyama, M. *J. Biol. Chem.* **2006**, *281*, 8981.

(8) Klabunde, T.; Eicken, C.; Sacchettini, J. C.; Krebs, B. *Nat. Struct. Biol.* **1998**, *5*, 1084.

(9) Cuff, M. E.; Miller, K. I.; van Holde, K. E.; Hendrickson, W. A. *J. Mol. Biol.* **1998**, *278*, 855.

(10) Sendovski, M.; Kanteev, M.; Ben-Yosef, V. S.; Adir, N.; Fishman, A. *J. Mol. Biol.* **2011**, *405*, 227.

(11) Li, Y.; Wang, Y.; Jiang, H.; Deng, J. *Proc. Natl. Acad. Sci. USA* **2009**, *106*, 17002.

(12) Virador, V. M.; Reyes Grajeda, J. P.; Blanco-Labra, A.; Mendiola-Olaya, E.; Smith, G. M.; Moreno, A.; Whitaker, J. R. *J. Agric. Food. Chem.* **2009**, *58*, 1189.

(13) Decker, H.; Hellmann, N.; Jaenicke, E.; Lieb, B.; Meissner, U.; Markl, J. *Integr. Comp. Biol.* **2007**, *47*, 631.

(14) Campello, S.; Beltramini, M.; Giordano, G.; Di Muro, P.; Marino, S. M.; Bubacco, L. *Arch. Biochem. Biophys.* **2008**, *471*, 159.

(15) Hatcher, L.; Karlin, K. *J. Biol. Inorg. Chem.* **2004**, *9*, 669.

(16) Decker, H.; Dillinger, R.; Tuczek, F. *Angew. Chem. Int. Ed.* **2000**, *39*, 1591.

(17) Root, R. W. *J. Biol. Chem.* **1934**, *104*, 239.

(18) Klinman, J. P. *J. Biol. Chem.* **2006**, *281*, 3013.

(19) Prigge, S. T.; Eipper, B. A.; Mains, R. E.; Amzel, L. M. *Science* **2004**, *304*, 864.

(20) Prigge, S. T.; Kolhekar, A. S.; Eipper, B. A.; Mains, R. E.; Amzel, L. M. *Nat. Struct. Biol.* **1999**, *6*, 976.

(21) Evans, J. P.; Ahn, K.; Klinman, J. P. *J. Biol. Chem.* **2003**, *278*, 49691.

(22) Klinman, J. P. *Chem. Rev.* **1996**, *96*, 2541.

(23) Bauman, A. T.; Yukl, E. T.; Alkevich, K.; McCormack, A. L.; Blackburn, N. J. *J. Biol. Chem.* **2006**, *281*, 4190.

(24) Comba, P.; Knoppe, S.; Martin, B.; Rajaraman, G.; Rolli, C.; Shapiro, B.; Stork, T. *Chem. Eur. J.* **2008**, *14*, 344.

(25) Chen, P.; Solomon, E. I. *J. Am. Chem. Soc.* **2004**, *126*, 4991.

(26) Cramer, C. J.; Tolman, W. B. *Acc. Chem. Res.* **2007**, *40*, 601.

(27) Chen, P.; Bell, J.; Eipper, B. A.; Solomon, E. I. *Biochemistry* **2004**, *43*, 5735.

(28) Maiti, D.; Lee, D.; Gaoutchenova, K.; Würtele, C.; Holthausen, M. C.; Sarjeant, A. A. N.; Sundermeyer, J.; Schindler, S.; Karlin, K. D. *Angew. Chem., Int. Ed.* **2008**, *47*, 82.

(29) Maiti, D.; Narducci Sarjeant, A. A.; Karlin, K. D. *Inorg. Chem.* **2008**, *47*, 8736.

(30) Himes, R. A.; Karlin, K. D. *Curr. Opin. Chem. Biol.* **2009**, *13*, 119.

(31) Decker, A.; Solomon, E. I. *Curr. Opin. Chem. Biol.* **2005**, *9*, 152.

(32) Yoshizawa, K.; Kihara, N.; Kamachi, T.; Shiota, Y. *Inorg. Chem.* **2006**, *45*, 3034.

(33) Crespo, A.; Marti, M. A.; Roitberg, A. E.; Amzel, L. M.; Estrin, D. A. *J. Am. Chem. Soc.* **2006**, *128*, 12817.

(34) Huber, S. M.; Ertem, M. Z.; Aquilante, F.; Gagliardi, L.; Tolman, W. B.; Cramer, C. J. *Chem. Eur. J.* **2009**, *15*, 4886.

(35) Prigge, S. T.; Eipper, B.; Mains, R.; Amzel, L. M. *Science* **2004**, *304*, 864.

(36) Jaron, S.; Blackburn, N. *J. Biochemistry* **1999**, *38*, 15086.

(37) Würtele, C.; Gaoutchenova, E.; Harms, K.; Holthausen, M. C.; Sundermeyer, J.; Schindler, S. *Angew. Chem. Int. Ed.* **2006**, *45*, 3867.

(38) Maiti, D.; Lee, D.-H.; Gaoutchenova, K.; Würtele, C.; Holthausen, M. C.; Narducci Sarjeant, A. A.; Sundermeyer, J.; Schindler, S.; Karlin, K. D. *Angew. Chem. Int. Ed.* **2008**, *47*, 82.

(39) Maiti, D.; Fry, H. C.; Woertink, J. S.; Vance, M. A.; Solomon, E. I.; Karlin, K. D. *J. Am. Chem. Soc.* **2006**, *129*, 264.

(40) Peterson, R. L.; Himes, R. A.; Kotani, H.; Suenobu, T.; Tian, L.; Siegler, M. A.; Solomon, E. I.; Fukuzumi, S.; Karlin, K. D. *J. Am. Chem. Soc.* **2011**, *133*, 1702.

(41) Maiti, D.; Fry, H. C.; Wortink, J. S.; Vance, M. A.; Solomon, E. I.; Karlin, K. D. *J. Am. Chem. Soc.* **2007**, *129*, 264.

(42) Fry, H. C.; Scaltrito, D. V.; Meyer, G. J.; Karlin, K. D. *J. Am. Chem. Soc.* **2003**, *125*, 11866.

(43) Jaron, S.; Mains, R. E.; Eipper, B. A.; Blackburn, N. J. *Biochemistry* **2002**, *41*, 13274.

(44) Blackburn, N. J.; Pettingill, T. M.; Seagraves, K. S.; Shigeta, R. T. *J. Biol. Chem.* **1990**, *265*, 15383.

(45) Pettingill, T. M.; Strange, R. W.; Blackburn, N. J. *J. Biol. Chem.* **1991**, *266*, 16996.

(46) Reedy, B. J.; Blackburn, N. J. *J. Am. Chem. Soc.* **1994**, *116*, 1924.

(47) Boswell, J. S.; Reedy, B. J.; Kulathila, R.; Merkler, D.; Blackburn, N. J. *Biochemistry* **1996**, *35*, 12241.

(48) Jaron, S.; Blackburn, N. J. *Biochemistry* **2001**, *40*, 6867.

(49) Sorrell, T. N.; Borovik, A. S.; Shen, C. C. *Inorg. Chem.* **1986**, *25*, 589.

(50) Leslie, K. S.; Drago, R. S.; Griffis, A. B.; Hamilton, D. E.; O'Connor, C. J. *Inorg. Chem.* **1987**, *26*, 1951.

(51) Sorrell, T. N.; Borovik, A. S. *J. Am. Chem. Soc.* **1987**, *109*, 4255.

(52) Sorrell, T. N.; Malachowski, M. R. *Inorg. Chem.* **1983**, *22*, 1883.

(53) Kretzer, R. M.; Ghiladi, R. A.; Lebeau, E. L.; Liang, H. C.; Karlin, K. D. *Inorg. Chem.* **2003**, *42*, 3016.

(54) Lee, D.-H.; Hatcher, L. Q.; Vance, M. A.; Sarangi, R.; Milligan, A. E.; Narducci Sarjeant, A. A.; Incarvito, C. D.; Rheingold, A. L.; Hodgson, K. O.; Hedman, B.; Solomon, E. I.; Karlin, K. D. *Inorg. Chem.* **2007**, *46*, 6056.

(55) Fry, H. C.; Lucas, H. R.; Narducci Sarjeant, A. A.; Meyer, G. J.; Karlin, K. D. *Inorg. Chem.* **2008**, *47*, 241.

(56) Kolhekar, A. S.; Keutmann, H. T.; Mains, R. E.; Quon, A. S. W.; Eipper, B. A. *Biochemistry* **1997**, *36*, 10901.

(57) Pasquali, M.; Floriani, C.; Karlin, K. D.; Zubieta, J. *Copper(I)−Carbon Monoxide Chemistry: Recent Advances and Perspectives," In Copper Coordination Chemistry: Biochemical & Inorganic Perspectives*, **1983**.

(58) Himes, R. A.; Park, G. Y.; Barry, A. N.; Blackburn, N. J.; Karlin, K. D. *J. Am. Chem. Soc.* **2007**, *129*, 5352.

(59) Rondelez, Y.; Seneque, O.; Rager, M. N.; Duprat, A. F.; Reinaud, O. *Chem. Eur. J.* **2000**, *6*, 4218.

(60) Sorrell, T. N.; Jameson, D. L. *J. Am. Chem. Soc.* **1983**, *105*, 6013.

(61) Villacorta, G. M.; Lippard, S. J. *Inorg. Chem.* **1987**, *26*, 3672.

(62) Reedy, B. J.; Murthy, N. N.; Karlin, K. D.; Blackburn, N. J. *J. Am. Chem. Soc.* **1995**, *117*, 9826.

(63) Rhames, F.; Murthy, N.; Karlin, K.; Blackburn, N. *J. Biol. Inorg. Chem.* **2001**, *6*, 567.

(64) Magnus, K. A.; Ton-That, H.; Carpenter, J. E. *Chem. Rev.* **1994**, *94*, 727.

(65) Kitajima, N. *Encyclopedia of Inorganic Chemistry, "Copper: Hemocyanin/Tyrosinase Models"* **1997**, *2*, 822.

(66) Kitajima, N. In *Adv. Inorg. Chem.*; Sykes, A. G., Ed.; Academic Press: 1992; Vol. Volume 39, p 1.

(67) Ginsbach, J. W.; Kieber-Emmons, M. T.; Nomoto, R.; Noguchi, A.; Ohnishi, Y.; Solomon, E. I. *Proc. Nat. Acad. Sci.* **2012**, *109*, 10793.

(68) Kitajima, N.; Fujisawa, K.; Fujimoto, C.; Moro, n.; Hashimoto, S.; Kitagawa, T.; Toriumi, K.; Tasumi, K.; Nakamura, A. *J. Am. Chem. Soc.* **1992**, *114*, 1277.

(69) Suzuki, K.; Shimokawa, C.; Morioka, C.; Itoh, S. *Biochemistry* **2008**, *47*, 7108.

(70) Karlin, K. D.; Zuberbuhler, A. D., in 'Formation, Structure and Reactivity of Copper Dioxygen Complexes',ed. J. Reedijk, Bouwman, E., New York **1999**.

(71) Mirica, L. M.; Ottenwaelder, X.; Stack, T. D. P. *Chem. Rev.* **2004**, *104*, 1013.

(72) Lewis, E. A.; Tolman, W. B. *Chem. Rev.* **2004**, *104*, 1047.

(73) Que, L.; Tolman, W. B. *Angew. Chem. Int. Ed.* **2002**, *41*, 1114.

(74) Stack, T. D. P. *Dalton Trans.* **2003**, 1881.

(75) Kitajima, N.; Moro, n. *Chem. Rev.* **1994**, *94*, 737.

(76) Karlin, K. D.; Tyeklár, Z. *in 'Bioinorganic Chemistry of Copper', New York* **1993**.

(77) Karlin, K. D.; Kaderli, S.; Zuberbühler, A. D. *Acc. Chem. Res.* **1997**, *30*, 139.

(78) Tolman, W. B. *Acc. Chem. Res.* **1997**, *30*, 227.

(79) Karlin, K. D.; Gultneh, Y. *Prog. Inorg. Chem.* **1987**, *35*, 219.

(80) Kitajima, N.; Fujisawa, K.; Morooka, Y.; Toriumi, K. *J. Am. Chem. Soc.* **1989**, *111*, 8975.

(81) Tyeklar, Z.; Jacobson, R. R.; Wei, N.; Murthy, N. N.; Zubieta, J.; Karlin, K. D. *J. Am. Chem. Soc.* **1993**, *115*, 2677.

(82) Jacobson, R. R.; Tyeklar, Z.; Farooq, A.; Karlin, K. D.; Liu, S.; Zubieta, J. *J. Am. Chem. Soc.* **1988**, *110*, 3690.

(83) Hayashi, H.; Fujinami, S.; Nagatomo, S.; Ogo, S.; Suzuki, M.; Uehara, A.; Watanabe, Y.; Kitagawa, T. *J. Am. Chem. Soc.* **2000**, *122*, 2124.

(84) Komiyama, K.; Furutachi, H.; Nagatomo, S.; Hashimoto, A.; Hayashi, H.; Fujinami, S.; Suzuki, M.; Kitagawa, T. *Bull. Chem. Soc. Jpn.* **2004**, *77*, 59.

(85) Karlin, K. D.; Kaderli, S.; Zuberbuhler, A. D. *Acc. Chem. Res.* **1997**, *30*, 139.

(86) Liang, H.-C.; Karlin, K. D.; Dyson, R.; Kaderli, S.; Jung, B.; Zuberbühler, A. D. *Inorg. Chem.* **2000**, *39*, 5884.

(87) Blackburn, N. J.; Strange, R. W.; Farooq, A.; Haka, M. S.; Karlin, K. D. *J. Am. Chem. Soc.* **1988**, *110*, 4263.

(88) Pidcock, E.; Obias, H. V.; Abe, M.; Liang, H.-C.; Karlin, K. D.; Solomon, E. I. *J. Am. Chem. Soc.* **1999**, *121*, 1299.

(89) Magnus, K. A.; Hazes, B.; Tonthat, H.; Bonaventura, C.; Bonaventura, J.; Hol, W. G. J. *Proteins: Struct. Funct. Bioinform.* **1994**, *19*, 302.

(90) Tolman, W. B. *Acc. Chem. Res.* **1997**, *30*, 227.

(91) Zhang, C. X.; Liang, H. C.; Kim, E. I.; Shearer, J.; Helton, M. E.; Kim, E.; Kaderli, S.; Incarvito, C. D.; Zuberbuhler, A. D.; Rheingold, A. L.; Karlin, K. D. *J. Am. Chem. Soc.* **2003**, *125*, 634.

(92) Itoh, S.; Taki, M.; Nakao, H.; Holland, P. L.; Tolman, W. B.; Que, L.; Fukuzumi, S. *Angew. Chem. Int. Ed.* **2000**, *39*, 398.

(93) Lewis, E. A.; Tolman, W. B. *Chem. Rev.* **2004**, *104*, 1047.

(94) Karlin, K. D.; Nasir, M. S.; Cohen, B. I.; Cruse, R. W.; Kaderli, S.; Zuberbuehler, A. D. *J. Am. Chem. Soc.* **1994**, *116*, 1324.

(95) Zhang, C. X.; Kaderli, S.; Costas, M.; Kim, E.-i.; Neuhold, Y.-M.; Karlin, K. D.; Zuberbühler, A. D. *Inorg. Chem.* **2003**, *42*, 1807.

(96) Fry, H. C.; Scaltrito, D. V.; Karlin, K. D.; Meyer, G. J. *J. Am. Chem. Soc.* **2003**, *125*, 11866.

(97) Fujusawa, K.; Tanaka, M.; Moro, n.; Kitajima, N. *J. Am. Chem. Soc.* **1994**, *116*, 12079.

(98) Chen, P.; Root, D. E.; Campochiano, C.; Fujisawa, K.; Solomon, E. I. *J. Am. Chem. Soc.* **2003**, *125*, 466.

(99) Spencer, D. J. E.; Aboelella, N. W.; Reynolds, A. M.; Holland, P. L.; Tolman, W. B. *J. Am. Chem. Soc.* **2002**, *124*, 2108.

(100) Aboelella, N. W.; Lewis, E. A.; Reynolds, A. M.; Brennessel, W. W.; Cramer, C. J.; Tolman, W. B. *J. Am. Chem. Soc.* **2002**, *124*, 10660.

(101) Jazdzewski, B. A.; Reynolds, A. M.; Holland, P. L.; Jr., V. G. Y.; Kaderli, S.; Zuberbuhler, A. D.; Tolman, W. B. *J. Biol. Inorg. Chem.* **2003**, *8*, 381.

(102) Weitzer, M.; Schindler, S. *Inorg. Chem.* **2003**, *42*, 1800.

(103) Halfen, J. A.; Mahapatra, S.; Wilkinson, E. C.; Kaderli, S.; Young, V. G.; Que, L.; Zuberbuhler, A. D.; Tolman, W. B. *Science* **1996**, *271*, 1397.

Chapter 2:

Light-Induced Copper-CO and Copper-O_2 Reactivity

Abstract

The study of the binding of small molecules like carbon monoxide and dioxygen to (L)Copper(I) compounds where 'L' is a tridentate ligand is of particular interest to gain fundamental insights into the coordination chemistry and O_2-activation occurring in the active site of the enzymes peptidylglycine α-hydroxylating monooxygenase (PHM) and dopamine β-monooxygenase (DβM) where the copper ions have also a tridentate first coordination sphere (although the type of donors and coordination environment are different) and bind such small molecules at a single metal center. The stability and reactivity of such tridentate chelating ligand-copper(I) compounds towards small molecules is, however, often very solvent-dependent as the fourth available coordination site of the copper can be easily occupied by a solvent molecule. In this study, (L)Copper(I)(CO) compounds bearing tridentate N-donor chelating ligands ([(nQ2)CuI(CO)]+ (**1**) and [(BzQ2)CuI(CO)]+ (**2**) were photo-excited using UV light (355 nm) inducing carbon monoxide release and allowing fast CO and/or O_2 coordination to the copper. Second-order rate constants and kinetic parameters determined revealed an overall slower copper/CO and Cu/O_2 reaction chemistry occurring for these compounds in comparison with previously

studied copper complexes with tetradentate ligands. Evidence for the formation of a mononuclear 1:1 Cu/O_2 adduct at low temperature in acetone solvent supported by the tridentate ligand nQ_2 was also shown.

1. Introduction

Carbon monoxide has been used for decades as redox-inactive surrogate of dioxygen to investigate on O_2 binding occurring in the active site of enzymes that modulate the reactivity of such a wide-spread oxidative agent.[1-10] Carbon monoxide coordination to transition metal ions has also been very useful to gain fundamental insights on the ligand environment surrounding metals i.e. electron-donating properties of ligands, sterics, coordination environment, etc... Early studies of carbon monoxide photo-release from myoglobin and hemoglobin, in fact, greatly improved our understanding of both CO dissociation from and CO binding to the iron ion, shedding light on the multi-step processes involved in the chemistry occurring in proteins i.e. geminate recombination after CO photo-ejection, protein conformational changes, and kinetic barriers associated with the various steps of binding and dissociation of CO. It is from the pioneering studies of Gibson and co-workers[11,12] that the so called 'flash-and-trap' method has been employed, in combination with transient absorption spectroscopy, to examine the O_2 binding to iron. Starting from $[(P)Fe^{II}(CO)]^{2+}$ (P = protein), the method allowed characterization of O_2 binding to iron(II) through competitive coordination of CO and O_2 to the metal after CO photo-release. The success of this approach stimulated its application to the study of the binding of small molecules to other metal ions as well. The first work where CO was successfully photo-released from a copper coordination compound was reported by Scaltrito and co-workers[13] where ultra-violet light (355 nm) was used to excite the tetradentate ligand-copper compound $[(TMPA)Cu^{I}(CO)]^{+}$ (see Chart 1 for ligand structure: TMPA = ^{D}L with D = Py) allowing kinetics and thermodynamics of the following CO re-binding to the copper to be determined. After these studies, the 'flash-and-trap' method was utilized also for other copper coordination compounds, in analogy with the studies conducted by Gibson et al. for

the iron proteins and full kinetic and thermodynamic characterization was performed for the binding of both CO and O_2 to copper(I) compounds bearing tetradentate N-donor chelating ligands (Chart 1, ^{D}L ligands).[14-16] The studies were performed in several solvents revealing the importance of solvent effects on the binding of copper compounds with small molecules. In fact, such effects play a key role in modulating both stability and reactivity of copper coordination compounds through both electrostatic interactions and coordination of the solvent to the metal. The latter strongly depends on the number and type of atom donors surrounding the copper, the electron-donating capability of the ligand, the 'bite' angle by which a chelating ligand binds the copper, the oxidation state of the metal, etc... In the case of tetradentate N-donor chelating ligand environments like those for which previous laser experiments have been performed, the solvent may or may not coordinate copper(I) ion complex formed after photoexcitation, depending on the factors listed above.

For neutral tridentate pyridyl-(or quinolyl-)based N-donor chelating ligand-copper compounds, on the other hand, where one additional coordination position is available on the copper ion, solvent binding to the copper becomes thermodynamically more favorable. This is one of the reasons why copper(I) compounds supported by such ligands are sometimes not reactive with O_2 at low temperature, even at high concentrations of copper. Itoh and coworkers showed for a few cases that dangling arms bearing aromatic groups linked to the alkyl nitrogen through a long (poly-)methylene chain (two or more methylene groups) interact with the copper through π-d interactions to such an extent that the copper(I)/O_2 chemistry is, then, completely inhibited.[17] These ligand-copper π-d effects have been shown <u>not</u> to occur in the case of the ligand BzQ_2 employed here (Chart 1) that has a dangling arm having a shorter methylene chain (only one methylene group) as a linker with the alkyl nitrogen of the ligand. Ligand denticity (i.e. 3N vs. 4N) has also been shown to

have significant effects on the Cu(I)/O_2 chemistry for synthetic ligand-copper systems.[18,19] In this work, $[(L)Cu^{I}(CO)]^{+}$ compounds were synthesized using a modification of the synthetic procedure used by Itoh and co-workers[17] where the corresponding acetonitrile compounds, $[(L)Cu^{I}(CH_3CN)]^{+}$, were dissolved in CO-saturated ethanol (EtOH) at low temperature followed by solvent removal. Two $[(L)Cu^{I}(CO)]^{+}$ compounds, ($[(nQ_2)Cu^{I}(CO)]^{+}$ (**1**) and $[(BzQ_2)Cu^{I}(CO)]^{+}$ (**2**), both supported by L = bis(2-quinolylmethyl)amine tridentate ligands were synthesized in this manner for this study. Both ligands have a 'dangling' arm that does not coordinate copper(I) being either a neopentyl- (nQ_2) or a benzyl- (BzQ_2) functional group (Chart 1). The ligand BzDMM (N,N-bis(3,5-dimethyl-4-methoxy-2-pyridylmethyl)benzylamine, Chart 1) was also synthesized in this study in an effort to stabilize a putative copper(II)-superoxide species, possibly, forming upon O_2 binding to its copper(I) complex ([(BzDMM)Cu^{I}]BArF) through the presence of the electron-donating methoxy functional groups (-OCH_3) present in the *para* position of the pyridine groups of the ligand. The dioxygen reactivity of [(BzDMM)Cu^{I}]BArF was tested, although the photochemistry of its carbonylated counterpart [(BzDMM)Cu^{I}(CO)]BArF led to non-reversible chemistry of the species formed upon laser excitation.

Chart 1. Ligands systems examined in this study (middle) and those from previous works (top) and complex formulas examined in this study (bottom).

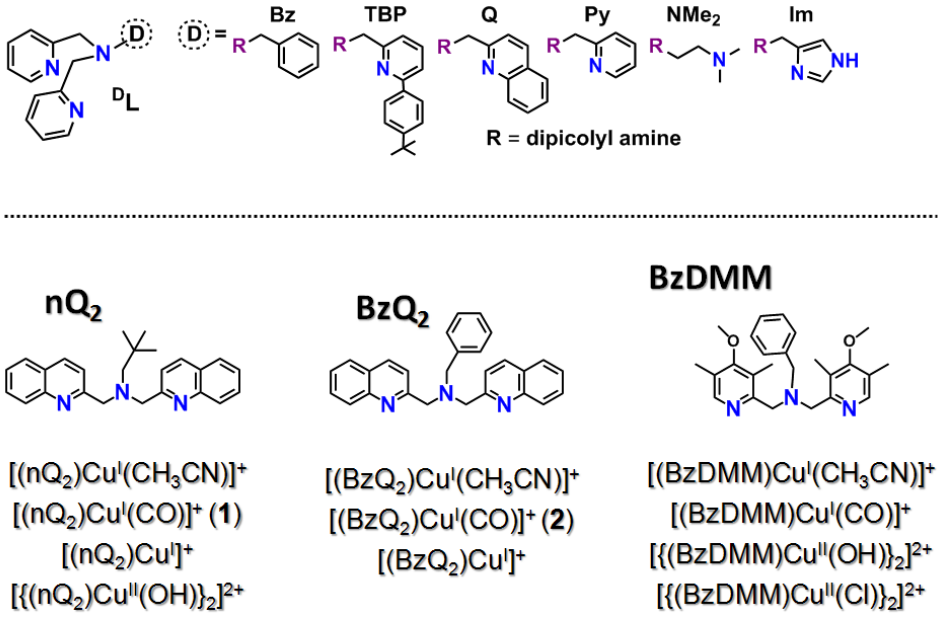

In this study, we explored the kinetics of CO and O_2 binding to copper(I) following photoexcitation of **1** and **2** at low temperature in acetone solvent and both second-order rate constants and activation parameters were determined.

2. Experimental

2.1 Materials

All compounds purchased were of the highest available purity from Sigma-Aldrich Chemical or Tokyo Chemical Industry (TCI) and they were used as received unless otherwise specified. Tetrahydrofuran (THF) was distilled under argon from

Na/benzophenone and degassed with argon before use. Pentane was distilled from calcium hydride under argon and also degassed before use. Diethyl ether was used after being passed through a 60 cm long column of activated alumina (Innovative Technologies) under argon. $[(Cu^{I}(CH_3CN)_4]BArF$ (BArF = $[B(C_6F_5)_4]^-$) was synthesized according to literature protocols[20] and $[(Cu^{I}(CH_3CN)_4]PF_6$ was purchased from Sigma-Aldrich Chemical. The identity and purity of other compounds used in this study were verified by ^1H NMR or/and elemental analysis.

2.2 O_2-Free Techniques and Cryogenics

Synthesis and manipulations of copper complexes were performed employing Schlenk techniques or carried out in an MBraun glovebox (with O_2 and H_2O levels below 1 ppm). UV-Vis spectra were recorded with a Cary 50 Bio spectrophotometer equipped with a liquid nitrogen chilled Unisoku USP-203-A cryostat.

2.3 NMR Measurements

NMR spectroscopy was performed on Bruker 300 and 400 MHz instruments with spectra calibrated to either internal tetramethylsilane (TMS) standard or to residual protio solvent.

2.4 CO and O_2 Solubility in acetone

The solubility of CO (0.01169 mol/L) and O_2 (0.01134 mol/L) in acetone at 25 ^{o}C and temperature-dependent solubility data were used as available in the literature.[21,22] The formula used for the temperature dependence of the molar fraction solubility of CO in acetone was the following:

$\ln \chi = -26.890 + (723.58 / T) + [3.0376 (\ln T)]$

where χ is the molar fraction solubility of CO in acetone and T is the temperature, in Kelvin, while the correspondent curve utilized for O_2 was the following:

$\ln \chi = -24.3100 + (649.40 / T) + [2.6414 (\ln T)]$

2.5 Gas Mixing

Carbon monoxide (CO; Air Gas East, grade 2.3) used for the experiments in acetone was treated by passing through an R & D Separations oxygen/moisture trap (Agilent Technologies OT3-4). Red rubber tubing (Fisher Scientific; inner diameter: 1/4 in.; thickness: 3/16 in.) was used to attach the gas cylinders fitted with appropriate regulators to two MKS Instruments Mass-Flo Controllers (MKS Type 1179A) regulated by an MKS Instruments Multi-Channel Flow Ratio/Pressure Controller (MKS Type 647C). The gas mixtures (N_2/CO and O_2/CO) were determined by the set flow rates of the two gases. For example, a 10% CO mixture would be made by mixing CO at a rate of 10 standard cubic centimeters per minute (sccm) with N_2 at 90 sccm for a total flow of 100 sccm. By varying the ratio of CO and N_2 with the gas mixer, the concentration of the gases were determined by taking the percentage of the gas added and multiplying by the solubility of the corresponding gas in acetone. For example, if [CO] = X and [N_2] = Y, if the CO/N_2 flow rate is 3/7 (or 30% of the total gas flow is CO), then, the concentration of CO and N_2 in acetone are [CO] = (0.30 · X) and [N_2] = (0.70 · Y).

2.6 Laser Flash Photolysis

Experimental information for the setup of the Nd:YAG flash-photolysis apparatus has been previously reported.[23] The apparatus was equipped with a liquid nitrogen chilled

Unisoku USP-203-A cryostat. The samples, **1** and **2**, were irradiated with λ_{exc} = 355 nm pulsed light (8 mJ/pulse) and data were collected at the monitored wavelengths from averages of 60 laser pulses. Samples (~ 1.5 mM) were prepared under an inert atmosphere (drybox) in 1 cm quartz cuvettes with four polished windows made custom by Quark glass. The cuvettes were equipped with a 14/20 joint and Schlenk stopcock. Gas mixtures were added to sample solutions through direct bubbling through a 24-inch needle (19-gauge) for 5 seconds for 10 times with intervals of 10 seconds between each time. During data collection the gas flowed through the headspace of the sample solution into the cuvette.

2.7 Ligand and Complex Syntheses

Synthesis of N,N-bis(2-quinolylmethyl)neopentylamine (nQ_2)

The compound 2-quinolinecarboxaldehyde (3 g, 0.013 mol) and neopentylamine (1.13 g, 0.013 mol) were stirred in 1,2-dichloroethane (DCE, 500 mL) and the mixture was heated using a heat gun for 15 minutes. The mixture was then cooled to room temperature using an ice bath and sodium triacetoxyborohydride (4.5 g, 0.021 mol) was slowly added and allowed to react under agitation for one hour. More sodium triacetoxyborohydride (4.5 g, 0.021 mol) was, then, added to the mixture that was allowed to stir overnight. The progress of the reaction was checked by TLC (Alumina). A solution of concentrated HCl was used to acidify the reaction mixture to pH = 1 and the aqueous phase was, then, treated with an aqueous solution of NaOH (0.5 M) until pH = 14 was reached. CH_2Cl_2 (DCM, 50 mL x 5) was, then, used to extract the deprotonated amines from the aqueous phase and the organic phase was, then, dried over Na_2SO_4 and the solvent was removed by evaporation. nQ_2 was isolated from the sample using an Alumina chromatography column (eluent: hexane:AcOEt - 80:20) in a 37% yield; ^{1}H-NMR ($CDCl_3$, 400 MHz) - 0.80 (9H, s,($-CH_3)_3$), 2.62 (2H, s,$-CH_2-$), 4.04

(4H, s, $–CH_2–N–CH_2–$), 7.48-7.54 (2H, t), 7.65-7.72 (2H, t), 7.74-7.82 (4H, t), 8.0-8.1 (2H, d), 8.1-8.2 (2H, d); HRMS (FAB^+) m/z - 370.22819, Calcd for $C_{25}H_{28}N_3$ - 370.22832.

Synthesis N,N-bis(2-quinolylmethyl)benzylamine (BzQ_2)

BzQ_2 was synthesized using the same experimental procedure used for nQ_2, however instead, 2-quinolinecarboxaldehyde (3 g, 0.013 mol) and benzylamine (2.04 g, 0.019 mol) were used and triacetoxyborohydride (4.5 g, 0.021 mol) was added to the mixture, twice. BzQ_2 was isolated in 50% yield. ^1H NMR ($CDCl_3$, 400 MHz) - 3.75 (2H, s,$–CH_2–$), 4.05 (4H, s, $–CH_2–N–CH_2–$), 7.30-7.33 (1H, d), 7.35-7.38 (2H, t), 7.40-7.45 (2H, d), 7.45-7.55 (2H, t), 7.6-7.7 (2H, t), 7.7-7.8 (4H, t), 8.1-8.2 (4H, d); HRMS (FAB^+) m/z - 390.19666, Calcd for $C_{27}H_{24}N_3$ - 390.19702.

Synthesis of N,N-bis(3,5-dimethyl-4-methoxy-2-pyridylmethyl)benzylamine (BzDMM)

2-Chloromethyl-4-methoxy-3,5-dimethylpyridine hydrochloride (6.37 g, 0.029 mol), benzylamine (1.5 g, 0.014 mol), and sodium carbonate (7.42 g, 0.070 mol) were stirred in acetonitrile (150 mL) for two days. The progress of the reaction was checked by TLC (Alumina). The solvent was removed by evaporation and BzDMM was isolated from the sample using an Alumina chromatography column (eluent: hexane:AcOEt - 75:25 and hexane:AcOEt - 25:75) in a 82% yield; ^1H-NMR ($CDCl_3$, 400 MHz) - 1.8-2.1 (6H, s,$(–CH_3)_2$), 2.1-2.4 (6H, s,$(–CH_3)_2$), 3.5-3.9 (15H, m,$–CH_2–$ and -O-CH_3), 7.0-7.4 (5H, m), 8.1-8.3 (2H, s); HRMS (FAB^+) m/z - 405.23960, Calcd for $C_{25}H_{31}N_3O_2$ - 405.24163.

Synthesis of [(nQ_2)Cu^I(CH_3CN)]BArF

Ligand nQ_2 (0.15 g, 0.41 mmol) and [$Cu^I(CH_3CN)_4$]BArF (0.372 g, 0.39 mmol) were dissolved in THF (2 mL) under argon. After stirring for 5 minutes, distilled/deoxygenated pentane (150 mL) was added causing precipitation of a yellow solid. The solvent was removed through cannula while applying a vacuum and the solid obtained was washed three times with pentane and was made re-precipitate from dichloromethane with pentane, and then dried under vacuum. The compound [(nQ_2)Cu^I(CH_3CN)]BArF was isolated in 63% yield. Crystals were obtained by vapor diffusion of ether into an acetone solution of the compound. ^{1}H NMR (THF d-8, 400 MHz) - 1.15 (9H, s,(–CH_3)$_3$), 2.45 (3H, s,(–CH_3CN)), 3.0 (2H, s,–CH_2–), 4.4 (4H, s, –CH_2–N–CH_2–), 7.65-7.8 (2H, d), 7.8-7.9 (2H, t), 8.0-8.15 (2H, t), 8.15-8.25 (2H, d), 8.6-8.7 (2H, d), 8.75-8.85 (2H, d); MS (FAB$^+$) m/z 432.2, Calcd for $C_{25}H_{27}CuN_3$ 432.15; Anal. Calcd for [(nQ_2)Cu^I(CH_3CN)](B(C_6F_5)$_4$) ($C_{51}H_{30}BCuF_{20}N_4$): C, 53.12; H, 2.62; N, 4.86%. Found: C, 52.76; H, 3.39; N, 4.54%.

Synthesis of [(nQ_2)Cu^I(CH_3CN)]PF_6

The compound [(nQ_2)Cu^I(CH_3CN)]PF_6 was synthesized for the purpose of obtaining crystals of X-ray quality. The procedure used for the synthesis was the same used for [(nQ_2)Cu^I(CH_3CN)]BArF with the difference that [($Cu^I(CH_3CN)_4$]PF_6 was used as source of copper and distilled/deoxygenated Et_2O was used for precipitation, instead of pentane.

Synthesis of [(BzQ_2)Cu^I(CH_3CN)]BArF

[(BzQ_2)Cu^I(CH_3CN)]BArF was synthesized using the same experimental procedure used for [(nQ_2)Cu^I(CH_3CN)]BArF mixing, instead, ligand BzQ_2 (0.15 g, 0.39 mmol) and [$Cu^I(CH_3CN)_4$]BArF (0.35 g, 0.39 mmol). Compound [(BzQ_2)Cu^I(CH_3CN)]BArF was

isolated in 63% yield. ^{1}H NMR (THF d-8, 400 MHz) - 2.44-2.45 (3H, s,(–CH_3CN)), 4.20-4.35 (4H,b s, –CH_2–N–CH_2–), 4.5-4.6 (2H,b s,–CH_2), 7.35-7.5 (3H), 7.6-7.7 (4H, t), 7.8-7.9 (2H, t), 8.0-8.1 (2H, t), 8.1-8.2 (2H,d), 8.55-8.65 (2H, d), 8.7-8.8 (2H, d); MS (FAB$^+$) m/z - 452.1, calcd for $C_{27}H_{23}CuN_3$ 452.1; Anal. Calcd for [(BzQ_2)Cu^I(CH_3CN)](B(C_6F_5)$_4$) ($C_{53}H_{26}BCuF_{20}N_4$): C, 54.26; H, 2.23; N, 4.78%. Two separate analyses: Found: C, 54.26; H, 2.98; N, 4.01%. Found: C, 53.58; H, 2.60; N, 3.59%.

Synthesis of [(BzDMM)Cu^I(CH_3CN)]BArF

Ligand BzDMM (0.100 g, 0.247 mmol) and [Cu^I(CH_3CN)$_4$]BArF (0.089 g, 0.247 mmol) were dissolved in THF (2 mL) under argon. After stirring for 5 minutes, distilled/deoxygenated pentane (150 mL) was added causing precipitation of a yellow solid. The solvent was removed through cannula while applying vacuum and the solid obtained was washed three times with pentane and dried under vacuum. The compound [(BzDMM)Cu^I(CH_3CN)]BArF was isolated in 60% yield. ^{1}H-NMR (THF d-8, 400 MHz) - 2.05-2.4 (15H, d,(–CH_3)$_4$ and CH_3-CN), 3.5-3.9 (15H, m,–CH_2– and -O-CH_3), 7.1-7.+5 (5H, m), 8.1-8.3 (2H, s).

Synthesis of [(nQ_2)Cu^I(CO)]BArF (1)

Syntheses of the two [(L)Cu^I(CO)]BArF compounds were performed using a modification of the procedure previously adopted by Itoh and co-workers.[17] [(nQ_2)Cu^I(CH_3CN)]BArF (0.1 g, 0.087 mmol) was dissolved in EtOH (5 mL) in a CO atmosphere at -80^{0}C and the mixture was stirred for 30 minutes. Addition of distilled/deoxygenated pentane caused precipitation of a white solid. The solvent was removed through filtration while applying a vacuum and the solid obtained was then, washed

three times with CO-saturated pentane and dried under vacuum. Compound $[(nQ_2)Cu^I(CO)]BArF$ was isolated in 75% yield. ^1H NMR (CD_2Cl_2, 400 MHz) - 1.10 (9H, s,$(–CH_3)_3$), 3.08 (2H, s,$–CH_2–$), 4.1-4.6 (4H, dd, $–CH_2–N–CH_2–$), 7.4-7.5 (2H, d), 7.7-7.8 (2H, t), 7.9-8.1 (4H, q), 8.3-8.4 (2H, d), 8.4-8.5 (2H, d); IR (MeTHF) 2094 cm^{-1} (C-O); MS (FAB^+) m/z 432.1, Calcd for $C_{25}H_{27}CuN_3$ 432.15; Anal. Calcd for $[(nQ_2)Cu^I(CO)](B(C_6F_5)_4)$ ($C_{50}H_{27}BCuF_{20}N_3O$): C, 52.67; H, 2.39; N, 3.69%. Found: C, 51.86; H, 3.20; N, 3.80%.

Synthesis of $[(nQ_2)Cu^I(CO)]PF_6$

Compound $[(nQ_2)Cu^I(CO)]PF_6$ was synthesized for crystallization purposes. The procedure used for the synthesis was the same used for $[(nQ_2)Cu^I(CO)]BArF$ with the difference that it was performed at -40 ^0C and that distilled/deoxygenated Et_2O was used for precipitation, instead of pentane.

Synthesis of $[(BzQ_2)Cu^I(CO)]BArF$ (2)

$[(BzQ_2)Cu^I(CO)]BArF$ was synthesized using the same experimental procedure used for $[(nQ_2)Cu^I(CO)]BArF$ using, instead, $[(BzQ_2)Cu^I(CH_3CN)]BArF$ (0.1 g, 0.085 mmol) as the starting compound. Compound $[(BzQ_2)Cu^I(CO)]BArF$ was isolated in 75% yield. ^1H NMR (CD_2Cl_2, 400 MHz) - 4.0-4.2 (2H, d,$–CH_2$), 4.2-4.3 (2H, s, $–CH_2$), 4.5-4.6 (2H, d, $–CH_2$), 7.3-7.4 (3H), 7.4-7.5 (4H, t), 7.7-7.8 (2H, t), 7.9-8.1 (4H), 8.3-8.35 (2H,d), 8.35-8.45 (2H, d); IR (MeTHF) 2092 cm^{-1} (C-O); MS (FAB^+) m/z - 452.1, Calcd for $C_{27}H_{23}CuN_3$ 452.1.

Synthesis of $[(BzDMM)Cu^I(CO)]BArF$

The syntheses of the $[(BzDMM)Cu^I(CO)]BArF$ compound was performed using the same procedure adopted for the synthesis of $[(BzDMM)Cu^I(CH_3CN)]BArF$ except for the

fact that the reaction was conducted in a CO-saturated atmosphere and both THF and pentane solvents were also saturated with CO gas prior contact with the copper(I) compounds. Compound [(BzDMM)Cu^{I}(CO)]BArF was isolated in 60% yield. Crystals were obtained by vapor diffusion of pentane into a THF solution of the compound. ^{1}H NMR (CD_2Cl_2, 400 MHz) - 1.10 (9H, s,$(–CH_3)_3$), 3.08 (2H, s,$–CH_2–$), 4.1-4.6 (4H, dd, $–CH_2–N–CH_2–$), 7.4-7.5 (2H, d), 7.7-7.8 (2H, t), 7.9-8.1 (4H, q), 8.3-8.4 (2H, d), 8.4-8.5 (2H, d); IR (THF) 2087 cm^{-1} (C-O).

Synthesis of [(nQ_2)Cu^{I}]BArF

This compound was prepared using a modification of a synthetic procedure previously used to synthesize [(BzQ_2)Cu^{I}]ClO_4.[17] Carbon monoxide was removed from [(nQ_2)Cu^{I}(CO)]BArF dissolving it in a methanol solution, first, and heating it at 70 ^{0}C for 30 min using on an oil bath. The solvent was then removed in vacuo whereupon a yellow oily material of [(nQ_2)Cu^{I}]BArF was isolated in a 95% yield. The sample has been made re-precipitate from dichloromethane with pentane, obtaining a yellow solid. ^{1}H NMR (CD_2Cl_2, 400 MHz) - 0.7-0.9 (9H, s,$(–CH_3)_3$), 2.3-3.9 (2H, d,$–CH_2–$), 4.0-5.0 (4H, s, $–CH_2–N–CH_2–$), 7.4-7.9 (4H, m), 8.0-8.3 (4H, s), 8.5-8.7 (4H, d); HRMS (FAB^{+}): m/z 432.14953, Calcd for $C_{25}H_{27}CuN_3$ 432.15010.

Synthesis of [(BzQ_2)Cu^{I}]BArF

This compound was prepared using the same synthetic procedure used to synthesize [(nQ_2)Cu^{I}]BArF. The yellow oily material of [(BzQ_2)Cu^{I}]BArF was isolated in a 95% yield. This sample was also made re-precipitate from dichloromethane with pentane, obtaining a yellow solid. ^{1}H NMR (CD_2Cl_2, 400 MHz) - 3.8-4.2 (2H,b s,$–CH_2$), 4.2-5.0 (4H,b s, $–CH_2–$

N–CH_2–), 6.9-7.1 (3H), 7.15-7.7 (4H, t), 7.7-7.9 (2H, t), 7.9-8.2 (2H), 8.1-8.2 (2H,d), 8.3-8.7 (4H, dd); HRMS (FAB^+): m/z 452.11825, calcd for $C_{27}H_{23}CuN_3$ 452.11880.

Synthesis of $[\{(nQ_2)Cu^{II}(OH)\}_2](ClO_4)_2$

Synthesis of the bis-μ-hydroxo compound $[\{(nQ_2)Cu^{II}(OH)\}_2](ClO_4)_2$ was performed using the procedure previously adopted by Itoh and co-workers for $[\{(BzQ_2)Cu^{II}(OH)_2\}_2](ClO_4)_2$.[17] The yield was 70% and crystals were obtained by vapor diffusion of ether into an acetone solution of the compound. MS (FAB^+) m/z 432.1, Calcd for $C_{25}H_{27}CuN_3$ 432.15.

Synthesis of $[\{(BzDMM)Cu^{II}(OH)\}_2](PF_6)_2$ and $[\{(BzDMM)Cu^{II}(Cl)\}_2](PF_6)_2$

Both compounds were synthesized, accidentally, during one the early attempts for the synthesis of the compound $[(BzDMM)Cu^{I}(CH_3CN)]PF_6$. Crystals of $[\{(BzDMM)Cu^{II}(OH)\}_2](PF_6)_2$ were obtained by diffusion of ether into THF solutions of the complex while crystals of $[\{(BzDMM)Cu^{II}(Cl)\}_2](PF_6)_2$ were obtained by vapor diffusion of either into dichloromethane (DCM) solutions of the complex, instead.

3. Results and Discussion

In this study, the tridentate ligand-copper-carbonyl compounds $[(nQ_2)Cu^{I}(CO)]^+$ (**1**) and $[(BzQ_2)Cu^{I}(CO)]^+$ (**2**) (Chart 2) were employed in laser experiments where CO was photo-released upon excitation of **1** and **2** in the presence of either $CO_{(g)}$ or $O_{2(g)}/CO_{(g)}$ mixtures in acetone solvent. Results were compared with those previously determined for the tridentate complex $[(BzPy_1)Cu^{I}(CO)]^+$ ($Bzpy_1$ = ^{D}L with D = Bz, Chart 1) and for the series of

tetradentate copper complexes $[(^{D}L)Cu^{I}(CO)]^{+}$ (see Chart 1 for ligand structures). Compound $[(nQ_2)Cu^{I}]^{+}$ was, instead, used to investigate the Cu/O_2 reactivity through benchtop experiments. In addition, crystal structures of the new complexes $[(nQ_2)Cu^{I}(CO)]^{+}$ (**1**), $[(nQ_2)Cu^{I}(CH_3CN)]^{+}$, $[\{(nQ_2)Cu^{II}(OH)\}_2]^{2+}$, and also $[(BzDMM)Cu^{I}(CO)]BArF$, $[\{(BzDMM)Cu^{II}(OH)\}_2](PF_6)_2$, $[\{(BzDMM)Cu^{II}(Cl)\}_2](PF_6)_2$ (see BzDMM ligand structure in Chart 1) were determined and were compared with those of analogous compounds, previously determined.

Chart 2. Ligand-copper(I) carbonyl complexes examined in this work for photolysis experiments.

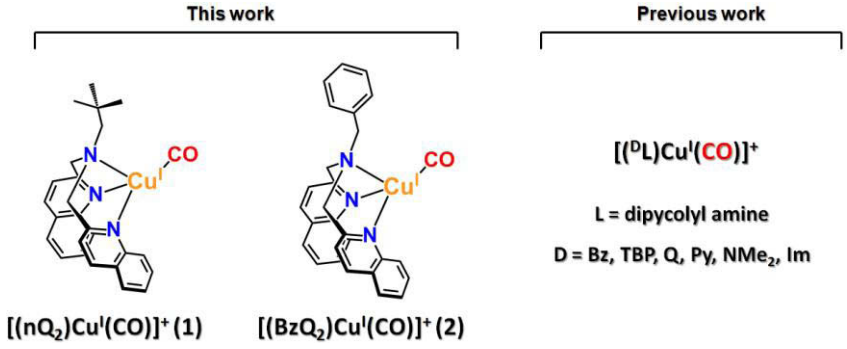

3.1 X-Ray Crystallography of $[(nQ_2)Cu^{I}(CH_3CN)]PF_6$, $[(nQ_2)Cu^{I}(CO)]PF_6$, $[(BzDMM)Cu^{I}(CO)]BArF$, $[\{(BzDMM)Cu^{II}(OH)\}_2](PF_6)_2$, $[\{(BzDMM)Cu^{II}(Cl)\}_2](PF_6)_2$, and $[\{(nQ_2)Cu^{II}(OH)\}_2](ClO_4)_2$

ORTEP diagrams of the crystal structures resolved in this work for the complexes derived from the nQ_2 ligand, $[(nQ_2)Cu^{I}(CH_3CN)]PF_6$ (A), $[(nQ_2)Cu^{I}(CO)]PF_6$ (B), and

[{(nQ_2)Cu^{II}(OH)}$_2$](ClO_4)$_2$ (C), are shown in Figure 1. The diagrams in Figure 2, instead, show the structures resolved for complexes supported by the BzDMM ligand. Selected bond lengths and angles are indicated in Table 1 for the acetonitrile complex [(nQ_2)Cu^{I}(CH_3CN)]PF_6, in Table 2 for the carbon monoxide complexes [(nQ_2)Cu^{I}(CO)]PF_6 and [(BzDMM)Cu^{I}(CO)]BArF, and in Table 3 for the dicopper(II) bis-μ-hydroxo complexes [{(nQ_2)Cu^{II}(OH)}$_2$](ClO_4)$_2$ and [{(BzDMM)Cu^{II}(OH)}$_2$](PF_6)$_2$, along with the dicopper(II) bis-μ-chloride complex [{(BzDMM)Cu^{II}(Cl)}$_2$](PF_6)$_2$.

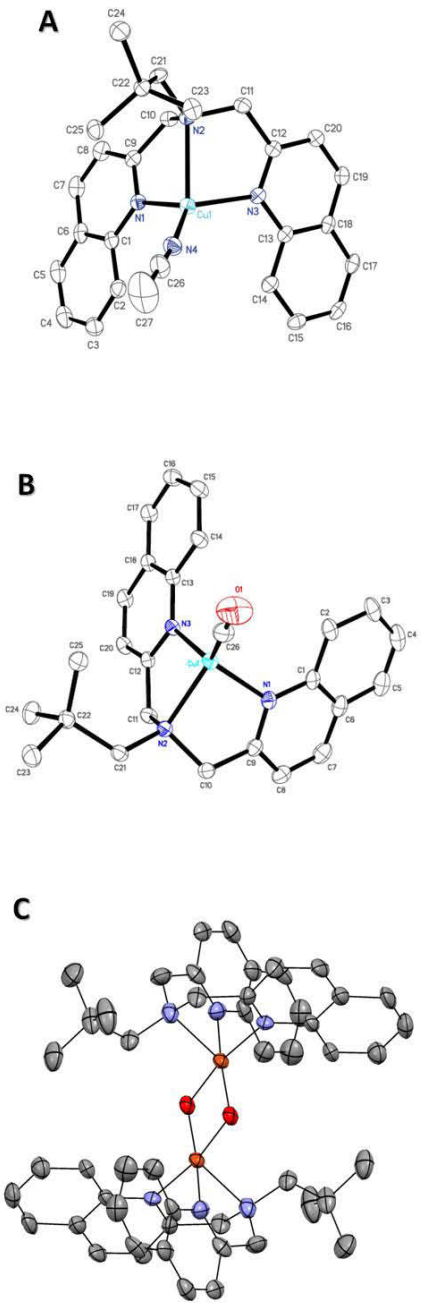

Figure 1. ORTEP diagrams of (A) $[(nQ_2)Cu^{I}(CH_3CN)]PF_6$, (B) $[(nQ_2)Cu^{I}(CO)]PF_6$, and (C) $[\{(nQ_2)Cu^{II}(OH)\}_2](ClO_4)_2$. Both hydrogen atoms and the counterions have been omitted for clarity.

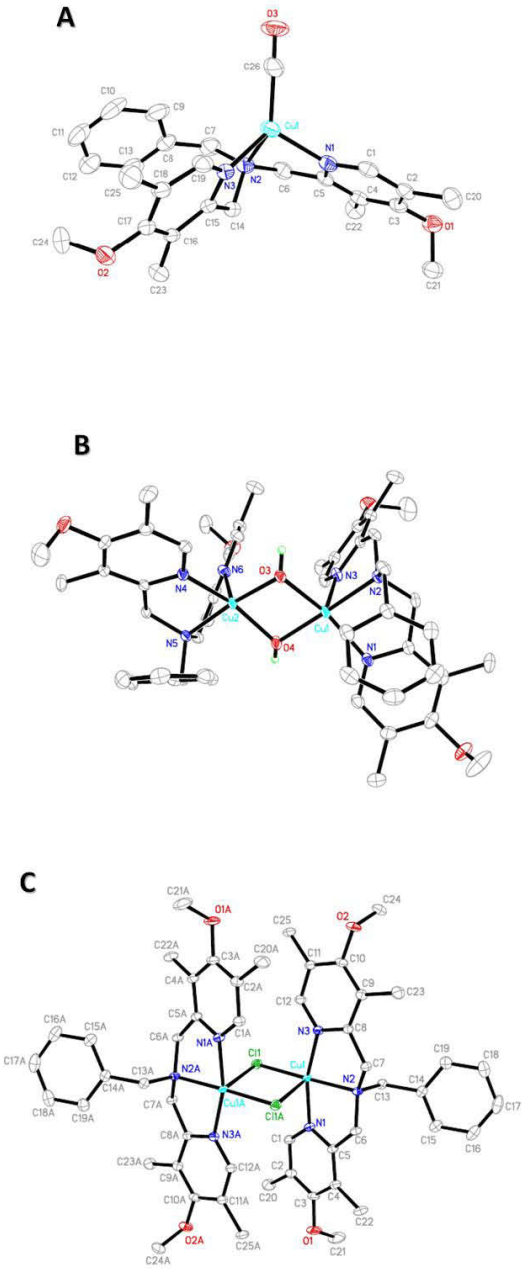

Figure 2. ORTEP diagrams of (A) [(BzDMM)Cu^{I}(CO)]BArF, (B) [{(BzDMM)Cu^{II}(OH)}$_2$](PF$_6$)$_2$, and (C) [{(BzDMM)Cu^{II}(Cl)}$_2$](PF$_6$)$_2$. Both hydrogen atoms (except for the OH groups in Figure 2B) and the counterions have been omitted for clarity.

Copper(I) is tetracoordinated in both $[(nQ_2)Cu^I(CH_3CN)]^+$ and $[(nQ_2)Cu^I(CO)]^+$ where two nitrogens from the quinolyl groups, one nitrogen from the alkylamino group, and one nitrogen atom from $-CH_3CN$ (in $[(nQ_2)Cu^I(CH_3CN)]^+$) or a carbon atom from CO (in $[(nQ_2)Cu^I(CO)]^+$) are the atom donors. The angles $N_{quinoline}$-Cu-$N_{alkylamine}$ of ~ 81^0C found here ('$N_{Q\ or\ P}$-Cu-N_{alk}' in Tables 1 and 2) are smaller than those typically found in the N-donor tetracoordinate analogue compounds previously characterized (~95^0C)[24-31] and their value is, instead, in line with that found for the tridentate $[(BzPy_1)Cu^I(CO)]^+$ previously reported (Chart 1, $Bzpy_1$ = ^{D}L with D = Bz, and Table 1).[14]

Table 1. Selected bond lengths and bond angles for the copper(I)-acetonitrile species $[(nQ_2)Cu^I(CH_3CN)]^+$ and $[(BzPY_1)Cu^I(CH_3CN)]^+$.

BOND LENGTHS (Å)	$[(BzPy_1)Cu(CH_3CN)]^{+,\ a}$	$[(nQ_2)Cu(CH_3CN)]^+$
Cu-N_{CN}	1.900(5)	1.915(2)
Cu-N_{alk}	2.309(5)	2.319(1)
Cu-$N_{Q\ or\ P}$ (avg)	2.016(4)	2.025(1)
BOND ANGLES (°)		
N_{CN}-Cu-$N_{Q\ or\ P}$ (avg)	116.0(2)	122.85(6)
N_{CN}-Cu-N_{alk}	133.3(2)	127.90(6)
$N_{Q\ or\ P}$-Cu-N_{alk} (avg)	79.4(2)	80.64(5)
$N_{Q\ or\ P}$-Cu-$N_{Q\ or\ P}$	123.8(2)	108.53(6)

[a] Crystallized as BArF (=$[B(C_6F_5)_4]^-$) salt.[32]

The Cu^I-N(≡C) bond length in $[(nQ_2)Cu^I(CH_3CN)]^+$ (1.915(2) Å) is, although by a small extent, greater than that found in the previously characterized tridentate copper compound $[(BzPy_1)Cu^I(CH_3CN)]^+$ (1.900(5) Å)[32] suggesting a stronger bond in the latter case. It has

been previously demonstrated that the presence of a substituent in the 6th carbon position of the pyridyl ring causes a steric repulsion between the substituent and the copper ion.[33,34] Consequently, the greater Cu^{I}-N(=C) bond length found in the crystal structure of $[(nQ_2)Cu^{I}(CH_3CN)]^+$ might be caused by this effect, possibly pushing the acetonitrile ligand away from the copper in $[(nQ_2)Cu^{I}(CH_3CN)]^+$. This is supported by the fact that longer Cu-N bonds (Cu-N_{CN}, Cu-N_{Alk}, and Cu-$N_{Q\ or\ P}$ in Table 1) are found for the latter complex compared to those found in $[(BzPy_1)Cu^{I}(CH_3CN)]^+$.

Table 2. Selected bond lengths and bond angles for the copper(I)-CO species $[(nQ_2)Cu^{I}(CO)]^+$, $[(BzQ_2)Cu^{I}(CO)]^+$, $[(BzDMM)Cu^{I}(CO)]^+$, and $[(BzPY_1)Cu^{I}(CO)]^+$.

BOND LENGTHS (Å)	$[(nQ_2)Cu(CO)]^+$	$[(BzQ_2)Cu(CO)]^{+\,a}$	$[(BzDMM)Cu(CO)]^{+\,b}$	$[(BzPy_1)Cu(CO)]^{+\,b}$
Cu-C	1.795(2)	1.797(4)	1.805(5)	1.815(2)
C-O	1.118(3)	1.121(4)	1.126(7)	1.123(2)
Cu-N_{alk}	2.134(1)	2.109(3)	2.131(3)	2.159(1)
Cu-$N_{Q\ or\ P}$ (avg)	2.047(2)	2.040(3)	2.041(2)	2.048(1)
BOND ANGLES (°)				
C-Cu-$N_{Q\ or\ P}$ (avg)	128.21(7)	124.8(1)	121.8(2)	121.96(7)
C-Cu-N_{alk}	129.67(7)	122.9(1)	126.0(2)	129.94(7)
$N_{Q\ or\ P}$-Cu-N_{alk} (avg)	82.91(5)	83.2(1)	81.6(1)	80.81(6)
$N_{Q\ or\ P}$-Cu-$N_{Q\ or\ P}$	101.33(5)	104.2(1)	111.0(1)	108.95(6)

[a] Crystallized as ClO_4^- salt[17] [b] Crystallized as BArF salt (=$[B(C_6F_5)_4]^-$).[32]

The Cu^{I}-C(O) bond length in $[(nQ_2)Cu^{I}(CO)]^+$ is, essentially, the same with that found for $[(BzQ_2)Cu^{I}(CO)]^+$ (1.795(2) Å vs. 1.797(4) Å). This suggests a similar bond strength between the copper and the C(-O) in the two compounds while a slightly longer Cu^{I}-C(O) bond in

$[(BzDMM)Cu^{I}(CO)]^{+}$ (1.805(5) Å) would suggest a weaker bond for this compound. The C-O bond length found for the two quinolyl-based compounds is also very similar to one another. This shows that the extent of electronic π back-donation from the copper to the CO fragment is about the same in the two cases. A quite big difference between the structures of $[(nQ_2)Cu^{I}(CO)]^{+}$ and $[(BzQ_2)Cu^{I}(CO)]^{+}$ is, instead, the presence of what seems to be an intra-molecular electronic π-π interaction between the phenyl group of BzQ_2 and one the two quinolyls in $[(BzQ_2)Cu^{I}(CO)]^{+}$. This seems to bring the alkyl nitrogen of the ligand BzQ_2 closer to the copper ion. On the basis of these results, we propose that the electron-donating capability of nQ_2 and BzQ_2 is comparable to one another. The C-O bond in both $[(nQ_2)Cu^{I}(CO)]^{+}$ (1.118(3) Å) and $[(BzQ_2)Cu^{I}(CO)]^{+}$ (1.121(4) Å) is slightly shorter than that found for $[(BzPy_1)Cu^{I}(CO)]^{+}$ (1.123(2) Å) and $[(BzDMM)Cu^{I}(CO)]^{+}$ (1.126(7) Å) which is indicative of a more pronounced electron-withdrawing ability of the quinolyl functional groups present in nQ_2 and BzQ_2 *versus* the pyridyl donors present in the $BzPy_1$ and BzDMM ligands.

Crystal structures also show that Cu^{I}-C(O), Cu-$N_{alkylamine}$ (Cu-N_{alk} in Table 2), and Cu-$N_{Q\ or\ P}$ bonds are all shorter in both $[(nQ_2)Cu^{I}(CO)]^{+}$ and $[(BzQ_2)Cu^{I}(CO)]^{+}$ compared to those found in $[(BzPY_1)Cu^{I}(CO)]^{+}$ indicating that the compounds bearing bis-quinolyl ligands (**1** and **2**) have more 'compact' structures than $[(BzPY_1)Cu^{I}(CO)]^{+}$.

The structure of two new dicopper(II) bis-μ-hydroxo compounds, $[\{(nQ_2)Cu^{II}(OH)\}_2](ClO_4)_2$ (Figure 1C) and $[\{(BzDMM)Cu^{II}(OH)\}_2](PF_6)_2$ (Figure 2B), are also reported in this work and are compared with the previously determined structure of the analog compound $[\{(BzQ_2)Cu^{II}(OH)\}_2](ClO_4)_2$ (Table 3).[17] Assuming that electron-donating properties of the two ligands, nQ_2 and BzQ_2, are comparable to one another (*vide infra*), th longer Cu-O bond and O···O distances, and shorter Cu···Cu distance found for the

$N_3CuO2CuN_3$ moiety in $[\{(BzQ_2)Cu^{II}(OH)\}_2]^{2+}$ *versus* $[\{(nQ_2)Cu^{II}(OH)\}_2]^{2+}$ might suggest that steric effects account for these differences. An inverted trend for the copper-alkyl nitrogen vs. copper-quinoline nitrogen bond lengths found within the complexes supported by ligands having a dangling benzyl arm, like in $[\{(BzQ_2)Cu^{II}(OH)\}_2](ClO_4)_2$ and in $[\{(BzDMM)Cu^{II}(OH)\}_2](PF_6)_2$ has also been observed here ($Cu\text{-}N_{alk}$ vs. $Cu\text{-}N_Q$ in Table 3). In fact, copper-alkyl nitrogen bonds are, typically, longer than copper-quinolyl (or pyridyl-) nitrogen bonds in these kinds of complexes. This trend is, instead, inverted for $[\{(BzQ_2)Cu^{II}(OH)\}_2]^{2+}$ and somewhat for $[\{(BzDMM)Cu^{II}(OH)\}_2]^{2+}$. We suggest that a steric distortion of the $N_3CuO_2CuN_3$ moiety is induced by the ligands BzQ_2 and BzDMM in $[\{(BzQ_2)Cu^{II}(OH)\}_2]^{2+}$ and $[\{(BzDMM)Cu^{II}(OH)\}_2]^{2+}$. Interestingly, even though the benzyl group in both BzQ_2 and BzDMM is separated from the alkyl nitrogen by only one methylene group, it seems that π-π stacking interactions can still take place between the phenyl portion of the benzyl group and one of the two quinolyl (or pyridyl-) groups in each of the two BzQ_2 (or BzDMM) ligands in the dicopper(II) bis-μ-hydroxo complexes $[\{(BzQ_2)Cu^{II}(OH)\}_2]^{2+}$ and $[\{(BzDMM)Cu^{II}(OH)\}_2]^{2+}$. These intra-molecular interactions are not present in $[\{(nQ_2)Cu^{II}(OH)\}_2]^{2+}$ because of the aliphatic nature of the nQ_2 dangling arm (neopentyl). The π-π interaction between the benzyl group and one of the two quinolines rings in $[\{(BzQ_2)Cu^{II}(OH)\}_2]^{2+}$ 'stretches' one of the two copper-quinoline nitrogen bonds ($Cu\text{-}N_Q$) from 2.328 Å in $[\{(nQ_2)Cu^{II}(OH)\}_2]^{2+}$ to 2.370 Å in $[\{(BzQ_2)Cu^{II}(OH)\}_2]^{2+}$ moving the one quinolyl group that is <u>not</u> involved in the π-π stacking away from the copper ion in $[\{(BzQ_2)Cu^{II}(OH)\}_2]^{2+}$ and 'compressing', instead, the copper-alkyl nitrogen bond ($Cu\text{-}N_{Alk}$) that is considerably shorter in $[\{(BzQ_2)Cu^{II}(OH)\}_2]^{2+}$ compared with that found in $[\{(nQ_2)Cu^{II}(OH)\}_2]^{2+}$ (2.036(9) Å vs. 2.328(7) Å, respectively). Since the electron-donating capability of the alkyl nitrogen is greater than that of the quinolyl nitrogen, the net effect is

electron density moving from the ligand to the copper making the metal ion less positive in $[\{(BzQ_2)Cu^{II}(OH)\}_2]^{2+}$. This, in turn, weakens the electrostatic interaction between copper and the oxo ligands making the Cu-O bond length slightly longer in $[\{(BzQ_2)Cu^{II}(OH)\}_2]^{2+}$ compared with that found in $[\{(nQ_2)Cu^{II}(OH)\}_2]^{2+}$ (1.942(8) Å vs. 1.931(4) Å). The greater O···O distance found in $[\{(BzQ_2)Cu^{II}(OH)\}_2]^{2+}$ is also reflected in a wider O-Cu-O and a narrower Cu-O-Cu angles in the latter complex in comparison with those found in $[\{(nQ_2)Cu^{II}(OH)\}_2]^{2+}$.

Table 3. Comparison of selected bond lengths and bond angles between the bis-μ-hydroxo dicopper(II) compounds $[\{(nQ_2)Cu^{II}(OH)\}_2](ClO_4)_2$, $[\{(BzDMM)Cu^{II}(OH)\}_2](PF_6)_2$, $[\{(BzQ_2)Cu^{II}(OH)\}_2](ClO_4)_2$, and the bis-$\mu$-chloride dicopper(II) complex $[\{(BzDMM)Cu^{II}(Cl)\}_2](PF_6)_2$.

BOND LENGTHS (Å)	$[\{(nQ_2)Cu^{II}(OH)_2\}_2]^{2+}$	$[\{(BzDMM)Cu^{II}(OH)_2\}_2]^{2+}$	$[\{(BzQ_2)Cu^{II}(OH)_2\}_2]^{2+}$[a]	$[\{(BzDMM)Cu^{II}(Cl)_2\}_2]^{2+}$
Cu-O or Cu-Cl (avg)	1.931(4)	1.940(1)	1.942(8)	2.5078(5)
O···O or Cl···Cl	2.426	2.501	2.464	3.777
Cu···Cu	3.004	2.948	3.003	3.344
Cu-N_{alk}	2.328(7)	2.040(2)	2.036(9)	2.036(1)
Cu-$N_{Q\ or\ P}$ (avg)	2.027(5)	2.113(2)	2.20(1)	1.973(1)
BOND ANGLES (°)				
O(Cl)-Cu-O(Cl)	77.84(2)	79.98(6)	78.8(2)	97.12(1)
O(Cl)-Cu-N_{alk}	109.33(2)	177.90(6)	133.2(2)	89.38(4)
O(Cl)-Cu-$N_{Q\ or\ P}$ (avg)	131.33(2)	100.74(6)	113.3(2)	97.17()
Cu-O(Cl)-Cu	102.2(2)	99.67(7)	101.2(2)	82.88(4)
$N_{Q\ or\ P}$-Cu-N_{alk} (avg)	80.82(2)	80.42(6)	79.5(2)	82.58(6)
$N_{Q\ or\ P}$-Cu-$N_{Q\ or\ P}$	89.94(2)	107.47(6)	107.7(2)	164.73(6)

[a] From Itoh and co-workers.[17]

Another interesting aspect concerning the $[\{(nQ_2)Cu^{II}(OH)\}_2](ClO_4)_2$ crystal resolved here is a quite unique super-structure found where the crystal packing of molecules (cations and anions) are such that channels form (Figure 3). The details of such are not given, but could be derived from the X-ray structural information (CIF file). It may be of future interest to investigate the possible absorption and/or reactivity properties towards substrates and small molecules of such crystals.

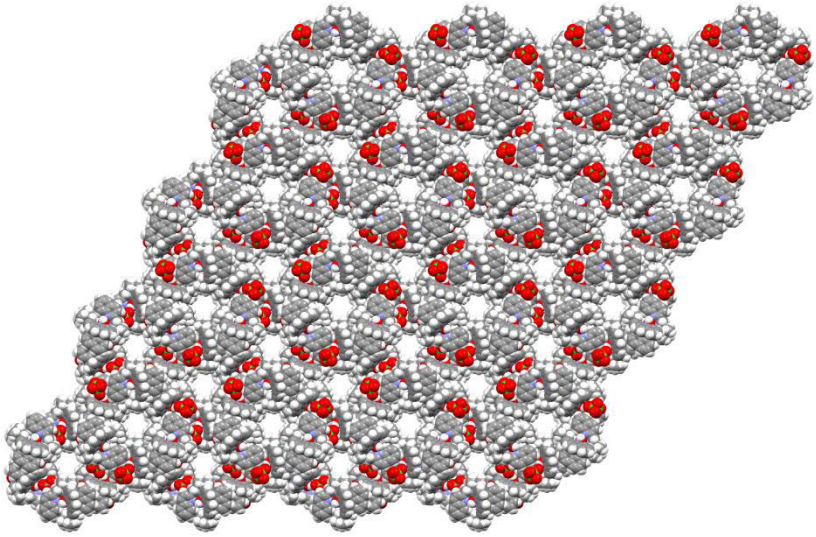

Figure 3. Super-molecular structure found for $[\{(nQ_2)Cu^{II}(OH)\}_2](ClO_4)_2$ crystals.

3.2 Infrared Spectroscopy (ν_{CO} in MeTHF and THF Solvents)

Infrared spectroscopy was performed for compounds **1**, **2**, and $[(BzDMM)Cu^{I}(CO)]^+$ to investigate possible effects of the different dangling arm (neopentyl vs. benzyl) for the quinolyl-based ligands on the electron-donating properties of nQ_2 and BzQ_2. CO stretching frequencies found in synthetic copper(I)-carbonyl compounds typically fall in the range 2035-2137 cm^{-1}.[29,35-41] The values found in this work for **1**, **2**, and $[(BzDMM)Cu^{I}(CO)]^+$

(Table 4) are consistent with these findings and are also in line with that previously determined for the N-donor tridentate complex $[(BzPY_1)Cu^I(CO)]^+$.[14]

Table 4. CO stretching frequences (ν_{CO}) for **1** and **2** in MeTHF, and for $[(BzDMM)Cu^I(CO)]^+$ and $[(BzPY_1)Cu^I(CO)]^+$ in THF.

Compound	ν_{CO} (cm^{-1})
$[(nQ_2)Cu^I(CO)]^+$	2094
$[(BzQ_2)Cu^I(CO)]^+$	2092
$[(BzDMM)Cu^I(CO)]^+$	2087[a]
$[(BzPY1)Cu^I(CO)]^+$	2093[a,b]

[a] Determined in THF [b] From a previous work.[14]

The presence of a different dangling arm in **1** compared to **2** (neopentyl vs. benzyl) does not seem to have a big effect on the electron density donated from the ligand to the copper ion in solution with an observed frequency difference of just 2 cm^{-1} (2094 cm^{-1} vs. 2092 cm^{-1}). A noticeable effect of the ligand environment seems to occur for the complex $[(BzDMM)Cu^I(CO)]^+$, instead, where a lower value of the CO stretching frequency may indicate a greater electron-donating ability of BzDMM compared to nQ_2, BzQ_2, and $BzPY_1$ inducing a stronger π-back donation from the ligand moiety to the copper(I) ion (2087 cm^{-1} vs. 2092-2094 cm^{-1}). Values of ν_{CO} determined for copper-containing proteins where the metal is coordinated to three imidazole ligands are typically 20-40 cm^{-1} lower than those found for these synthetic analogues.[35,38] That illustrates the remarkable electron-donating ability of the imidazole ligand compared with pyridyl and quinolyl functional groups.

3.3 CO Binding to Copper(I) in Acetone Solvent: Laser Experiments

Laser experiments where the copper(I)-carbonyl complex $[(BzDMM)Cu^{I}(CO)]^{+}$ was photoexcited with UV light (355 nm) were conducted in MeTHF. Although difference spectra consistent with formation of $[(BzDMM)Cu^{I}(CH_3CN)]^{+}$ (λ_{max} = 315 nm, ε = 3600 M^{-1} cm^{-1}) from $[(BzDMM)Cu^{I}(CO)]^{+}$ appeared in the region ~ 380-430 nm (Figure 4), low energy difference spectra also appeared, (> 550 nm, Figure 4) suggesting formation of additional species upon laser excitation of $[(BzDMM)Cu^{I}(CO)]^{+}$. In addition, decrease of the initial difference absorption signal upon laser excitation suggested that formation of the additional products occurs in a non-reversible fashion, namely, the starting compound $[(BzDMM)Cu^{I}(CO)]^{+}$ is not reversibly re-formed after each laser pulse. Thus, further studies on the photochemistry of this system were not conducted.

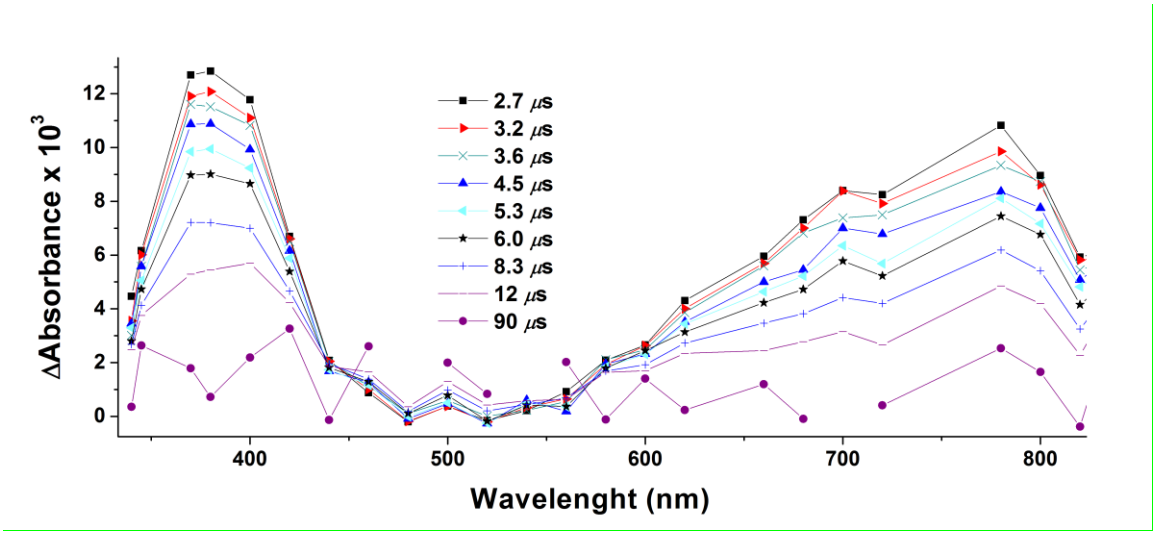

Figure 4. Transient absorption difference spectra collected at the indicated delay times after 355 nm laser excitation (8 mJ/pulse, 8-10 ns fwhm) of $[(BzDMM)Cu^{I}(CO)]^{+}$ in MeTHF.

Spectra of the complexes [(nQ_2)Cu^I]BArF and [(BzQ_2)Cu^I]BArF dissolved in acetone solvent (Figures 5A and 6A, in black) and spectra collected after bubbling CO gas through these copper(I) solutions (Figures 5A and 6A, in red) are presented in Figures 5A and 6A. Photo-release of carbon monoxide upon laser excitation of [(nQ_2)Cu^I(CO)]$^+$ (**1**) or [(BzQ_2)Cu^I(CO)]$^+$ (**2**) should also yield [(nQ_2)Cu^I]$^+$ or [(BzQ_2)Cu^I]$^+$ in acetone and the difference spectra shown in Figures 5B and 6B are expected to appear in such transient absorption experiments after photoexcitation of **1** or **2**.

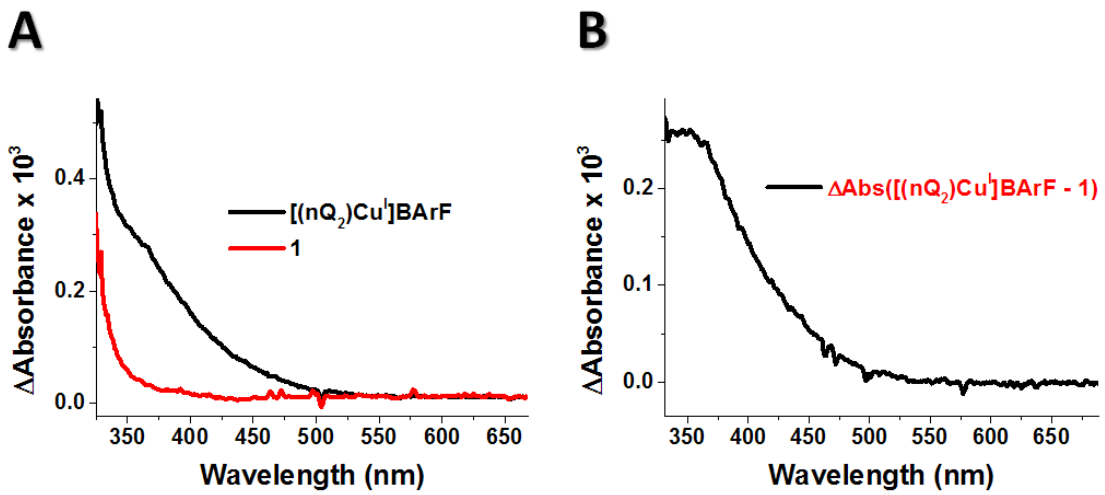

Figure 5. (A) Absorption spectrum collected before (black line) and after (red line) CO bubbling into a solution of [(nQ_2)Cu^I]BArF in acetone (150 μM) at room temperature. (B) Absorption difference spectrum (Abs([(nQ_2)Cu^I]BArF) - Abs(**1**)).

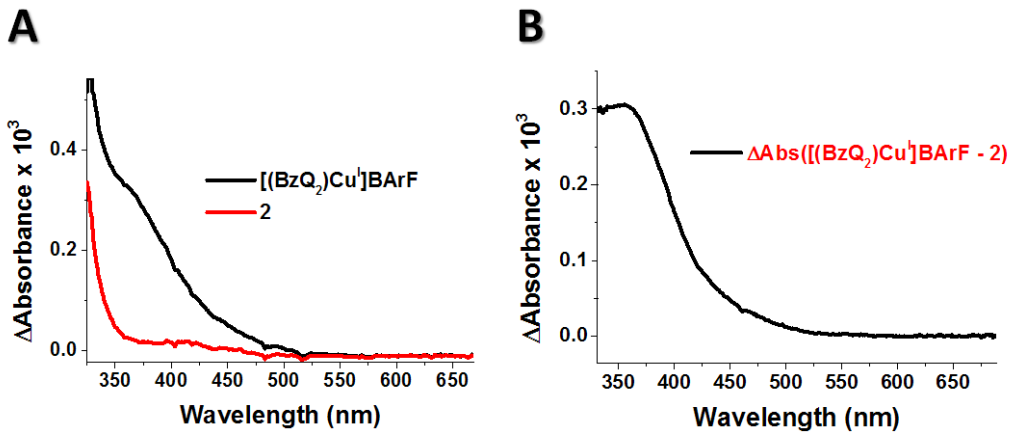

Figure 6. (A) Absorption spectrum collected before (black line) and after (red line) CO bubbling into a solution of $[(BzQ_2)Cu^I]BArF$ in acetone (10 μM) at room temperature. (B) Absorption difference spectrum (Abs($[(BzQ_2)Cu^I]BArF$) - Abs(**2**)).

Copper-carbon bond cleavage was induced in $[(nQ_2)Cu^I(CO)]^+$ (**1**) by irradiation with UV light (355 nm) at low temperature in acetone solvent. The peak at ~ 370 nm is consistent with the formation of either the species $[(nQ_2)Cu^I]^+$ or both the species $[(nQ_2)Cu^I]^+$ and $[(nQ_2)Cu^I(acetone)]^+$ after laser excitation of **1**. Transient absorption difference spectra observed at longer delay times were consistent with binding of CO to either $[(nQ_2)Cu^I]^+$ or $[(nQ_2)Cu^I(acetone)]^+$ (Figure 7A) yielding $[(nQ_2)Cu^I(CO)]^+$. This conclusion is supported by the observed [CO]-dependent monoexponential decay of the peak observed at ~ 370 nm over a microsecond time regime (Figure 7B).

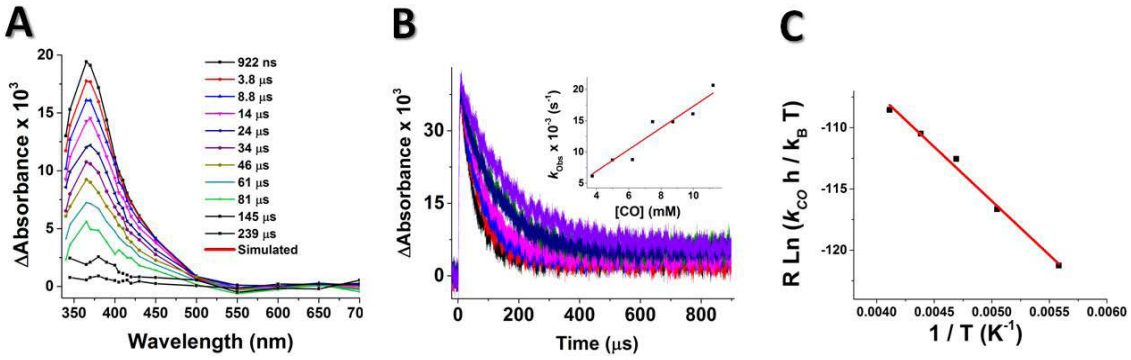

Figure 7. (A) Transient absorption difference spectra collected at the indicated delay times after 355 nm laser excitation (8 mJ/pulse, 8-10 ns fwhm) of **1** in acetone (B) Representative absorption changes monitored at 370 nm after photoexcitation of **1** at various ratios of $O_{2(g)}/N_{2(g)}$ at -94 ^{0}C in acetone. The inset shows the plots for the determination of k_{CO}. (C) Eyring plot for the determination of the activation parameters associated with the rate constants k_{CO}.

A similar behavior was observed after photoexcitation of $[(BzQ_2)Cu^I(CO)]^+$ (**2**) in acetone (see Figures 8 and 9).

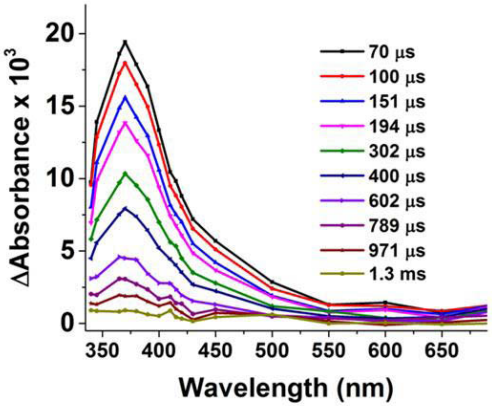

Figure 8. Transient absorption difference spectra collected at the indicated delay times after 355 nm laser excitation (8 mJ/pulse, 8-10 ns fwhm) of $[(BzQ_2)Cu^I(CO)]^+$ (**2**) in acetone at -94 ^{0}C.

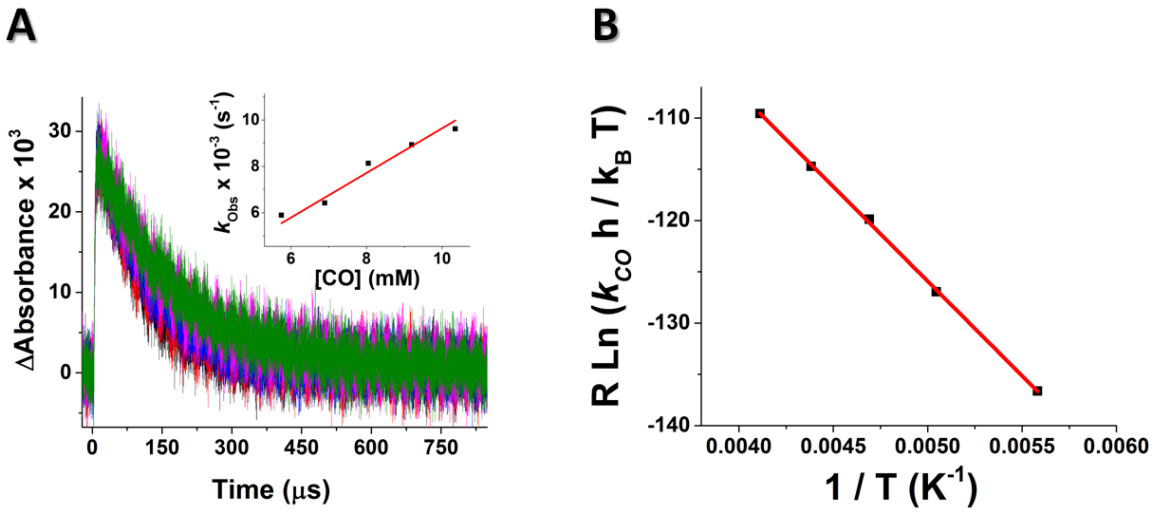

Figure 9. (A) Representative absorption changes monitored at 370 nm after photo-excitation of **2** at various ratios of $O_{2(g)}/N_{2(g)}$ at -74^{0}C in acetone. The inset shows the plots for the determination of k_{CO}. (B) Eyring plot for the determination of the activation parameters associated with the rate constants k_{CO}.

On the basis of the results observed here we propose the course of reactions in these systems to follow the pathways shown in Scheme 1 where a [CO]-dependent process occurs with CO binding to either $[LCu^{I}]^{+}$ or $[LCu^{I}(acetone)]^{+}$.

Scheme 1. Proposed mechanism for the CO photochemstry in acetone.

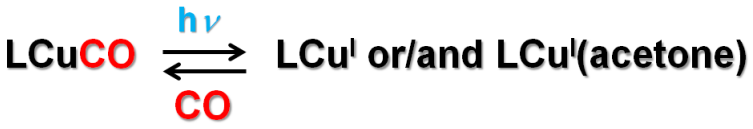

A study of the CO binding rate dependence was carried out in pseudo-first-order conditions (excess of CO) and second-order rate constants for CO coordination to copper(I) were determined for both **1** and **2** in the temperature range -30^{0}C /-94^{0}C. Eyring analyses were performed and activation parameters determined, revealing a relatively low activation enthalpy for the binding between CO and copper(I) (Figure 7C, and Table 5).

Table 5. Comparison of second-order rate constants and activation parameters for the binding of CO to $[(nQ_2)Cu^I(acetone)]^+$, $[(BzQ_2)Cu^I(acetone)]^+$, and previously studied compounds.

	k_{CO}[a]		$\Delta H^{\ddagger}$, [b]	$\Delta S^{\ddagger}$, [b]
Temp.	25^{0}C	-80^{0}C		
nQ_2	$(3.1 \pm 0.1)\cdot10^7$	$(2.9 \pm 0.1)\cdot10^6$	8.8 ± 0.4	-72 ± 2
BzQ_2	$(6.3 \pm 0.1)\cdot10^7$	$(7.2 \pm 0.1)\cdot10^5$	18.4 ± 0.2	-34 ± 1
$BzPy_1$[c]	$5.0\cdot10^8$	$2.8\cdot10^8$	0.7	-76
N4 ^{D}L[c]	$(0.97\text{-}2.8)\cdot10^9$	$(0.95\text{-}3.9)\cdot10^8$	5.7-9.1	-(59-35)

[a] k_{CO}, M^{-1} s^{-1} [b] ΔH, kJ mol^{-1} [b] ΔS, J K^{-1} mol^{-1} [c] Values determined in THF.[14] 'N4 ^{D}L' refers to the tetradentate ligands with D = Im, NMe_2, Py, Q, and TBP.[14]

The negative activation entropy found from laser flash-photolysis experiments for both compounds **1** and **2** is consistent with an associative process where CO coordinates a copper(I) that is weakly or not bound to a solvent molecule (acetone). The higher activation barrier (18.4 vs. 8.8 kJ mol^{-1}) and the less negative activation entropy (-34 vs. -72 kJ K^{-1} mol^{-1}) found for the binding of CO to $[(BzQ_2)Cu^I(acetone)]^+$ compared to $[(nQ_2)Cu^I(acetone)]^+$ are both consistent with a stronger Cu^I-O(acetone) bond in the compound bearing the BzQ_2 ligand. C-O stretching frequencies found for **1** and **2** in MeTHF solution suggest a just

slightly stronger electron-donating ability of nQ_2 vs. BzQ_2 (ν_{CO} = 2094 cm^{-1} for **1** vs. 2092 cm^{-1} for **2**) which might make the acetone a stronger ligand in $[(BzQ_2)Cu^{I}(acetone)]^{+}$. This interpretation would be in line with what menationed above for the activation parameters determined here. A comparison of the activation parameters obtained for the binding of CO to $[(nQ_2)Cu^{I}(acetone)]^{+}$ and $[(BzQ_2)Cu^{I}(acetone)]^{+}$ with those previously determined for $[(BzPy_1)Cu^{I}(acetone)]^{+}$ ($Bzpy_1$ = ^{D}L with D = Bz, Chart 1) and the tetradentate N-donor ligand-copper compound series $[(^{D}L)Cu^{I}(solv)]^{+}$ (see Chart 1 for ligand structures) in THF revealed a similar or greater activation enthalpy for the quinolyl-based tridentate compounds (Table 5). Although the comparison has being made between different systems in different solvents (acetone vs. THF) it could be, still, reasonable to expect such a trend on the basis of the more positive Cu(II)/Cu(I) redox potentials for complexes of tridentates vs. tetradentate N-donor ligands (3 vs. 4 for N4 ^{D}L) and because of the presence of quinolyl vs. pyridyl groups (nQ_2 and BzQ_2 vs. $BzPy_1$) that is likely more electron-withdrawing then for the case of complexes with quinolyl ligand donors.

Radiance dependence studies were also carried out for **1** in MeTHF. The absorption change was found to be linear with the laser fluence over a ~ 0-50 mJ cm^{-2} range indicating that a monophotonic process was involved in the CO photo-release from **1** (Figure 10).

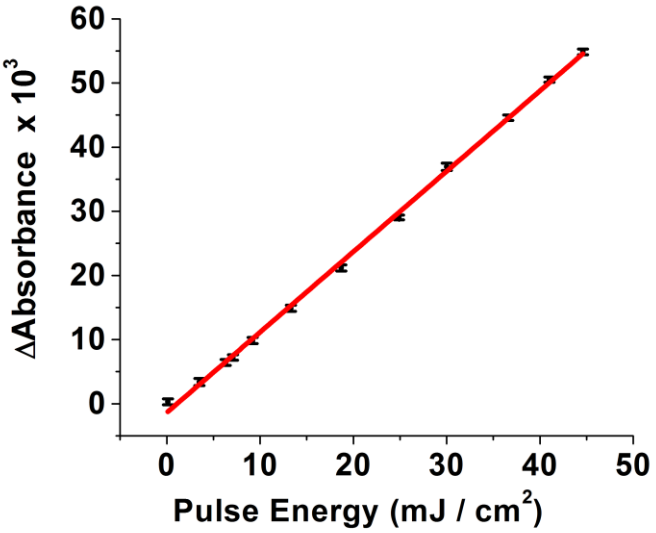

Figure 10. Magnitude of the absorption change as a function of the incident irradiance for **1**. Measurements collected at 370 nm, 0.5 μs delay time, -94^{0}C in MeTHF.

3.4 Dioxygen Binding to Copper(I) in Acetone Solvent: Benchtop Experiments

Tridentate N-donor copper(I) compounds supported by both pyridyl[18,19,42-44] and quinolyl[17] ligands have been shown to react with dioxygen at low temperature to give dicopper(III) bis-μ-oxo or/and dicopper(II) side-on peroxo 2:1 Cu/O_2 compounds.[17,18] In fact, in certain instances, substitution with a methyl group on the C-6 of the pyridyl groups leads to a decrease of the electron-donating ability of the nitrogen on the pyridyl groups towards the copper affording selective formation of dicopper(II) side-on peroxo instead of dicopper(III) bis-μ-oxo adducts.[44]

In addition to the interesting photochemistry observed for the complex $[(BzDMM)Cu^{I}(CO)]^{+}$ (see above), oxygenation of $[(BzDMM)Cu^{I}(CH_3CN)]^{+}$ at -80 ^{0}C in MeTHF also resulted in the formation of an intermediate. The spectrum showing an absorption maximum at 390 nm (Figure 11) suggests a dicopper(III) bis-μ-oxo species to be

formed. The presence of a dicopper(II) side-on peroxo moiety cannot be excluded *a priori*. However, dicopper(II) side-on peroxo complexes usually possess a strong absorption (λ_{max}) at ~360-365 nm, instead. On the other hand, based on the initial concentration of $[(BzDMM)Cu^{I}(CH_3CN)]^{+}$ (209 μM) and assuming a 100% conversion of $[(BzDMM)Cu^{I}(CH_3CN)]^{+}$ to the oxygenated intermediate, an extinction coefficient of $\varepsilon_{390\ nm}$ = 9700 M^{-1} cm^{-1} has been determined. This value is very similar with that estimated for the dicopper(III) bis-μ-oxo complex $[\{(BzPy_1)Cu^{III}(O)\}_2]^{2+}$ in THF ($\varepsilon_{390\ nm}$ = 8000 M^{-1} cm^{-1}).[32] This is in favor of the hypothesis of the formation of the bis-μ-oxo complex $[\{(BzDMM)Cu^{III}(O)\}_2]^{2+}$ upon the addition of dioxygen to $[(BzDMM)Cu^{I}(CH_3CN)]^{+}$ performed here.

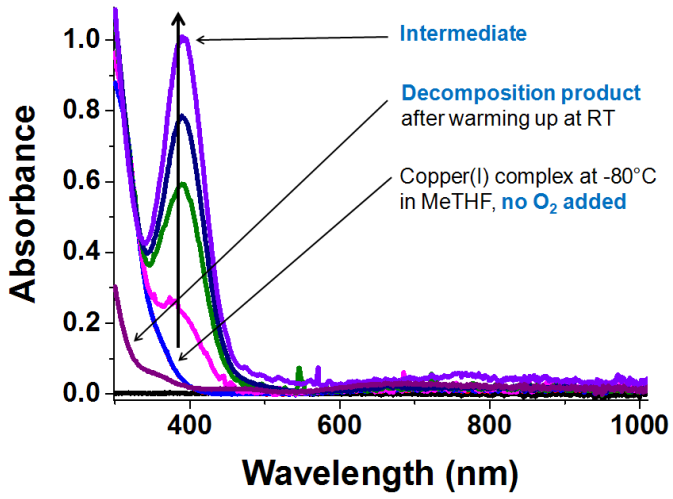

Figure 11. Absorption spectral change after introduction of O_2 into a MeTHF solution of $[(BzDMM)Cu^{I}(CH_3CN)]BArF$ (209 μM) at -80 ^{0}C, to give a dioxygen adduct (bis-μ-oxo-dicopper(III) or side-on peroxo-dicopper(II) species) with $\varepsilon_{390\ nm}$ = 9700 M^{-1} cm^{-1}.

As for copper(I)-dioxygen chemistry of complexes of the quinolyl containing ligand systems, the story is different. Addition of dioxygen to either MeTHF or acetone solutions of both $[(nQ_2)Cu^I(CH_3CN)]BArF$ and $[(BzQ_2)Cu^I(CH_3CN)]BArF$ resulted in no reaction occurring (Figure 12).

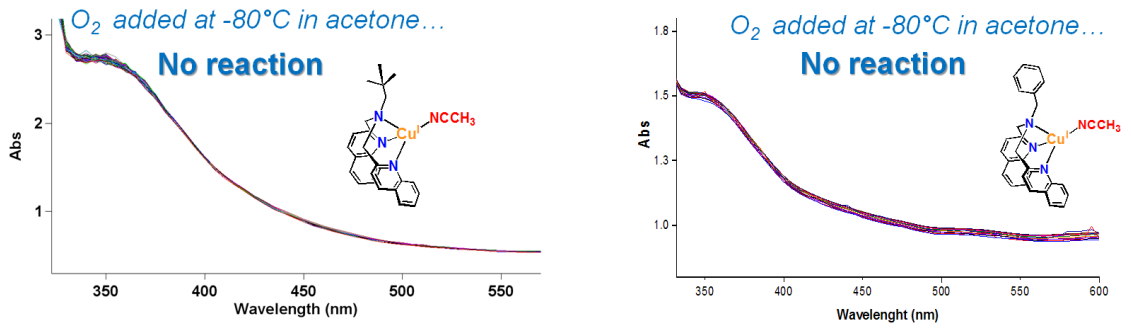

Figure 12. Addition of O_2 into a acetone solutions of $[(nQ_2)Cu^I(CH_3CN)]BArF$ and $[(BzQ_2)Cu^I(CH_3CN)]BArF$ at -80 ^{0}C resulted in no reaction.

However, the compound $[(BzQ_2)Cu^I]ClO_4$ (λ_{max} = 362 nm, $\varepsilon \approx 5200$ M^{-1} cm^{-1}) has been previously shown by Itoh and coworkers to react with dioxygen at -94^{0}C in acetone solvent giving a mixture of side-on peroxo and bis-μ-oxo dicopper compounds. This was confirmed by resonance Raman (rR) spectroscopy combined with $^{18}O_2$ isotopic substitution studies although not all the isotopic shifts could be assigned.[17] From the same work, it was instead shown that the reaction of $[(PheQ_2)Cu^I]ClO_4$ with dioxygen (where the '$PheQ_2$' ligand has the same structure with BzQ_2 except for having two methylene groups, instead of one, separating the central alkyl nitrogen with the dangling phenyl group) yielded a dicopper(II) side-on peroxo complex as a major product. The previous studies mentioned above showed

that the acetonitrile molecule coordinating the copper(I) ion in such tridentate copper(I) complexes needs to be removed for the reaction between copper(I) and dioxygen to occur.

Thus, similar synthetic procedures were introduced to the study of nQ_2 and BzQ_2 copper complexes here. Introduction of dioxygen into an acetone solution of $[(nQ_2)Cu^I]BArF$ (2 mM, λ_{max} = 363 nm, ε = 3900 M^{-1} cm^{-1}) performed here at -94^{0}C gave the spectral changes shown in Figure 13 where a peak at 361 nm appeared after oxygenation (Figure 13A, in blue). In about one hour, the decay observed led to the development of a new peak with λ_{max} = 351 nm. The same oxygenation experiment was also performed at a higher concentration of the copper(I) complex (5 mM) to confirm the presence of a second peak in the low energy region (λ_{max} = 575 nm) appearing together with that found at 351 nm (Figure 13B). A comparison of absorption maxima (λ_{max}) and extinction coefficients (ε) found here to those found for previously characterized compounds is shown in Table 6.

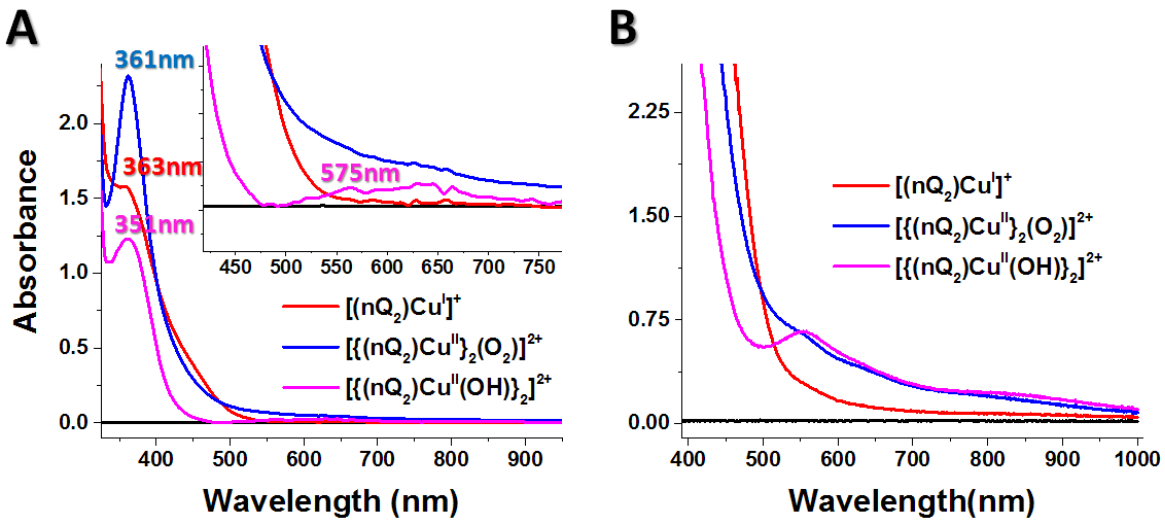

Figure 13. (A) Absorption spectral change after introduction of O_2 into a 2 mM acetone solution of $[(nQ_2)Cu^I]^+$ at -94 ^{0}C (in red). (B) Same experiment performed using a higher concentration of $[(nQ_2)Cu^I]^+$ (5 mM).

Table 6. Comparison of spectroscopic features of $[\{(nQ_2)Cu^{II}\}_2(O_2)]^{2+}$ with those of previously characterized compounds.

COMPOUND	λ_{max}, nm (ε, $M^{-1}cm^{-1}$)
nQ_2-peroxo dicopper(II)	361 (11300) 515 broad (460)
BzQ_2-peroxo dicopper(II)	362 (13000), 535 (1800) [a]
$PheQ_2$-peroxo dicopper(II)	360 (18000), 515 broad (1000) [a]

[a] previously characterized.[17]

Keeping in mind the oxygenation chemistry previously observed for $[(BzQ_2)Cu^{I}]^{+}$ and comparing λ_{max} and ε values in Table 6 to one another we propose the blue spectrum shown in Figure 13 to represent the dicopper(II) side-on peroxo species $[\{(nQ_2)Cu^{II}\}_2(O_2)]^{2+}$. Given the chemistry previously observed for the oxygenation of both $[(BzQ_2)Cu^{I}]^{+}$ and $[(PheQ_2)Cu^{I}]^{+}$, however, the presence of the bis-μ-oxo compound $[\{(nQ_2)Cu^{III}\}_2(O)_2]^{2+}$, which may be in equilibrium with the peroxo complex $[\{(nQ_2)Cu^{II}\}_2(O_2)]^{2+}$, cannot be ruled out. Additional studies (especially rR) could shed more light on this question. The spectroscopic features of the species formed after that represented by the blue spectrum during the oxygenation reaction of $[(nQ_2)Cu^{I}]^{+}$ (Figure 13, in magenta: λ_{max} = 351 nm, ε = 9900 M^{-1} cm^{-1} and λ_{max} = 575 nm, ε = 390 M^{-1} cm^{-1}) resembles a bis-μ-hydroxo complex,[45-47] comparing well with the spectrum of the authentic nQ_2-bis-μ-hydroxo dicopper(II), $[\{(nQ_2)Cu^{II}(OH)\}_2]^{2+}$, synthesized in this work (see above). The comparison presented in Figure 14 shows a good match between bands for both the high and the low energy regions.

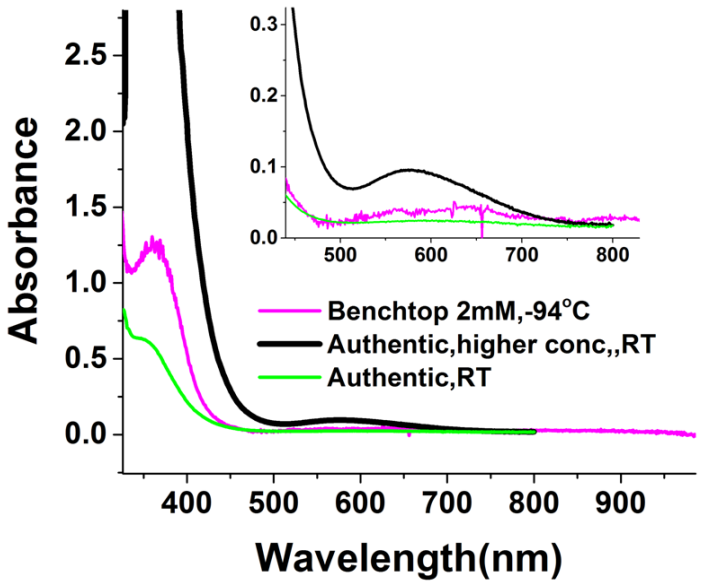

Figure 14. Comparison between the spectrum from the oxygenation experiment (in magenta) and that from the authentic $[\{(nQ_2)Cu^{II}(OH)_2]^{2+}$ compound prepared at two different concentrations (green and black spectra).

On the basis of the evidence shown here and considering the copper(I)/O_2 chemistry previously observed for the analogue compounds $[(BzQ_2)Cu^I]^+$ and $[(PheQ_2)Cu^I]^+$ under the same experimental conditions, we propose the mechanism shown in Scheme 2 for the reactivity of $[(nQ_2)Cu^I]^+$ with O_2.

Scheme 2. Proposed mechanism for $[(nQ_2)Cu^I]^+/O_2$ reactivity in acetone.

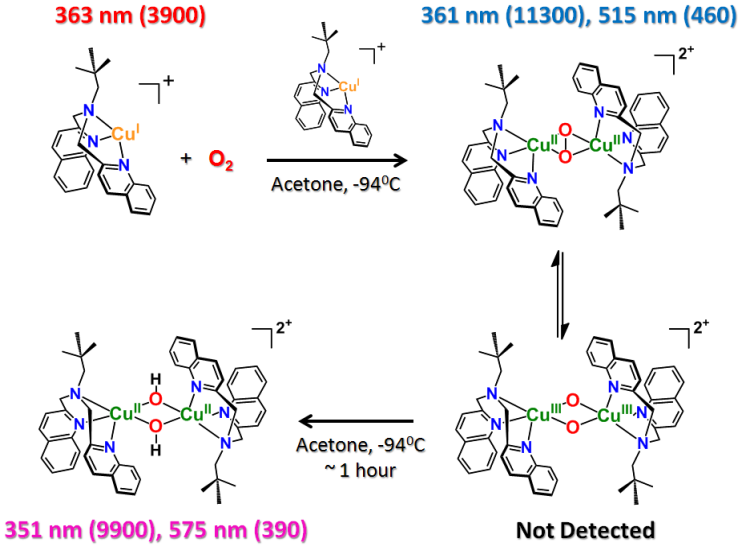

In this Scheme, $[(nQ_2)Cu^I]^+$ reacts with O_2 at low temperature to give the dicopper(II) side-on peroxo species $[\{(nQ_2)Cu^{II}\}_2(O_2)]^{2+}$ as a major product. That is in equilibrium with a non-detectable mount of bis-μ-oxo compound, $[\{(nQ_2)Cu^{III}\}_2(O_2)]^{2+}$, which slowly converts to the bis-μ-hydroxo species $[\{(nQ_2)Cu^{II}(OH)\}_2]^{2+}$, that probably formed through hydrogen atom abstraction from the acetone solvent by the bis-μ-oxo complex.

3.5 Dioxygen Binding to Copper(I) in Acetone Solvent: Laser Experiments

A study of the binding between O_2 and copper(I) with possible detection of a 1:1 Cu:O_2 intermediate supported by the tridentate chelating ligand nQ_2 was also attempted. The flash-and-trap method, previously employed for tetradentate copper compounds,[14,15] was adopted.

The experiments were performed in a solution saturated with a 99% : 1% $O_{2(g)}$: $CO_{(g)}$ gas mixture ratio and 355 nm pulsed laser light was used to induce CO photo-release from **1**.

According to the reaction mechanism depicted in Scheme 1, O_2 could bind any of the species that form after CO photoejection, i.e. the 'naked' copper species $[(nQ_2)Cu^I]^+$ (LCu^I) and/or the solvento-species $[(nQ_2)Cu^I(acetone)]^+$ ('LCu^I(Acetone)' in Scheme 3).

Scheme 3. Possible O_2 reactive species.

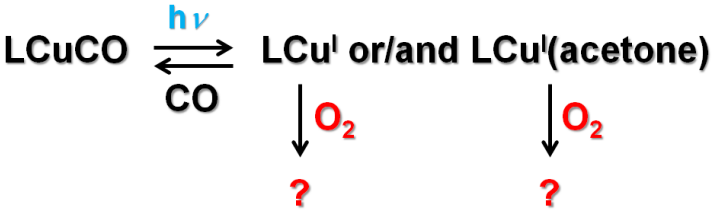

The two options for O_2 binding to copper(I), according to Scheme 3, are both possible: $[(nQ_2)Cu^I]^+ + O_2 \rightarrow [(nQ_2)Cu^{II}(O_2)]^+$ and/or $[(nQ_2)Cu^I(acetone)]^+ + O_2 \rightarrow [(nQ_2)Cu^{II}(O_2)]^+$ as acetone may or may not or may just weakly coordinate copper(I) in $[(nQ_2)Cu^I]^+$ after photoexcitation of **1**.

As an interesting and possibly significant contrast to what observed in the laser experiment performed in the present work when only $CO_{(g)}$ was present, is that transient absorption difference spectra collected in the presence of $O_{2(g)}$ displayed, instead, an increase of the signal in the range 405-440 nm (Figure 15A). This increase was coupled with a faster

decay rate of the peak representing the species $[(nQ_2)Cu^I]^+$ or $[(nQ_2)Cu^I(acetone)]^+$ (Figure 17B).

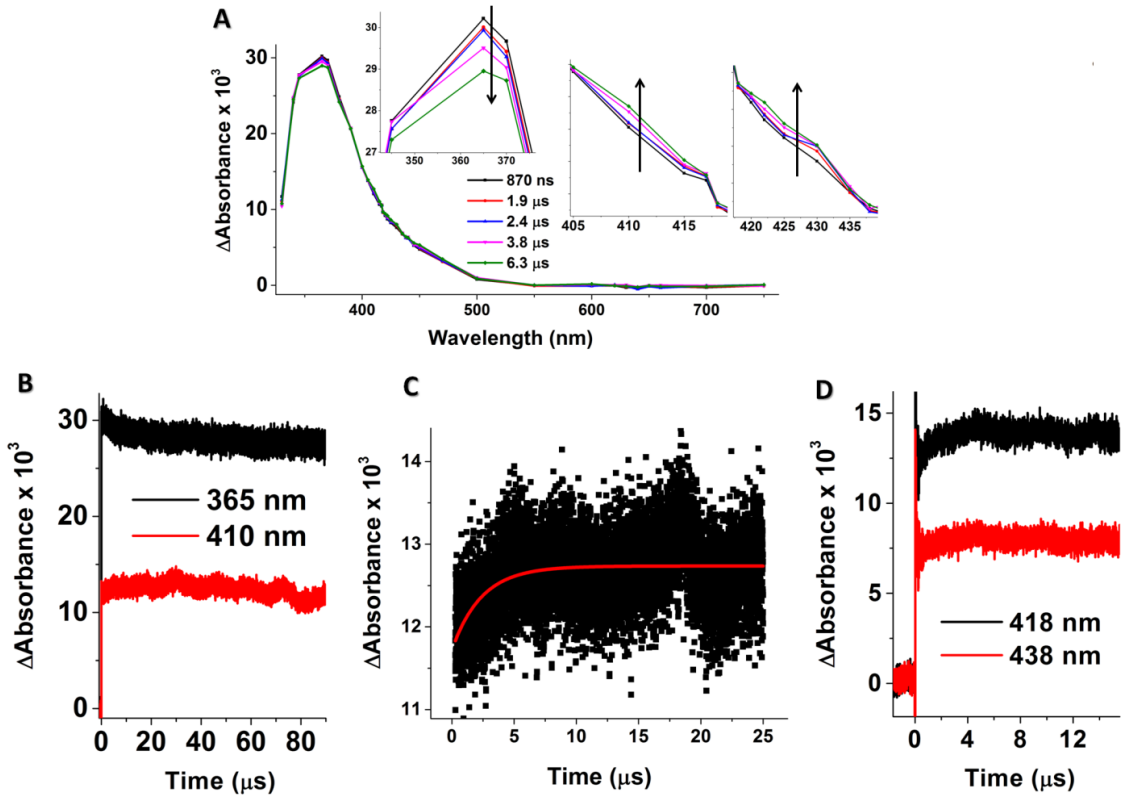

Figure 15. (A) Transient absorption difference spectra collected at the indicated delay times after 355 nm laser excitation (8 mJ/pulse, 8-10 ns fwhm) of **1** in acetone at -94 ^{0}C in the presence of O_2 (B) Representative absorption changes monitored in the experiment shown in A (C) First-order mono-exponential fit of the growth observed at 410 nm in A (D) Confirmation of the absorption increase in the range 405-440 nm in a separate experiment.

The growth of the absorption difference observed at 410 nm was fitted with a mono-exponential function and the observed rate constant was determined to be k_{obs} = (4.20 ± 0.03)·10^5 s^{-1}. Considering that the experiment was conducted in a 99%/1% O_2/CO gas mixture at -94^{0}C ([O_2] = 0.0124 M and [CO] = 1.2 x 10^{-4} M) it was, then, possible to provide

an estimate for the second-order rate constant for dioxygen binding to $[(nQ_2)Cu^{I}]^{+}$ or $[(nQ_2)Cu^{I}(acetone)]^{+}$ using the 'k_{fast}' kinetic model shown in Scheme 4 (top). In this model, competition for coordination of CO and O_2 to the copper(I) is taken into account and a value of $k_{O2} = (3.38 \pm 0.02)\cdot 10^{7}$ M^{-1} s^{-1} was determined (the value $k_{CO} = (1.73\ 0.06)\cdot 10^{6}$ M^{-1} s^{-1} calculated for the experiment when only CO was present was used). It should be pointed out that this value of k_{O2} has been determined from a single dioxygen/carbon monoxide concentration ratio and that, thus, it should be intended as a rough estimate of the range where the value of the real second-order rate constant should be (*vide infra*). The presence of the mentioned absorption changes was also confirmed in a separate experiment were the absorption increase at 418 nm and 428 nm was also monitored (Figure 15D). We propose that such increase of the absorbance difference is due to the formation of the 1:1 copper/O_2 species $[(nQ_2)Cu(O_2)]^{+}$. In this case, it is possible to adopt the 'classical' kinetic model used in previous flash-and-trap experiments for the competitive binding of CO and O_2 to copper(I) indicated in Scheme 4.

Scheme 4. Flash-and-trap kinetic model.

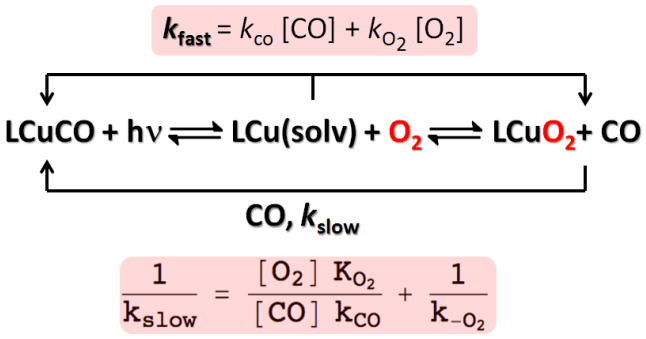

Second-order rate constants for the binding of O_2 to $[(nQ_2)Cu^I]^+$ or $[(nQ_2)Cu^I(acetone)]^+$ were determined, in this case, using the 'k_{slow}' model (Scheme 4, bottom) and activation parameters were obtained through temperature-dependent studies and Eyring analysis (Figure 16 and Table 7).

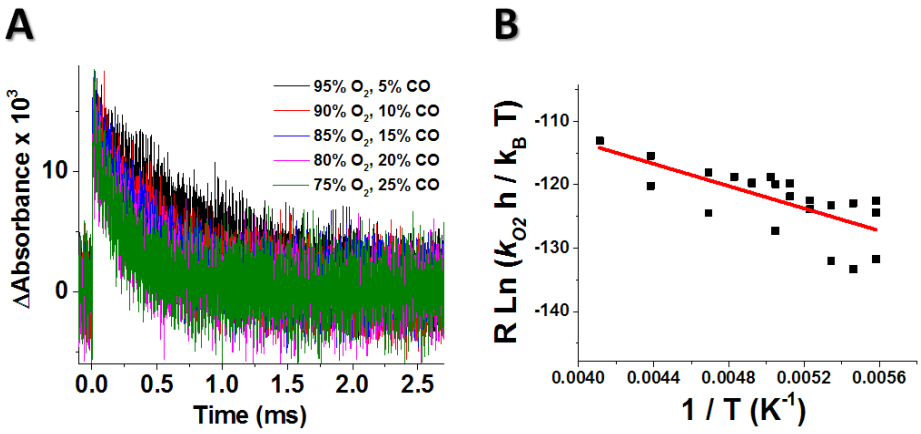

Figure 16. (A) Representative absorption changes monitored at 418 nm after photo-excitation of **1** at various ratios of $O_{2(g)}/CO_{2(g)}$ at -94^{0}C in acetone (B) Determination of the activation parameters for the rate constants k_{O2}.

The k_{O2} value determined with the 'k_{slow}' model extrapolated at -94^{0}C, (8.5 ± 1.4) · 10^5 M^{-1} s^{-1}) and that determined from the fast growth observed at 410 nm from a single dioxygen/carbon monoxide concentration ratio using the 'k_{fast}' model, (3.38 ± 0.02)·10^7 M^{-1} s^{-1}, are off by almost two orders of magnitude. As mentioned, however, it should be kept in mind that the latter value has been determined using a 'single point' 99%/1% O_2/CO gas mixture analysis and the apparent inconsistency between the two k_{O2} values could be, then, considered reasonable.

Table 7. Comparison of second-order rate constants and activation parameters for the binding of O_2 to $[(nQ_2)Cu^I]^+$ or $[(nQ_2)Cu^I(acetone)]^+$ in acetone with $[(^DTMPA)Cu^I]^+$ in THF and in EtCN.

	k_{O2}[a]		$\Delta H^{\ddagger}$[b]	$\Delta S^{\ddagger}$[b]
Temp.	25°C	-80°C		
nQ_2	$(3.1 \pm 0.1)\cdot10^7$	$(2.9 \pm 0.1)\cdot10^6$	9 ± 2	-78 ± 10
N4 ^DL[c]	$(0.13\text{-}23)\cdot10^{10}$	$(0.7\text{-}1.8)\cdot10^8$	7.6-32	-45-(+80)
TMPA[d]	$5.8\cdot10^7$	$3.8\cdot10^4$	32	10

[a] k_{O2}, M^{-1} s^{-1} [b] ΔH, kJ mol^{-1} [b] ΔS, J K^{-1} mol^{-1} [c] Values determined in THF[15] Values determined in EtCN[48,49]. 'N4 ^DL' refers to the tetradentate ligands with D = Im, NMe_2, and Py.[14]

Although the activation enthalpy for O_2 binding to $[(nQ_2)Cu^I(acetone)]^+$ is comparable to those found for the tetradentate ligand-copper series $[(^DL)Cu^I]^+$ in THF, the overall value of the rate constants is greater in the latter case of about two orders of magnitude at all the temperatures probed in this work. This may be due to the more labile nature of the copper-solvent bond for ^DL compounds in THF compared with the nQ_2-based compound in acetone. A comparison of the activation parameters for the binding of O_2 to $[(nQ_2)Cu^I]^+$ or $[(nQ_2)Cu^I(acetone)]^+$ with those previously determined for $[(^DTMPA)Cu^I]^+$ in EtCN (^DTMPA = ^DL with D = Py, Chart 1) confirms and highlights the evidence that acetone is a good solvent to study the reactivity of this class of tridentate N-donor copper complexes with dioxygen. In fact, acetone binding to copper(I) is not as strong as nitrile solvents which, in some cases for the latter, can either slow down or completely shut-off the copper(I)/O_2 chemistry in such compounds. It would be possible to argue on whether or not O_2 coordinated, at all, to any of the copper(I) compounds shown in the reaction mechanism presented in Scheme 3. However, in case dioxygen did not display any reactivity with the copper compounds shown in Scheme 3, then, it should behave as an inert gas (N_2) and the

same results with those obtained when only $CO_{(g)}$ and $N_{2(g)}$ were present in solution should be obtained in the laser experiments. Such data analysis was performed and both activation enthalpy and entropy were found to be greater in the presence of O_2 ($\Delta H^{\ddagger}(O_2/N_2)$ and $\Delta S^{\ddagger}(O_2/N_2)$) compared to those found when only CO/N_2 gas mixtures were present in the reaction mixture: $\Delta H^{\ddagger}(O_2/N_2)$ = (11.2 ± 1.8) vs. $\Delta H^{\ddagger}(CO/N_2)$ = (8.8 ± 0.4) kJ mol^{-1} and $\Delta S^{\ddagger}(O_2/N_2)$ = (-61 ± 9) vs. $\Delta S^{\ddagger}(CO/N_2)$ = (-72 ± 2) kJ K^{-1} mol^{-1} suggesting that the presence of O_2 translated into new reactivity towards the copper(I) complexes shown in Scheme 3 and playing in favor of the interpretation that formation of the novel transient mononuclear 1:1 Cu/O_2 complex $[(nQ_2)Cu(O_2)]^+$, did occur.

4. Conclusions

Carbon monoxide and dioxygen fast binding kinetics towards copper(I) compounds supported by the N-donor, tripodal, tridentate chelating ligands nQ_2 and BzQ_2 were examined in acetone solvent and evidence for the possible formation of a new mononuclear 1:1 Cu/O_2 species, $[(nQ_2)Cu(O_2)]^+$, was presented. Reactions with both CO and O_2 were found to be slower for the tridentate copper(I) complexes examined here compared with the previously studied tetradentate N-donor copper-ligand systems. This might be due to a stronger binding of tridentate copper complexes with the solvent (here acetone) which leads to intrinsically greater activation barriers for the binding of small molecules with the copper ion. This study provides the first example of detection of a transient mononuclear 1:1 Cu/O_2 complex supported by a neutral tridentate N-donor ligand.

5. Acknowledgments

The following co-authors contributed to the work presented in this chapter:

Maxime A. Siegler, Gerald J. Meyer, and Kenneth D. Karlin

6. References

(1) Hofrichter, J.; Sommer, J. H.; Henry, E. R.; Eaton, W. A. *Proc. Natl. Acad. Sci. USA* **1983**, *80*, 2235.

(2) Hofrichter, J.; Henry, E. R.; Sommer, J. H.; Deutsch, R.; Ikeda-Saito, M.; Yonetani, T.; Eaton, W. A. *Biochemistry* **1985**, *24*, 2667.

(3) Murray, L. P.; Hofrichter, J.; Henry, E. R.; Ikeda-Saito, M.; Kitagishi, K.; Yonetani, T.; Eaton, W. A. *Proc. Natl. Acad. Sci. USA* **1988**, *85*, 2151.

(4) Spiro, T. G.; Soldatova, A. V.; Balakrishnan, G. *Coord. Chem. Rev.* **2013**, *257*, 511.

(5) Bonaventura, C.; Sullivan, B.; Bonaventura, J.; Bourne, S. *Biochemistry* **1974**, *13*, 4784.

(6) Ellerton, H. D.; Ellerton, N. F.; Robinson, H. A. *Prog. Biophys. Mol. Biol.* **1983**, *41*, 143.

(7) Alben, J. O.; Moh, P. P.; Fiamingo, F. G.; Altschuld, R. A. *Proc. Natl. Acad. Sci-Biol.* **1981**, *78*, 234.

(8) Einarsdottir, O.; Dyer, R. B.; Lemon, D. D.; Killough, P. M.; Hubig, S. M.; Atherton, S. J.; Juan J. Lbpez-Garriga, g.; Palmer, G.; Woodruff, W. H. *Biochemistry* **1993**, *32*, 12013.

(9) Stavrakis, S.; Koutsoupakis, K.; Pinakoulaki, E.; Urbani, A.; Saraste, M.; Varotsis, C. *J. Am. Chem. Soc.* **2002**, *124*, 3814.

(10) Okuno, D.; Iwase, T.; Shinzawa-Itoh, K.; Yoshikawa, S.; Kitagawa, T. *J. Am. Chem. Soc.* **2003**, *125*, 7209.

(11) Gibson, Q. H.; Greenwood, C. *Biochem. J.* **1963**, *86*, 541.

(12) Greenwood, C.; Gibson, Q. H. *J. Biol. Chem.* **1967**, *242*, 1782.

(13) Scaltrito, D. V.; Fry, H. C.; Showalter, B. M.; Thompson, D. W.; Liang, H.-C.; Zhang, C. X.; Kretzer, R. M.; Kim, E.-i.; Toscano, J. P.; Karlin, K. D.; Meyer, G. J. *Inorg. Chem.* **2001**, *40*, 4514.

(14) Lucas, H. R.; Meyer, G. J.; Karlin, K. D. *J. Am. Chem. Soc.* **2010**, *132*, 12927.

(15) Fry, H. C.; Scaltrito, D. V.; Karlin, K. D.; Meyer, G. J. *J. Am. Chem. Soc.* **2003**, *125*, 11866.

(16) Fry, H. C.; Lucas, H. R.; Narducci Sarjeant, A. A.; Karlin, K. D.; Meyer, G. J. *Inorg. Chem.* **2007**, *47*, 241.

(17) Kunishita, A.; Osako, T.; Tachi, Y.; Teraoka, J.; Itoh, S. *Bull. Chem. Soc. Jpn.* **2006**, *79*, 1729.

(18) Mirica, L. M.; Ottenwaelder, X.; Stack, T. D. P. *Chem. Rev.* **2004**, *104*, 1013.

(19) Lewis, E. A.; Tolman, W. B. *Chem. Rev.* **2004**, *104*, 1047.

(20) Liang, H. C.; Kim, E.; Incarvito, C. D.; Rheingold, A. L.; Karlin, K. D. *Inorg. Chem.* **2002**, *41*, 2209.

(21) Fischer, K.; Wilken, M. *J. Chem. Thermodyn.* **2001**, *33*, 1285.

(22) Battino, R. *IUPAC Solubility Data Series: Oxygen and Ozone; Pergamon: Oxford, New York* **1981**.

(23) Argazzi, R.; Bignozzi, C. A.; Heimer, T. A.; Castellano, F. N.; Meyer, G. J. *J. Phys. Chem.* **1994**, *33*, 5741.

(24) Fry, H. C.; Lucas, H. R.; Narducci Sarjeant, A. A.; Meyer, G. J.; Karlin, K. D. *Inorg. Chem.* **2008**, *47*, 241.

(25) Pasquali, M.; Marini, G.; Floriani, C.; Gaetanimanfredotti, A.; Guastini, C. *Inorg. Chem.* **1980**, *19*, 2525.

(26) Kitajima, N.; Fujisawa, K.; Fujimoto, C.; Moro, n.; Hashimoto, S.; Kitagawa, T.; Toriumi, K.; Tasumi, K.; Nakamura, A. *J. Am. Chem. Soc.* **1992**, *114*, 1277.

(27) Karlin, K. D.; Tyekl; xe; r, Z.; Farooq, A.; Haka, M. S.; Ghosh, P.; Cruse, R. W.; Gultneh, Y.; Hayes, J. C.; Toscano, P. J.; Zubieta, J. *Inorg. Chem.* **1992**, *31*, 1436.

(28) Ardizzoia, G. A.; Beccalli, E. M.; Lamonica, G.; Masciocchi, N.; Moret, M. *Inorg. Chem.* **1992**, *31*, 2706.

(29) Imai, S.; Fujisawa, K.; Kobayashi, T.; Shirasawa, N.; Fujii, H.; Yoshimura, T.; Kitajima, N.; Moro, n. *Inorg. Chem.* **1998**, *37*, 3066.

(30) Conry, R. R.; Ji, G. Z.; Tipton, A. A. *Inorg. Chem.* **1999**, *38*, 906.

(31) Reger, D. L.; Collins, J. E. *Organometallics* **1996**, *15*, 2029.

(32) Lucas, H. R.; Li, L.; Sarjeant, A. A. N.; Vance, M. A.; Solomon, E. I.; Karlin, K. D. *J. Am. Chem. Soc.* **2009**, *131*, 3230.

(33) Nagao, H.; Komeda, N.; Mukaida, M.; Suzuki, M.; Tanaka, K. *Inorg. Chem.* **1996**, *35*, 6809.

(34) Maiti, D.; Woertink, J. S.; Narducci Sarjeant, A. A.; Solomon, E. I.; Karlin, K. D. *Inorg. Chem.* **2008**, *47*, 3787.

(35) Lucas, H. R.; Karlin, K. D. *Met. Ions Life Sci.* **2009**, *6*, 295.

(36) Himes, R. A.; Park, G. Y.; Barry, A. N.; Blackburn, N. J.; Karlin, K. D. *J. Am. Chem. Soc.* **2007**, *129*, 5352.

(37) Pasquali, M.; Floriani, C.; Karlin, K. D.; Zubieta, J. *Copper(I) −Carbon Monoxide Chemistry: Recent Advances and Perspectives,' In Copper Coordination Chemistry: Biochemical & Inorganic Perspectives*, 1983.

(38) Rondelez, Y.; Seneque, O.; Rager, M. N.; Duprat, A. F.; Reinaud, O. *Chem. Eur. J.* **2000**, *6*, 4218.

(39) Jonas, R. T.; Stack, T. D. P. *Inorg. Chem.* **1998**, *37*, 6615.

(40) Fujisawa, K.; Ono, T.; Ishikawa, Y.; Amir, N.; Miyashita, Y.; Okamoto, K.; Lehnert, N. *Inorg. Chem.* **2006**, *45*, 1698.

(41) Dias, H. V. R.; Lu, H. L. *Inorg. Chem.* **1995**, *34*, 5380.

(42) Karlin, K. D.; Kaderli, S.; Zuberbuhler, A. D. *Acc. Chem. Res.* **1997**, *30*, 139.

(43) Osako, T.; Ueno, Y.; Tachi, Y.; Itoh, S. *Inorg. Chem.* **2003**, *42*, 8087.

(44) Osako, T.; Terada, S.; Tosha, T.; Nagatomo, S.; Furutachi, H.; Fujinami, S.; Kitagawa, T.; Suzuki, M.; Itoh, S. *Dalton Trans.* **2005**, 3514.

(45) Hatcher, L. Q.; Vance, M. A.; Narducci Sarjeant, A. A.; Solomon, E. I.; Karlin, K. D. *Inorg. Chem.* **2006**, *45*, 3004.

(46) Kitajima, N.; Moro-oka, Y. *Chem. Rev.* **1994**, *94*, 737.

(47) Obias, H. V.; Lin, Y.; Murthy, N. N.; Pidcock, E.; Solomon, E. I.; Ralle, M.; Blackburn, N. J.; Neuhold, Y.-M.; Zuberbühler, A. D.; Karlin, K. D. *J. Am. Chem. Soc.* **1998**, *120*, 12960.

(48) Weitzer, M.; Schindler, S.; Brehm, G.; Hormann, E.; Jung, B.; Kaderli, S.; Zuberbuehler, A. D. *Inorg. Chem.* **2003**, *42*, 1800.

(49) Zhang, C. X.; Liang, H. C.; Kim, E. I.; Shearer, J.; Helton, M. E.; Kim, E.; Kaderli, S.; Incarvito, C. D.; Zuberbuhler, A. D.; Rheingold, A. L.; Karlin, K. D. *J. Am. Chem. Soc.* **2003**, *125*, 634.

Chapter 3:

Wavelength-Dependent O_2 Photo Release from Mononuclear $LCuO_2$ Compounds

Abstract

Irradiation of the copper(II)-superoxide synthetic complexes $[(TMG_3tren)Cu^{II}(O_2)]^+$ (**1**) and $[(PV\text{-}TMPA)Cu^{II}(O_2)]^+$ (**2**) with visible light resulted in direct photo-generation of O_2 gas at low temperature (from -40^0C to -70^0C for **1** and from -125^0C to -135^0C for **2**) in 2-methyltetrahydrofuran (MeTHF) solvent. The quantum yield for O_2 release was wavelength-dependent: λ_{exc} = 436 nm, ϕ = 0.29 (for **1**), ϕ = 0.11 (for **2**), and λ_{exc} = 683 nm, ϕ = 0.035 (for **1**), ϕ = 0.078 (for **2**), and this process was followed by fast O_2-recombination with $[(TMG_3tren)Cu^{I}]^+$ (**3**) or $[(PV\text{-}TMPA)Cu^{I}]^+$ (**4**). The activation enthalpy for O_2 re-binding to the copper(I) center (~ 10 kJ mol^{-1}) and for (thermal) O_2 dissociation from the superoxide compound **1** (45 kJ mol^{-1}) were determined. TD-DFT studies, carried out for **1**, support the experimental results confirming the dissociative character of the excited states formed upon blue or red light laser excitation.

1. Introduction

Copper-containing proteins play a major role in O_2 transport and activation in biology. Thus, Cu^I/O_2 reactions and subsequent transformations are critical in this setting as well as in practical systems.[1-4] Initial O_2 adducts of copper(I) must form in all cases, including in O_2-carriers, oxygenases (oxygen transfer to the substrate) and oxidases (substrate oxidized by O_2), but these first formed species often further react with other electron/proton sources (which may be the substrate) to give Cu_n-peroxo, Cu^{II}-hydroperoxo[5,6] or perhaps Cu_n-oxyl[2,7-11] active species or intermediates. In peptidylglycine α-hydroxylating monooxygenase[12,13] and dopamine β-monooxygenase,[14] such O_2 activation occurs at a single copper center. An X-ray structure of a precatalytic complex along with chemical[15-18] and computational studies,[7,19-21] suggested an end-on bound Cu^{II}-superoxide species as the enzyme reactive intermediate effecting substrate hydrogen abstraction, further implicating the (bio)chemical importance of initially formed Cu^I/O_2 1:1 adducts, i.e., Cu^{II}-superoxide species.

Here, for the first time, we show that O_2 can be photo-ejected directly from the 1:1 mononuclear copper/O_2 compounds $[(TMG_3tren)Cu^{II}(O_2)]^+$ (**1**) and $[(PV\text{-}TMPA)Cu^{II}(O_2)]^+$ (**2**) using either 436 nm or 683 nm pulsed laser light (Scheme 1).

Scheme 1. Flash-photolysis studies of **1** and **2**.

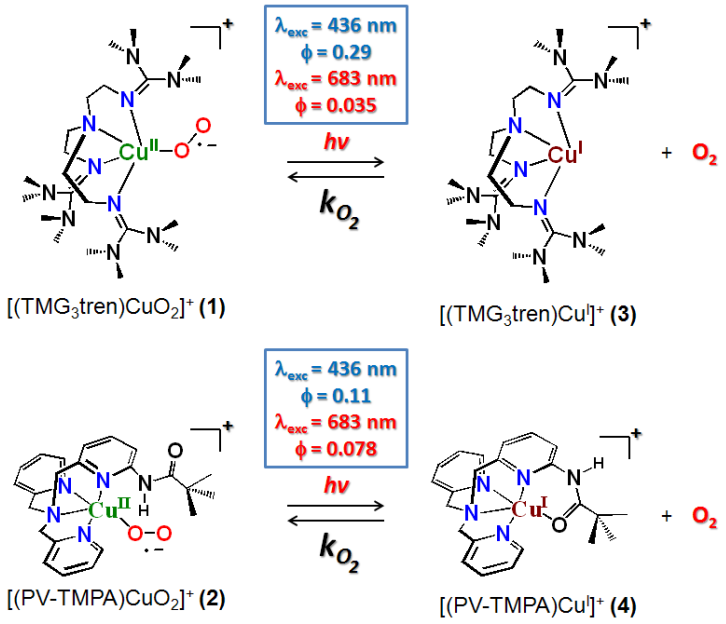

Interestingly, a different yield for O_2 release was observed with these two excitation wavelengths which is unusual compared to the O_2 photo-release found in heme systems, such as myoglobin.[22] Temperature-dependent kinetic and thermodynamic studies have been carried out to elucidate the nature of the barriers involved in the thermal O_2 binding and dissociation processes. Data are corroborated by DFT calculations that help to interpret the experimentally observed wavelength-dependent quantum yields for the O_2 photo-release from **1** and give new insights into the electron transfer process under study. To the best of our knowledge, this is the first time that a direct O_2 photo-ejection from 1:1 copper-superoxide adducts has been shown to occur.

2. Experimental

2.1 Materials and Methods

All materials purchased were of highest purity available from Sigma-Aldrich Chemical or Tokyo Chemical Indrusties (TCI) and were used as received, unless specified otherwise. 2-methyltetrahydrofuran (MeTHF) and tetrahydrofuran were distilled under an inert atmosphere from Na/benzophenone and degassed with argon prior to use. Pentane and acetonitrile were freshly distilled from calcium hydride under an inert atmosphere and degassed prior to use. Identity and purity of the compounds used in this study were verified by elemental analysis and/or ^{1}H-NMR spectroscopy.

Synthesis and manipulations of copper salts were performed according to standard Schlenk techniques or in an MBraun glovebox (with O_2 and H_2O levels below 1 ppm). UV-Vis spectra were recorded with a Cary 50 Bio spectrophotometer equipped with a liquid nitrogen chilled Unisoku USP-203-A cryostat. NMR spectroscopy was performed on Bruker 300 and 400 MHz instruments with spectra calibrated to either internal tetramethylsilane (TMS) standard or to residual protio solvent. $[Cu^I(MeCN)_4]BArF$, the ligands (TMG_3tren and PV-TMPA), and the related copper(I) complexes ($[(TMG_3tren)Cu^I]BArF$ and $[(PV\text{-}TMPA)Cu^I]BArF$) were synthesized by literature procedures.[23-25]

2.2 Determination of O_2 solubility in 2-MeTHF

The solubility of O_2 in 2-MeTHF was determined using mole fractions and temperature-dependent data given in the literature.[26] The mol fraction solubility of $O_{2(g)}$ in 2-MeTHF at one atmosphere and 311.03 K was extrapolated from the available data to be $5.79973 \cdot 10^{-4}$. Molar fraction solubility at different temperatures were obtained using the data available for

the molar fraction solubility of $O_{2(g)}$ in diethyl ether as a function of temperature[27] fitting the data to those experimentally determined from Ref. 26.

2.3 Gas Mixing

Carbon monoxide (CO; Air Gas East, grade 2.3) used for the flash-and-trap experiment performed for [(TMPA)Cu^{I}(CO)]BArF in 2-MeTHF was treated by passing through an R & D Separations oxygen/moisture trap (Agilent Technologies OT3-4). Dioxygen (O_2; Air Gas East, grade 4.4) was dried by passing the gas through a short column of supported P4010 (Aquasorb, Mallinkrodt). Red rubber tubing (Fisher Scientific; inner diameter: 1/4 in.; thickness: 3/16 in.) was used to attach the gas cylinders fitted with appropriate regulators to two MKS Instruments Mass-Flo Controllers (MKS Type 1179A) regulated by an MKS Instruments Multi-Channel Flow Ratio/Pressure Controller (MKS Type 647C). The gas mixtures (N_2/CO and O_2/CO for [(TMPA)Cu^{I}(CO)]BArF and N_2/O_2 for [(TMG_3tren)Cu(O_2)]BArF and [(PV-TMPA)Cu(O_2)]BArF) were determined by the set flow rates of the two gases. For example, a 10% O_2 mixture would be made by mixing O_2 at a rate of 10 standard cubic centimeters per minute (sccm) with CO at 90 sccm for a total flow of 100 sccm. By varying the ratio of O_2 and CO with the gas mixer, the concentration of the gases were determined by taking the percentage of the gas added and multiplying by the solubility of the corresponding gas in 2-MeTHF. For example, if [O_2] = 0.0087 M and [CO] = 0.0092 M at -70^{0}C, if the O_2/CO flow rate is 3/7 (or 30% of the total gas flow is O_2), then, the concentration of O_2 in 2-MeTHF = 0.30 x 0.0087 M = 0.0026 M and the concentration of CO = 0.70 x 0.0092 M = 0.0064 M.

2.4 Transient Absorption Experimental Details

Experimental information for the setup of the Nd:YAG flash-photolysis apparatus has been previously reported.[28] The apparatus was equipped with liquid nitrogen chilled Unisoku USP-203-A cryostat and a pressurized (~400 psi) H_2 Raman shifter tube to obtain the Stokes-shifted 683 and the anti-Stokes-shifted 436 nm excitation wavelengths. The samples, [(TMG_3tren)Cu(O_2)]BArF and [(PV-TMPA)Cu(O_2)]BArF, were irradiated with λ_{ex} = 436 nm or λ_{ex} = 683 nm pulsed light (15 mJ/pulse) and data were collected at the monitored wavelengths from averages of 60 laser pulses. Samples (320-360 μM) were prepared under an inert atmosphere (drybox) in 1 cm quartz cuvettes with four polished windows made custom by Quark glass. The cuvettes were equipped with a 14/20 joint and Schlenk stopcock. Gas mixtures were added to sample solutions through direct bubbling through a 24-inch needle (19-gauge) for 5 seconds for 10 times with intervals of 10 seconds between each time. During data collection the gas flowed through the headspace of the sample solution into the cuvette.

2.5 Data Treatment for Benchtop Titration Measurements

The equilibrium constant for the following chemical reaction

$$[(TMG_3tren)Cu^{I}]BArF + O_2 \rightleftharpoons [(TMG_3tren)Cu(O_2)]BArF$$

can be written as

$$K_{O2} = [LCuO_2] / [LCu^{I}] [O_2] \qquad \textbf{(1)}$$

having called TMG_3tren = L and having omitted the counter anion BArF for simplicity. Substitution of $[LCu^I] = [LCu^I]_0 - [LCuO_2]$ **(2)** into **(1)** (where $[LCu^I]_0$ is the initial concentration of LCu^I, before adding O_2), gives equation **(3)**:

$$[LCuO_2] / [O_2] = K_{O2}([LCu^I]_0 - [LCuO_2]) \qquad \textbf{(3)}$$

Considering, now, that O_2 does not absorb light at the wavelength λ = 449 nm, we choose to monitor LCu^I and $LCuO_2$. Consequently, the total observed absorbance at 449 nm will be given by the following equation:

$$\Delta Abs_{449} = \varepsilon^{Cu}{}_{449} [LCu^I] + \varepsilon^{CuO2}{}_{449} [LCuO_2] \qquad \textbf{(4)}$$

where $\varepsilon^{Cu}{}_{449}$ and $\varepsilon^{CuO2}{}_{449}$ are the extinction coefficients of LCu^I and $LCuO_2$ at 449 nm. Substituting equation **(2)** into equation **(4)** and rearranging gives:

$$[LCuO_2] = \Delta Abs_{449} / \Delta\varepsilon_{449} \qquad \textbf{(5)}$$

where $\Delta Abs_{449} = Abs^0{}_{449} - Abs_{449}$ is the optical density difference at 449 nm before ($Abs^0{}_{449}$) and after (Abs_{449}) adding O_2 to LCu^I

and

$\Delta\varepsilon_{449} = \varepsilon^{CuO2}{}_{449} - \varepsilon^{Cu}{}_{449}$ is the difference between the extinction coefficients of $LCuO_2$ and LCu^I at 449 nm.

Substitution of equation **(5)** into equation **(3)** and rearrangement gives the model used to fit the experimental data from the benchtop titration experiments performed in this work:

$$\Delta Abs_{449} = (K_{O2} [LCu^I]_0 \Delta\varepsilon_{449} [O_2]) / (1 + K_{O2} [O_2]) \qquad \textbf{(6)}$$

A fit of the experimental points ($[O_2]$; ΔAbs_{449}) with equation **(6)** will give the equilibrium constant K_{O2}. The same titration measurements performed at variable temperature give the correspondent values of the equilibrium constants and data can be fitted with the Van't Hoff equation $\ln(K_{O2}) = - (\Delta H^0 / RT) + (\Delta S^0 / R)$.

2.6 Model Used for Kinetic Studies

A kinetic 'relaxation' method[29,30] was used as a model for the reaction between $[(TMG_3tren)Cu^I]BArF$ and O_2 where the equilibrium concentrations of the species in solution were perturbed by laser excitation of $[(TMG_3tren)Cu(O_2)]BArF$ and the return to equilibrium was monitored spectroscopically. Consider, again, the following equilibrium:

$$[(TMG_3tren)Cu^I]BArF + O_2 \underset{k_{-O2}}{\overset{k_{O2}}{\rightleftharpoons}} [(TMG_3tren)Cu(O_2)]BArF$$

Again, TMG_3tren = L and the counter anion BArF was omitted for simplicity.

The rate of formation of $LCuO_2$ will be the following:

$$d[LCuO_2] / dt = k_{O2} [LCu^I] [O_2] - k_{-O2} [LCuO_2] \qquad \textbf{(7)}$$

At equilibrium, the net rate of formation of $LCuO_2$ will be zero:

$$d[LCuO_2] / dt = k_{O2} [LCu^I]_{eq} [O_2]_{eq} - k_{-O2} [LCuO_2]_{eq} = 0 \qquad \textbf{(8)}$$

Upon laser excitation of $[(TMG_3tren)Cu(O_2)]BArF$ we will alter the concentration of the species in solution as follows:

$$[LCu^I] = [LCu^I]_{eq} + \alpha$$

$$[O_2] = [O_2]_{eq} + \alpha \qquad \textbf{(9)}$$

$$[LCuO_2] = [LCuO_2]_{eq} - \alpha$$

Substitution of equations **(9)** into equation **(7)** and derivative with respect to α gives the following:

$$- d\alpha / dt = k_{O2} [LCu^I]_{eq} [O_2]_{eq} - k_{-O2} [LCuO_2]_{eq} + k_{O2}\alpha ([LCu^I]_{eq} + [LCuO_2]_{eq}) + k_{O2}\alpha^2 + k_{O2}\alpha$$

The summation of the first two terms on the right side of the equation is zero according to equation **(8)** and the term '$k_{O2}\alpha^2$' can be neglected since α is small. Consequently, the equation becomes:

$$- d\alpha / dt = \alpha (k_{O2} [LCu^{I}]_{eq} + k_{O2} [O_2]_{eq} + k_{-O2})$$

which gives a first order decay of α over time with decay constant:

$$k_{obs} = k_{O2}([LCu^{I}]_{eq} + [O_2]_{eq}) + k_{-O2}$$

In our experiments, $[O_2] >> [LCu^{I}]$ so we can assume that $[LCu^{I}]_{eq} + [O_2]_{eq} \approx [O_2]_0$ where $[O_2]_0$ is the total concentration of O_2 present in solution at all times. The observed rate constant is then

$$k_{obs} = k_{O2} [O_2]_0 + k_{-O2} \qquad \textbf{(10)}$$

Fitting the experimental data ($[O_2]_0$; k_{obs}) with equation **(10)** will, then, give a line with slope k_{O2} and intercept k_{-O2}. The same measurements performed at variable temperature give the corresponding rate constants (k_{O2} and k_{-O2}) and data can be fitted with the Eyring equation $\ln(k\, h / k_B T) = - (\Delta H^{\ddagger} / RT) + (\Delta S^{\ddagger} / R)$ (where h = Planck constant, k_B = Boltzmann constant, T = temperature, and k = rate constant) for both k_{O2} and k_{-O2}.

Equilibrium constants, K_{O2}, were calculated from the ratio k_{O2} / k_{-O2} at each temperature and the relevant Van't Hoff plot was determined.

2.7 Quantum Efficiency Measurements

Samples were prepared by bubbling $O_{2(g)}$ in solutions of [(TMG$_3$tren)Cu^{I}]BArF and [(PV-TMPA)Cu^{I}]BArF in dried and distilled 2-MeTHF at -130^{0}C. The absorbance of the samples at 436 nm and 683 nm (i.e. 0.082 at 683 nm) were monitored using a Cary 50 Bio

spectrophotometer equipped with a liquid nitrogen chilled Unisoku USP-203-A cryostat. Two actinometers were used: $[Ru(bpy)_3]Cl_2$ in CH_3CN at room temperature (RT) for the measurement at 436 nm and $[Os(bpy)_3](PF_6)_2$ in CH_3CN at RT for the measurements at 683 nm and their solutions were prepared to ensure to match the optical density of $[(TMG_3tren)Cu(O_2)]BArF$ and [(PV-TMPA)Cu(O2)]BArF at the relative excitation wavelengths. Data collection for the change in absorbance (ΔA) at the correspondent λ_{max} values (450 nm) where the change in extinction coefficients ($\Delta\varepsilon$) are known was made. The quantum yield at the two excitation wavelengths were calculated with equation **(11)**:

$$\Phi(LCuO_2) = (\Delta A_{450}^{Cu} / \Delta A_{450}^{Actin}) (\Delta\varepsilon_{450}^{Actin} / \Delta\varepsilon_{450}^{Cu}) (n_{MeTHF}^2 / n_{CH3CN}^2) \qquad \textbf{(11)}$$

where 'Actin' is $[Ru(bpy)_3]Cl_2$ in CH_3CN at RT for the 436 nm excitation wavelength and $[Os(bpy)_3](PF_6)_2$ in CH_3CN at RT for the 683 nm excitation wavelength. The values $\Delta\varepsilon_{450}^{[Ru(bpy)3]Cl2} = -10600\ M^{-1}cm^{-1}$,[31] $\Delta\varepsilon_{450}^{[Os(bpy)3](PF6)2} = -7300\ M^{-1}cm^{-1}$,[32] $\Delta\varepsilon_{450}^{Cu} \equiv \Delta\varepsilon_{450}^{[(TMG3tren)Cu(O2)]BArF} = -3134\ M^{-1}cm^{-1}$, and $\Delta\varepsilon_{450}^{Cu} \equiv \Delta\varepsilon_{450}^{[(PV\text{-}TMPA)Cu(O2)]BArF} = 5531\ M^{-1}cm^{-1}$ (determined in this work) where used. For the refractive index, the value 1.34163 for CH_3CN (n_{CH3CN}) at 298.15 K has been used[33] whereas a temperature correction of 0.00045 per Kelvin has been added to the refractive index of 2-MeTHF at 293.15 K (1.40751)[34] to obtain the refractive index which has been used for 2-MeTHF at 143.15 K in equation **(11)** (n_{MeTHF}): 1.40751 + [0.00045·(293.15-143.15)] = 1.47501.

2.8 DFT Calculations

Theoretical studies were carried out by our collaborators, Dr. Dimitrios G. Liakos and Prof. Frank Neese from the Max Planck Institute (Germany) and Jhon E. Zapata Rivera from Universitat Rovira i Virgili (Spain), and the text and figures describing the results come from them. The calculations were performed with the ORCA 2.9.0 program.[35] A DFT spin-unrestricted formalism has been used and the Becke88[36] exchange and Perdew86[36] correlation nonlocal functionals were used as implemented in ORCA (BP86) for geometry optimizations whereas the Becke's three-parameter hybrid functional with the correlation functional of Lee, Yang, and Parr (B3LYP)[37-39] was used for the single point calculations as well as for the relaxed energy scans done to examine the reaction pathway. The def-2-TZVP basis set[40,41] present in ORCA was used for all atoms. Relativistic effects were accounted for through the ZORA[42,43] module implemented in ORCA and also Van der Waals forces[44-46] were considered in the calculations. Relaxed energy scans along the copper-oxygen distance were performed on the ground state triplet potential energy surface of $[(TMG_3tren)Cu(O_2)]^+$.

3. Results and Discussion

3.1 Flash-Photolysis Experiments

Oxygenation of **3** at low temperature in MeTHF was accompanied by a drastic color change of the solution, from colorless to green, forming the previously well characterized compound **1**[47-49] and leading to the red spectrum shown in Figure 1A.

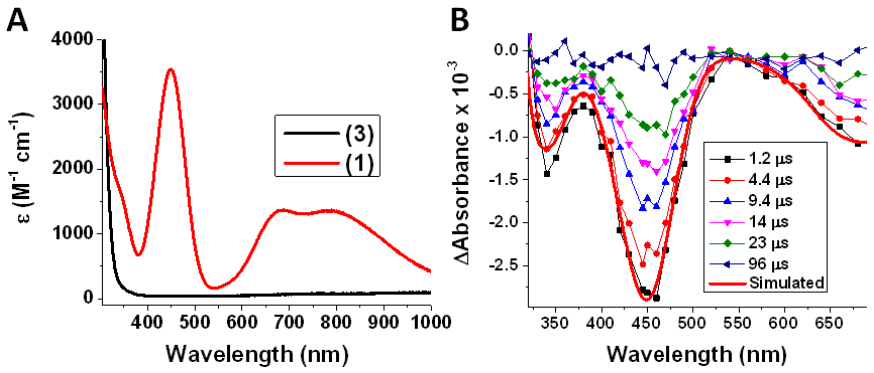

Figure 1. (A) Absorption spectrum of $[(TMG_3tren)Cu^{II}(O_2)]^+$ (**1**) (red line) obtained from oxygenation of $[(TMG_3tren)Cu^{I}]^+$ (**3**) (black line) at 218 K in MeTHF. (B) Transient absorption difference spectra collected at the indicated delay times after 436 nm laser excitation (15 mJ/pulse, 8-10 ns fwhm) of **1** in MeTHF at 218 K. Overlaid in red on the experimental data is a simulated spectrum (Abs(**3**) - Abs(**1**)).

Oxygenation of $[(PV\text{-}TMPA)Cu^{I}]^+$ (**4**) at low temperature also yielded the previously characterized mononuclear copper/O_2 species $[(PV\text{-}TMPA)Cu^{II}(O_2)]^+$ (**2**) (Figure 2A).[25]

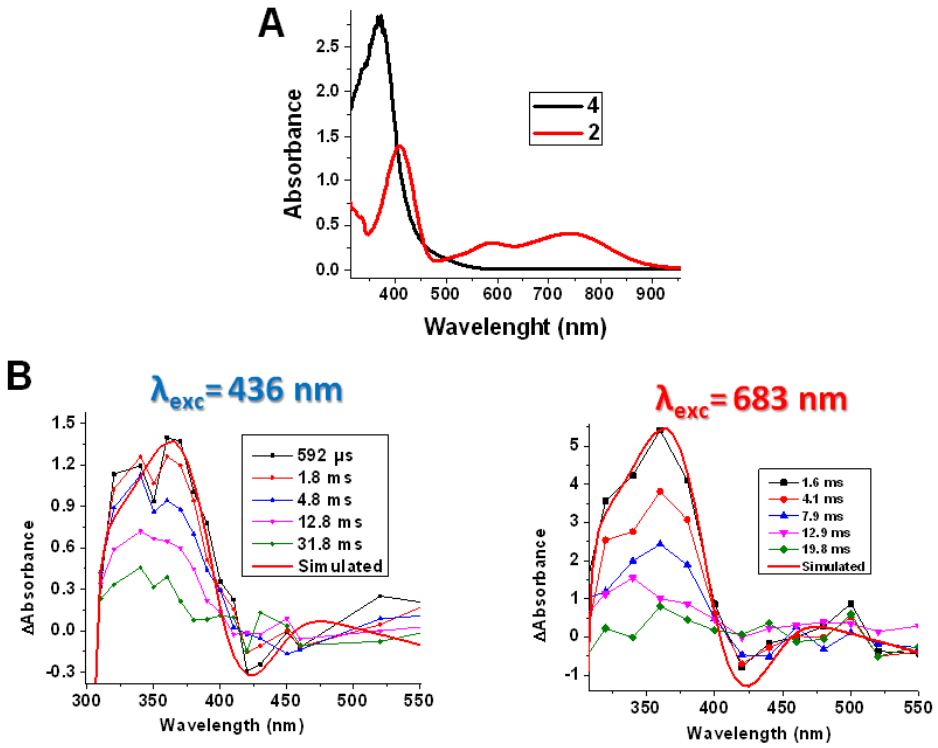

Figure 2. (A) Absorption spectrum of $[(PV\text{-}TMPA)Cu^{II}(O_2)]^+$ (**2**) (red line) obtained from oxygenation of $[(PV\text{-}TMPA)Cu^{I}]^+$ (**4**) (black line) at 143 K in MeTHF. (B) Transient absorption difference spectra collected at the indicated delay times after 436 nm and 683 nm laser excitation of **2** in MeTHF at 143 K. Overlaid in red on the experimental data is a simulated spectrum (Abs(**4**)- Abs(**2**)).

Cleavage of the copper-oxygen bond was, then, induced upon laser excitation of **1** and **2** (λ_{exc} = 436 or 683 nm) as shown by the transient absorption spectral data collected after laser excitation that were in complete agreement with those expected for O_2 photo-release from **1** to yield **3** (Figure 1B) and from **2** to yield **4** (Figure 2B).

The products of the reaction (**3**, O_2 and **4**, O_2, respectively) were excitation wavelength independent (Figures 3 and 2B), although the quantum yields differed markedly: ϕ = 0.29 for **1** and ϕ = 0.11 for **2** (λ_{exc} = 436 nm), ϕ = 0.035 for **1** and ϕ = 0.078 for **2** (λ_{exc} = 683 nm).

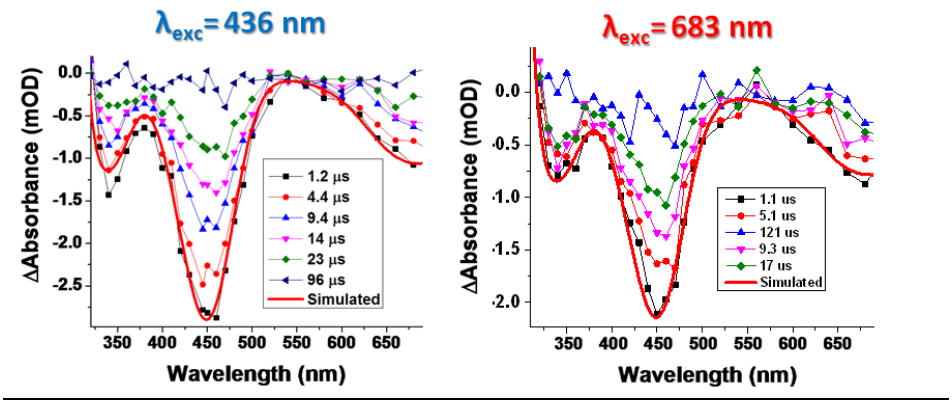

Figure 3. Transient absorption difference spectra collected at the indicated delay times after 436 nm and 683 nm laser excitation of $[(TMG_3tren)Cu^{II}(O_2)]^+$ (**1**) in MeTHF at 218 K. Overlaid in red on the experimental data is a simulated spectrum (Abs($[(TMG_3tren)Cu^{I}]^+$ (**3**))- Abs(**1**)).

The appearance of the products, **3** and **4**, occurred within the instrument response time indicating an O_2 time release of less than 10 ns. The follow-up thermal reaction of $[(TMG_3tren)Cu^{I}]^+$ (**3**) with O_2 led to the formation of the initial compound **1** as shown in Figure 1B. Kinetic parameters for O_2 coordination to **3** were quantified based on microsecond time scale data. Thus, a plot of the observed rate constants versus the O_2 concentration under pseudo-first-order conditions (excess of O_2) revealed a linear correlation (Figure 4) that allowed the determination of the second-order rate constants for O_2 coordinating to **3**, i.e., k_{O2} = 2.1 x 10^6 $M^{-1}s^{-1}$ at –80 °C . For the same temperature, this compares to k_{O2} = 6.6 x 10^5 $M^{-1}s^{-1}$ for **4** (Table 1).

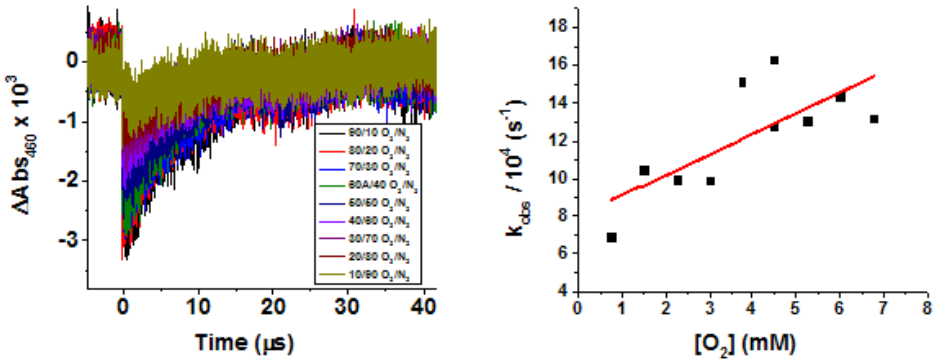

Figure 4. Left: Representative absorption changes monitored at 460 nm at various ratios of $O_{2(g)}/N_{2(g)}$ at -40 ^{0}C in 2-MeTHF for $[(TMG_3tren)Cu^{I}]^+$ (**3**) + O_2. Right: determination of k_{O2} and k_{-O2} fitting data with equation **(10)**.

The linear plots of k_{obs} vs. $[O_2]$ had a positive intercept that was indicative of the presence of an equilibrium between the reacting species, O_2 and $[(TMG_3tren)Cu^{I}]^+$ (**3**). Such a positive intercept was not observed for the coordination of O_2 to $[(PV\text{-}TMPA)Cu^{I}]^+$ (**4**), instead, indicating a quantitative formation of $[(PV\text{-}TMPA)Cu^{II}(O_2)]^+$ (**2**) from reaction of **4** with O_2. Consequently, rate constants for O_2 dissociation from **2** and equilibrium constants for the reaction between **4** and O_2 to give **2** could not be determined here. However, we were able to determine the equilibrium constant, K_{O2}, at several temperatures in MeTHF solvent through benchtop titration experiments for the binding of O_2 to **3**, to give **1** (Figure 5 and Table 1).

Figure 5. Determination of the equilibrium constant for the binding of [(TMG$_3$tren)Cu^{I}]BArF to O_2 at -65^{0}C in 2-MeTHF solvent.

Equilibrium constant values were also determined from laser experiments as follows. Under pseudo-first-order conditions, the rate law for O_2 binding to [(TMG$_3$tren)Cu^{I}]$^+$ (**3**) is expressed by the equation $k_{obs} = k_{O2}[O_2] + k_{-O2}$ where k_{obs} is the observed rate constant, k_{O2} is the second-order rate constant for the binding between **3** and O_2, and k_{-O2} is the first-order rate constant for the dissociation reaction of O_2 from **1** (see section 2.6 of this chapter).

Table 1. Comparison of kinetic and thermodynamic parameters for O_2 binding and dissociation for [(L)Cu] adducts.

TMG_3tren[c]

	k_{O2}	k_{-O2}	K_{O2}
$\Delta H^{\ddagger}$ or ΔH^{0}[a]	10 ± 6	45 ± 7	-40 ± 2
$\Delta S^{\ddagger}$ or ΔS^{0}[b]	-70 ± 26	42 ± 34	-134 ± 11
k or K 25°C	$(2.7 \pm 1.2)\cdot 10^{7}$	$(1.5 \pm 0.8)\cdot 10^{7}$	≈ 1
k or K -80°C	$(2.1 \pm 1.0)\cdot 10^{6}$	$(5.2 \pm 2.0)\cdot 10^{2}$	$(6.3 \pm 1.9)\cdot 10^{3}$

PV-TMPA[c]

	k_{O2}	k_{-O2}	K_{O2}
$\Delta H^{\ddagger}$ or ΔH^{0}[a]	9 ± 1	-	-
$\Delta S^{\ddagger}$ or ΔS^{0}[b]	-97 ± 7	-	
k or K 25°C	$(4.8 \pm 2.8)\cdot 10^{7}$	-	-
k or K -80°C	$(6.6 \pm 3.5)\cdot 10^{5}$	-	-

TMPA[d]

	k_{O2}	k_{-O2}	K_{O2}
$\Delta H^{\ddagger}$ or ΔH^{0}[a]	7.62	58.0	-48.5
$\Delta S^{\ddagger}$ or ΔS^{0}[b]	-45.1	105	-140
k or K 25°C	$1.3\cdot 10^{9}$	$1.3\cdot 10^{8}$	15.4
k or K -80°C	$1.4\text{-}1.6\cdot 10^{8}$	240	$6.5\cdot 10^{5}$

[a] ΔH, kJ mol^{-1} [b] ΔS, J K^{-1} mol^{-1} [c] In MeTHF, this work [d] In THF, determined through flash-and-trap method.[50] Values for [(TMPA)-Cu] in MeTHF have been found to be the same as in THF within experimental errors.[51]

The values of k_{-O2} and k_{O2} were determined from laser experiments, as a function of temperature through which the equilibrium constants were determined from the ratio k_{O2} / k_{-O2}. Van't Hoff analysis of the equilibrium constants determined with the two different methods (titration experiments and laser experiments) led to the same thermodynamic parameters within the experimental errors and are consistent with values found in a previous report by Roth and co-workers (Table 2 and Figure 6 and 7).

Table 2. Comparison of thermodynamic parameters for O_2 binding to $[(TMG_3tren)Cu^I]^+$ determined with two different methods in 2-MeTHF solvent.

Experiment	$\Delta H^{0,a}$	$\Delta S^{0,b}$
Laser (λ_{exc}=436 nm)	-35 ± 7	-112 ± 35
Benchtop Titration	-40 ± 2	-134 ± 11
Previous work[52]	-35 ± 3	-96 ± 13

[a]ΔH^0 values are in kJ mol^{-1}[b]ΔS^0 values are in J K^{-1}mol^{-1}.

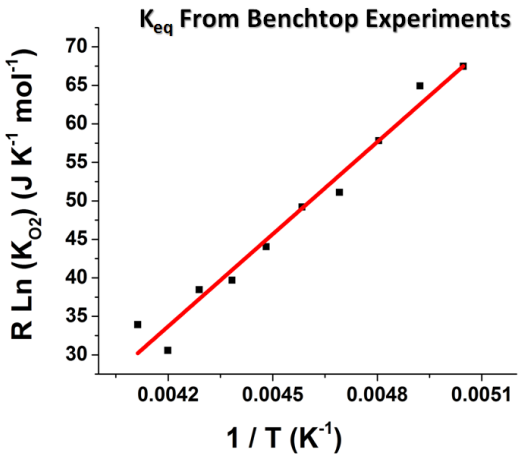

Figure 6. Van't Hoff plot for the variable temperature K_{O2} data for the binding of $[(TMG_3tren)Cu^I]$BArF to O_2 in 2-MeTHF solvent.

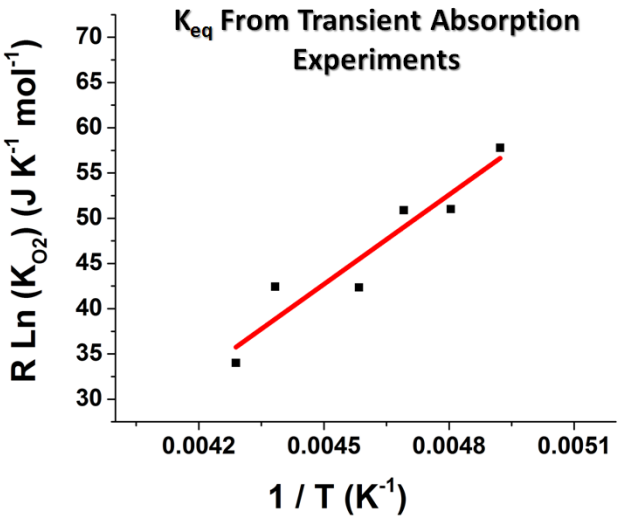

Figure 7. Van't Hoff plot for the equilibrium constants K_{O2} determined through transient absorption spectroscopy.

Furthermore, equilibrium constants found in this work follow a trend with solvent dielectric constant (***ε***) that was previously established. The equilibrium constant should favor the superoxide adduct as ***ε*** increases because of the stabilization of the charge separation present in $[(TMG_3tren)Cu^{II}(O_2)]^+$ (**1**). In fact, the equilibrium constant for the formation of **1** (K_{O2}) determined here at -60^{0}C fits well into a linear correlation together with the previously determined K_{O2} values in DMF (3030 and 4340)[52] and in chlorobenzene (216)[52,53] at -60^{0}C as a function of ***ε*** (Figure 8).

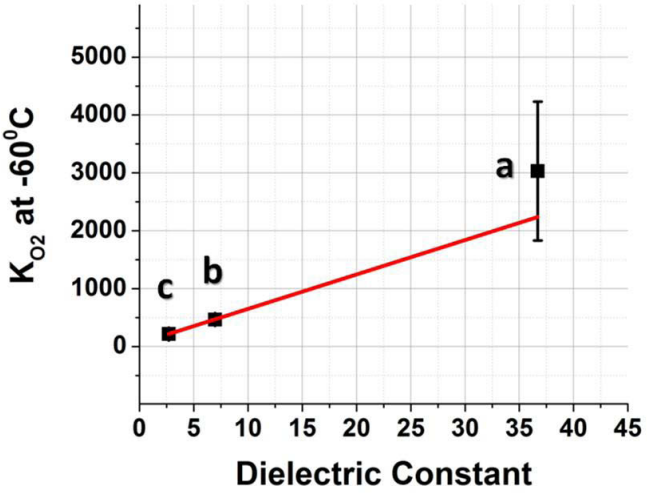

Figure 8. K_{O2} values determined at -60^{0}C in different solvents as follows: a) K_{O2}(DMF) = 3030 ± 4340 from Lanci et al. *J. Am. Chem. Soc.* 2007, 129, 14697; b) K_{O2}(MeTHF) = 467 ± 26 determined in this work; c) K_{O2}(chlorobenzene) = (K_{O2}(DMF) / 14) = 216 estimated from Lanci et al. *J. Am. Chem. Soc.* 2007, 129, 14697 and Lide, D. R. CRC Handbook of Chemistry and Physics, 74th ed.; CRC Press: Boca Raton, 1993. Dielectric constants for DMF, MeTHF, and chlorobenzene were taken as 37, 7, and 2.7, respectively.

Eyring analysis of the rate constants for both O_2 binding to $[(TMG_3tren)Cu^I]^+$ (**3**) and $[(PV\text{-}TMPA)Cu^I]^+$ (**4**) (k_{O2}) and O_2 dissociation from $[(TMG_3tren)Cu^{II}(O_2)]^+$ (**1**) (k_{-O2}) determined in the temperature range of -40^{0}C to -70^{0}C for **1** and **3** (Figure 9) and of -125^{0}C to -135^{0}C for **4** and (Figure 10) yielded the activation parameters shown in Table 1.

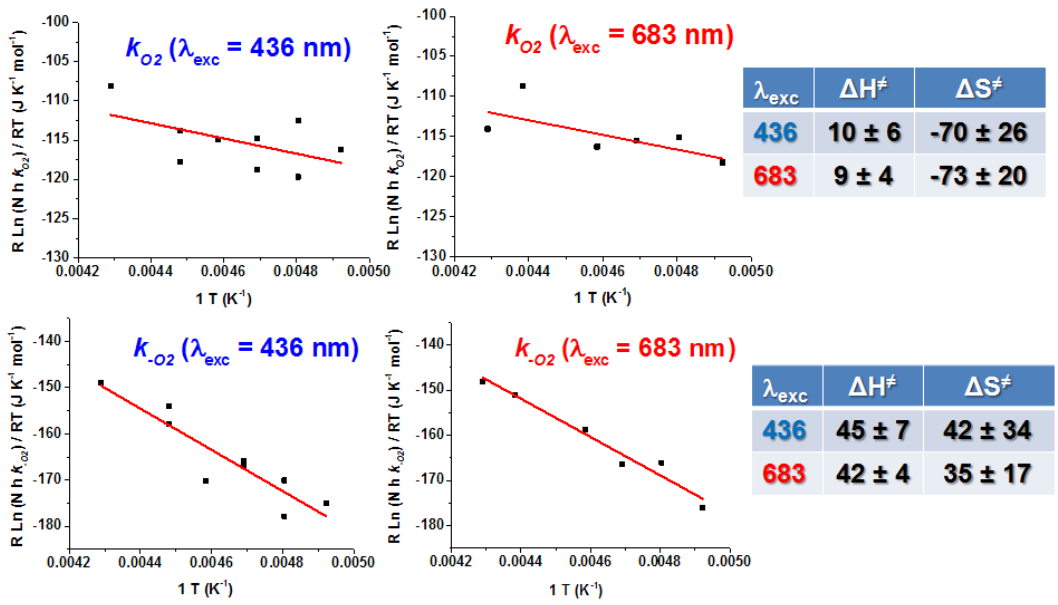

λ_{exc}	$\Delta H^{\neq}$	$\Delta S^{\neq}$
436	10 ± 6	-70 ± 26
683	9 ± 4	-73 ± 20

λ_{exc}	$\Delta H^{\neq}$	$\Delta S^{\neq}$
436	45 ± 7	42 ± 34
683	42 ± 4	35 ± 17

Figure 9. Determination of the activation parameters from the rate constants k_{O2} and k_{-O2} for $[(TMG_3tren)Cu^{I}]^{+}$ (**3**) and $[(TMG_3tren)Cu^{II}(O_2)]^{+}$ (**1**).

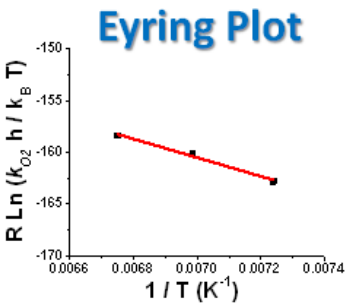

	k_{O2} (M^{-1} s^{-1})	
T (^{0}C)	PVTMPA	TMG_3tren
-125	(1.9 ± 0.2)·10^4	-
-130	(1.3 ± 0.1)·10^4	(1.9 ± 0.9)·10^5
-135	(9.1 ± 1.4)·10^3	-

Figure 10. Determination of the activation parameters for the reaction between $[(PV\text{-}TMPA)Cu^{I}]^{+}$ (**4**) and O_2 following laser excitation (λ_{exc} = 436 nm) of $[(PV\text{-}TMPA)Cu^{II}(O_2)]^{+}$ (**2**) in the temperature range 138 K to 148 K in MeTHF and comparison with the rate constant for the reaction between **4** and O_2 extrapolated at 143 K.

It is worthwhile to mention that the activation parameters found for $[(PV\text{-}TMPA)Cu^{I}]^{+}$ (**4**) represent an estimate as the second-order rate constants for O_2 coordination to **4** were determined at only three temperatures due to the instability of **4** above -125^{0}C in MeTHF. A comparison of activation and thermodynamic parameters determined in this study with those previously reported for the $[(TMPA)Cu^{II}(O_2)]^{+}$ adduct in MeTHF using $[(TMPA)Cu^{I}(CO)]^{+}$ and the 'flash-and-trap' method are also given in Table 1 (see Chart 1 for structure of ligands).

Chart 1. Structure of ligands for this work compared to the 'parent' TMPA ligand.

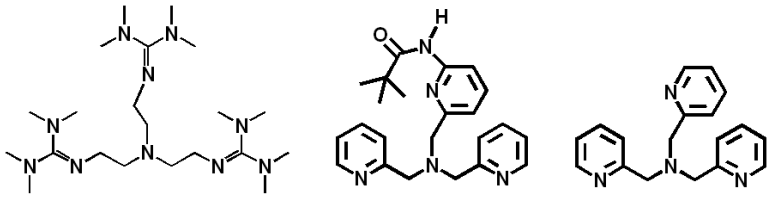

This TMPA-containing complex has been very well studied and it is the 'parent' ligand of PV-TMPA.[1a,14,15] The 'flash-and-trap' experiments, previously employed for $[(L)Cu^{I}(CO)]^{+}$ (L = ligand) compounds, allowed characterization of O_2 binding to copper(I) after CO photo-release through competitive coordination of CO and O_2.[50,54] The kinetic data obtained through the direct O_2 photo-ejection method described here are more straightforward to analyze compared to that of the 'flash-and-trap' method where the competitive binding of CO needs to be taken into account. Furthermore, in fast time scale studies of heme-copper

oxidases, it has been shown that the presence of CO and starting with a metal-CO adduct may interfere or alter the mechanism or rate of O_2 binding.[55]

The activation parameters found for the compounds studied here are quite similar to those determined for compounds using the flash-and-trap method. TMG_3tren, PV-TMPA, and TMPA offer an analogous coordination sphere to the copper all being tetradentate chelating ligands and it is reasonable to expect similar behavior of these copper compounds in the same experimental conditions (solvent, temperature, etc...). We interpret these consistencies as a strong evidence for the reliability of the new method we have employed here to study the reactivity of mononuclear copper compounds with O_2. The activation enthalpy found for the binding of O_2 to $[(TMG_3tren)Cu^I]^+$ (**3**) and $[(PV\text{-}TMPA)Cu^I]^+$ (**4**) falls within the same range (~ 10 kJ mol^{-1}). On the basis of the crystal structure of the starting compound $[(PV\text{-}TMPA)Cu^I]^+$,[25] the coordination within **4** mostly likely also includes an interaction between the copper(I) ion and the O-atom of the pivilamido group. As a consequence, one would expect a greater activation enthalpy for the reaction between O_2 and **4** compared with that between O_2 and **3** as the Cu(I)-O interaction needs to be 'disrupted' by the O_2 coordination to the copper only for **4** and not for **3**. Since the $\Delta H^{\ddagger}$ values for the binding of O_2 to **3** and **4** fall, instead, into the same range, this suggests a quite weak interaction for the $Cu^I\text{-}O_{(carbonyl)}$ coordination in **4**. The activation entropy estimated for the reaction involving O_2 coordination to **3** and to **4** is, instead, smaller for the latter. This suggests a mechanism where O_2 coordination to **4** leads to a 'highly ordered' transition state where <u>both</u> O_2 and the pivalamido O-atom are interacting with the copper center; for O_2 reacting with **3**, there is of course no pivalamido group present. The activation enthalpy and entropy for O_2 coordination to $[(TMPA)Cu^I]^+$ previously determined (Table 1) are smaller and less negative, respectively, compared with those found for **3** and **4**. The smaller

activation enthalpy for the binding of O_2 to $[(TMPA)Cu^{I}]^{+}$ can be interpreted on the basis of a stronger Cu-O_2 interaction in the transition state for $[(TMPA)Cu^{I}]^{+}$ compared to that for **3** and **4** due to an 'easier' spatial approach of O_2 to the copper(I) in $[(TMPA)Cu^{I}]^{+}$. In fact, the presence of guanidino groups which extend out away from the copper and its ligands in **3**, and of the Cu^{I}-$O_{(carbonyl)}$ coordination, in **4**, could explain or help support this hypothesis. The less negative activation entropy found for the coordination of O_2 to $[(TMPA)Cu^{I}]^{+}$ can be explained, instead, accounting for the smaller molecular reorganization occurring upon O_2 binding to $[(TMPA)Cu^{I}]^{+}$ due to the absence of guanidino groups or specific Cu(I)-O interactions in $[(TMPA)Cu^{I}]^{+}$ compared with **3** and **4**. Similar arguments can be used to explain the difference between the activation enthalpy found for the O_2 dissociation from $[(TMPA)Cu^{II}(O_2)]^{+}$ with the 'flash-and-trap' method and those found, here, for **1** and **2**, although the large activation entropy found for O_2 dissociation from $[(TMPA)Cu^{II}(O_2)]^{+}$ seems difficult to explain.

3.2 DFT and TD-DFT Calculations

TD-DFT calculations carried out here were aimed to shed light on the photochemically initiated O_2 dissociation and its observed excitation wavelength dependence. Findings from these TD-DFT calculations were in line with the previously assigned electronic ground state for $[(TMG_3tren)Cu^{II}(O_2)]^{+}$ (**1**).[49,52,56,57] In this rather peculiar electronic structure, the central copper ion is in a d^9 configuration and it is coordinated to a superoxide ligand. The singly occupied MOs (SOMOs) are of copper $3d_{z2}$ and $O_2^{\bullet-}$-π^*_v character. The orthogonality of these two orbitals leads to a S = 1 ground state multiplicity in which the spin in both SOMOs are aligned parallel (Figure 11).

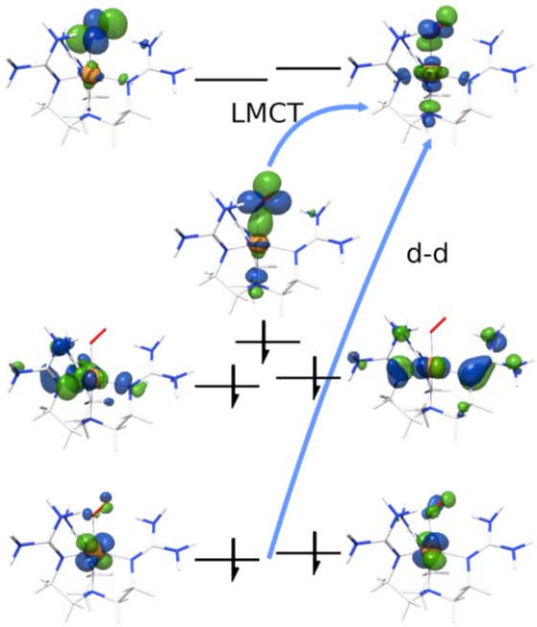

Figure 11. Localized orbital description for $[(TMG_3tren)Cu(O_2)]^+$ (**1**).

In a spin-unrestricted description, the highest occupied spin-down orbital has mainly oxygen π^*_σ-character and it is bonding with respect to the Cu^{II}-superoxide Cu-O bond. The lowest unoccupied orbitals in the spin-down manifold are the empty partner orbitals of the two SOMOs. Importantly, the unoccupied $3d_{z2}$ orbital is strongly σ-antibonding with respect to the Cu-O bond. Excitation from the bonding π^*_σ-based orbital to the antibonding d_{z2} orbital corresponds to a ligand-to-metal charge transfer (LMCT) excitation that formally leads to a Cu(I)-$^3O_2$ electronic configuration. Importantly, this state leads to a dramatic weakening of the Cu-O bond to the point that the excited state becomes dissociative (Figure 12).

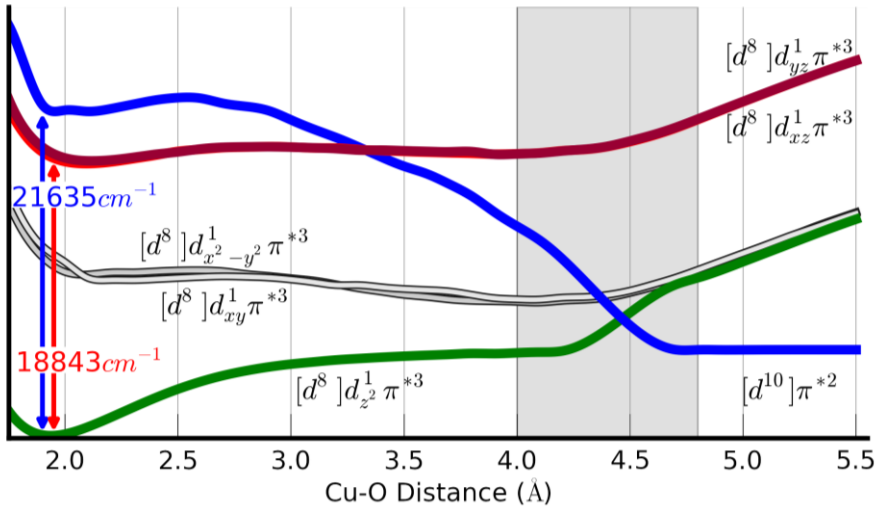

Figure 12. TD-DFT calculated excited state potential energy surfaces (PESs) as a function of copper-oxygen bond distance.

According to TD-DFT calculations, the position of the vertical LMCT excitation occurs at 21635 cm^{-1}, in reasonable agreement with the band maximum around 22900 cm^{-1}. Slightly lower in energy are a pair of nearly degenerate d-d excitations from the d_{xz}/d_{yz}-based orbitals, again, to the d_{z2}-based orbital.

As it is evident from Figure 13, the energies of the d_{z2} and π^* orbitals are, upon elongation of the Cu-O bond, resulting in a change from a triplet superoxide ground state $[d^8]\ d_{z2}^1\pi^{*3}$ to a triplet $d^{10}\pi^{*2}$ state.

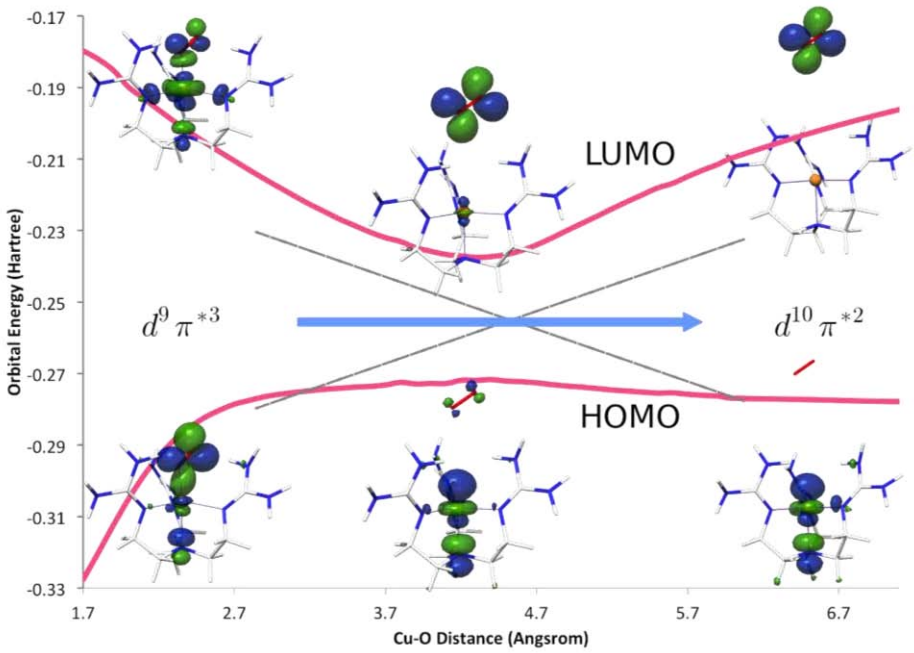

Figure 13. TD-DFT calculated energy and shape of the beta HOMO and beta LUMO orbitals as a function of copper-oxygen bond distance.

The triplet ground state potential energy surface of $[(TMG_3tren)Cu^{II}(O_2)]^+$ (**1**) (Figure 12, green line) shows a minimum at a Cu-O distance of about 1.9 Å. The calculated excited state energy at the same Cu-O bond distance was 18843 cm^{-1} (530 nm) for the d-d and 21635 cm^{-1} (462 nm) for the LMCT excited states and consistent with the experimentally observed electronic transitions for these states. Moreover, the character of both excited states at a Cu-O bond distance of 1.9 Å is dissociative (Figure 12). The LMCT excited state (blue line) crosses the ground state at a Cu-O distance of about 4.5 Å. Although the energy of the d-d excited states (red lines) also decreases at short Cu-O distances due to the weakened ligand field upon $Cu\text{-}O_2$ bond lengthening, it never reaches the ground state energy, instead. However, as the dissociative LMCT state crosses the d-d excited states there is an

opportunity for the system to cross from one of the d-d excited surfaces to the dissociative LMCT surface. Hence, there can also be O_2 dissociation following d-d excitation, provided that these states live long enough to reach the crossing regime. The exact crossing will probability depend on many details the discussion of which is outside the scope of this work. Given the finite probability for surface hopping much lower quantum yields are expected for the d-d states. This is in agreement with the observations for O_2 photo-release observed experimentally following excitation of **1** with either red (ϕ_{683} = 0.035) or blue light (ϕ_{436} = 0.29). The theoretical results are also consistent with the activation enthalpy for the O_2 dissociation from **1** observed experimentally ($\Delta H^{\ddagger}_{experim}$ = 45 kJ mol^{-1} vs. $\Delta H^{\ddagger}_{comput}$ = 67 kJ mol^{-1}).

Finally, the crossing between the ground state (Figure 12, in green) and LMCT (Figure 12, in blue) surfaces explains the fact that an association barrier is observed. The calculated barrier from TD-DFT (~ 24 kJ mol^{-1}) is in the right ballpark but slightly overestimates the experimentally measured barrier (~ 10 kJ mol^{-1}).

4. Conclusions

Summarizing, we report here the first example of a photodissociation of molecular oxygen from cupric-superoxide complexes, thus also representing a new approach to study the kinetics and the thermodynamics of formation of 1:1 L-copper(I)/O_2 compounds. Copper-oxygen bond breaking is induced in [(TMG$_3$tren)Cu^{II}(O_2)]$^+$ (**1**) and [(PV-TMPA)Cu^{II}(O_2)]$^+$ (**3**) through laser excitation either into the LMCT band, using 436 nm light, or into the d-d electronic transitions, using 683 nm light. Interestingly, the yield of O_2

release was wavelength-dependent. Such a wavelength dependence differs markedly from that observed with hemes. For example, the O_2 adduct of myoglobin photo-released O_2 results in a quantum yield of 0.3 with Soret (λ_{exc} = 488 nm) and Q (λ_{exc} = 580 nm) band excitation.[22] Formation and decay of $[(TMG_3tren)Cu^I]^+$ and $[(PV\text{-}TMPA)Cu^I]^+$ formed *in situ* have been observed and both activation and thermodynamic parameters for the Cu/O_2 reactions have been determined. TD-DFT calculations reveal that only the LMCT state is dissociative. However, surface hopping can explain the observed photodissociation upon d-d excitations. Additional experimental studies are on their way to further characterize the excited states involved in the copper-oxygen bond breaking process using ultra-fast laser spectroscopy.

5. Acknowledgments

The following co-authors contributed to the work presented in this chapter:

Dimitrios G. Liakos, Jhon E. Zapata Rivera, Frank Neese, Gerald J. Meyer, and Kenneth D. Karlin

6. References

(1) Fukuzumi, S.; Karlin, K. D. *Coord. Chem. Rev.* **2013**, *257*, 187.

(2) Himes, R. A.; Karlin, K. D. *Curr. Opin. Chem. Biol.* **2009**, *13*, 119.

(3) Solomon, E. I.; Ginsbach, J. W.; Heppner, D. E.; Kieber-Emmons, M. T.; Kjaergaard, C. H.; Smeets, P. J.; Tian, L.; Woertink, J. S. *Faraday Discuss.* **2011**, *148*, 11.

(4) Allen, S. E.; Walvoord, R. R.; Padilla-Salinas, R.; Kozlowski, M. C. *Chem. Rev.* **2013**, *113*, 6234.

(5) Maiti, D.; Lee, D.; Gaoutchenova, K.; Würtele, C.; Holthausen, M. C.; Sarjeant, A. A. N.; Sundermeyer, J.; Schindler, S.; Karlin, K. D. *Angew. Chem., Int. Ed.* **2008**, *47*, 82.

(6) Maiti, D.; Narducci Sarjeant, A. A.; Karlin, K. D. *Inorg. Chem.* **2008**, *47*, 8736.

(7) Comba, P.; Knoppe, S.; Martin, B.; Rajaraman, G.; Rolli, C.; Shapiro, B.; Stork, T. *Chem. Eur. J.* **2008**, *14*, 344.

(8) Decker, A.; Solomon, E. I. *Curr. Opin. Chem. Biol.* **2005**, *9*, 152.

(9) Yoshizawa, K.; Kihara, N.; Kamachi, T.; Shiota, Y. *Inorg. Chem.* **2006**, *45*, 3034.

(10) Crespo, A.; Marti, M. A.; Roitberg, A. E.; Amzel, L. M.; Estrin, D. A. *J. Am. Chem. Soc.* **2006**, *128*, 12817.

(11) Huber, S. M.; Ertem, M. Z.; Aquilante, F.; Gagliardi, L.; Tolman, W. B.; Cramer, C. J. *Chem. Eur. J.* **2009**, *15*, 4886.

(12) Blackburn, N.; Rhames, F.; Ralle, M.; Jaron, S. *J. Biol. Inorg. Chem.* **2000**, *5*, 341.

(13) Prigge, S. T.; Mains, R. E.; Eipper, B. A.; Amzel, L. M. *Cell Mol. Life Sci.* **2000**, *57*, 1236.

(14) Stewart, L. C.; Klinman, J. P. *Annu. Rev. Biochem.* **1988**, *57*, 551.

(15) Evans, J. P.; Ahn, K.; Klinman, J. P. *J. Biol. Chem.* **2003**, *278*, 49691.

(16) Klinman, J. P. *Chem. Rev.* **1996**, *96*, 2541.

(17) Klinman, J. P. *J. Biol. Chem.* **2006**, *281*, 3013.

(18) Bauman, A. T.; Yukl, E. T.; Alkevich, K.; McCormack, A. L.; Blackburn, N. J. *J. Biol. Chem.* **2006**, *281*, 4190.

(19) Chen, P.; Solomon, E. I. *J. Am. Chem. Soc.* **2004**, *126*, 4991.

(20) Cramer, C. J.; Tolman, W. B. *Acc. Chem. Res.* **2007**, *40*, 601.

(21) Chen, P.; Bell, J.; Eipper, B. A.; Solomon, E. I. *Biochemistry* **2004**, *43*, 5735.

(22) Ye, X.; Demidov, A.; Champion, P. M. *J. Am. Chem. Soc.* **2002**, *124*, 5914.

(23) Raab, V.; Kipke, J.; Burghaus, O.; Sundermeyer, J. *Inorg. Chem.* **2001**, *40*, 6964.

(24) Liang, H. C.; Kim, E.; Incarvito, C. D.; Rheingold, A. L.; Karlin, K. D. *Inorg. Chem.* **2002**, *41*, 2209.

(25) Peterson, R. L.; Himes, R. A.; Kotani, H.; Suenobu, T.; Tian, L.; Siegler, M. A.; Solomon, E. I.; Fukuzumi, S.; Karlin, K. D. *J. Am. Chem. Soc.* **2011**, *133*, 1702.

(26) Fischer, K.; Wilken, M. *J. Chem. Thermodyn.* **2001**, *33*, 1285.

(27) Battino, R. IUPAC Solubility Data Series: Oxygen and Ozone; Pergamon: Oxford, New York **1981**.

(28) Argazzi, R.; Bignozzi, C. A.; Heimer, T. A.; Castellano, F. N.; Meyer, G. J. *J. Phys. Chem.* **1994**, *33*, 5741.

(29) Eigen, M.; DeMayer, L. 'Techniques of Organic Chemistry', Vol VIII, Part 2, Chapter 18 (Eds., Friess, S.L., Lewis, E.S., and Weissberger, A.) , Wiley Interscience, New York **1963**.

(30) Czerlinski, G. H. 'Chemical Relaxation', Dekker, New York **1966**.

(31) Yoshimura, A.; Hoffman, M. Z.; Sun, H. *J. Photochem. Photobiol. A* **1993**, *70*, 29.

(32) Bergeron, B. V.; Kelly, C. A.; Meyer, G. J. *Langmuir* **2003**, *19*, 8389.

(33) Iloukhani, H.; Almasi, M. *Thermochim. Acta* **2009**, *495*, 139.

(34) Preus, S.; Kilsa, K.; Wilhelmsson, L. M.; Albinsson, B. *Phys. Chem. Chem. Phys.* **2010**, *12*, 8881.

(35) Neese, F. *ORCA,* version 2.9.0; Max-Planck Institut für Bioanorganische Chemie: Mülheim, Germany.

(36) Perdew, J. P. *Phys. Rev. B* **1986**, *33*, 8822.

(37) Becke, A. D. *Phys. Rev. A* **1988**, *38*, 3098.

(38) Becke, A. D. *J. Chem. Phys.* **1993**, *98*, 1372.

(39) Becke, A. D. *J. Chem. Phys.* **1993**, *98*, 5648.

(40) Schaefer, A.; Horn, H.; Ahlrichs, R. *J. Chem. Phys.* **1992**, *97*, 2571.

(41) Weigend, F.; Ahlrichs, R. *Phys. Chem. Chem. Phys.* **2005**, *7*, 3297.

(42) van Lenthe, E.; Baerends, E. J.; Snijders, J. G. *J. Chem. Phys.* **1993**, *99*, 4597.

(43) van Wullen, C. *J. Chem. Phys.* **1998**, *109*, 392.

(44) Grimme, S.; Anthony, J.; Ehrlich, S.; Krieg, H. *J. Chem. Phys.* **2010**, *132*, 154104.

(45) Grimme, S. *J. Comput. Chem.* **2006**, *27*, 1787.

(46) Grimme, S. *J. Comput. Chem.* **2004**, *25*, 1463.

(47) Schatz, M.; Raab, V.; Foxon, S. P.; Brehm, G.; Schneider, S.; Reiher, M.; Holthausen, M. C.; Sundermeyer, J.; Schindler, n. *S Angew. Chem., Int. Ed.* **2004**, *43*, 4360.

(48) Würtele, C.; Gaoutchenova, E.; Harms, K.; Holthausen, M. C.; Sundermeyer, J.; Schindler, S. *Angew. Chem. Int. Ed.* **2006**, *45*, 3867.

(49) Woertink, J. S.; Tian, L.; Maiti, D.; Lucas, H. R.; Himes, R. A.; Karlin, K. D.; Neese, F.; Würtele, C.; Holthausen, M. C.; Bill, E.; Sundermeyer, J. r.; Schindler, S.; Solomon, E. I. *Inorg. Chem.* **2010**, *49*, 9450.

(50) Fry, H. C.; Scaltrito, D. V.; Karlin, K. D.; Meyer, G. J. *J. Am. Chem. Soc.* **2003**, *125*, 11866.

(51) Data will be published in future works.

(52) Lanci, M. P.; Smirnov, V. V.; Cramer, C. J.; Gauchenova, E. V.; Sundermeyer, J.; Roth, J. P. *J. Am. Chem. Soc.* **2007**, *129*, 14697.

(53) Lide, D. R. *CRC Handbook of Chemistry and Physics, 74th ed.; CRC Press: Boca Raton* **1993**.

(54) Lucas, H. R.; Meyer, G. J.; Karlin, K. D. *J. Am. Chem. Soc.* **2010**, *132*, 12927.

(55) Einarsdóttir, Ó.; Funatogawa, C.; Soulimane, T.; Szundi, I. *BBA-Bioenergetics* **2012**, *1817*, 672.

(56) Poater, A.; Cavallo, L. *Inorg. Chem.* **2009**, *48*, 4062.

(57) Zapata-Rivera, J.; Caballol, R.; Calzado, C. J. *J. Comput. Chem.* **2011**, *32*, 1144.

Chapter 4:

One-Photon Two-Electron Oxidation of Peroxide to O_2 from Dicopper(II) Compounds

Abstract

Absorption of a single visible photon by the binuclear copper(II) μ–η^2-η^2-(side-on) peroxo compounds $[(N3)Cu^{II}_2(O_2)]^{2+}$ (**1**) and $[(N5)Cu^{II}_2(O_2)]^{2+}$ (**2**) resulted in two-electron transfer oxidation of the peroxo moiety by the dicopper(II) moiety and liberation of dioxygen gas, whereas light excitation of the dicopper peroxo compounds with a μ-1,2-(end-on) binding mode, $[(TMPA)Cu^{II}_2(O_2)]^{2+}$ (**3**) and $[(PV\text{-}TMPA)Cu^{II}_2(O_2)]^{2+}$ (**4**), did not result in the release of dioxygen. The second-order rate constants for O_2 coordination to the dicopper centers were determined as k_{O2} = 1.5 × 10^4 M^{-1} s^{-1}, at –80 °C, which increased to k_{O2} = (0.32–2.8) × 10^7 M^{-1} s^{-1} at 21^{0}C extrapolated by employing the activation parameters, also determined. The results provide rare examples of two-electron transfer chemistry triggered by absorption of a single photon.

1. Introduction

Single photon absorption followed by electron transfer generates one reducing and one oxidizing equivalent. The accumulation of more in molecular assemblies, through sequential photon absorption and electron transfer reactions, has proven to be difficult.[1] This is unfortunate as most reactions that yield useful fuels require multi-electron transfer chemistry.[2,3] A case in point is solar water oxidation that in addition to proton management requires four redox equivalents: two to form the O-O bond in peroxide; and an additional two to yield dioxygen gas.[4-13] The last two are particularly important as the release of peroxide or superoxide can give rise to unwanted radical chemistry.[14] Here we report that upon absorption of a single photon, the final two electrons can be transferred from peroxide to copper to liberate O_2 gas from well-defined dicoppper peroxo compounds. The dicopper peroxo compounds displayed peroxide-to-copper charge transfer absorption bands that harvest light across the entire visible region. The data suggests that this photoreactivity provides a unique example of multi-electron transfer chemistry initiated by absorption of a single photon.[15-17]

2. Experimental

2.1 Materials

All materials purchased were of the highest purity available from Sigma-Aldrich Chemical or Tokyo Chemical Industry (TCI) and were used as received, unless specified otherwise. Tetrahydrofuran was distilled under an inert atmosphere from Na/benzophenone and degassed with argon prior to use. Pentane and acetone were freshly distilled from calcium hydride and calcium sulfate, respectively, under an inert atmosphere and degassed prior to use. The N3 and N5 ligands were synthesized according with literature procedures.[18]

2.2 Synthetic Procedures

$[(N3)Cu^{I}_{2}(CH_3CN)_2](BArF)_2$ and $[(N5)Cu^{I}_{2}(CH_3CN)_2](BArF)_2$ (BArF = $B(C_6F_5)_4$) were synthesized by adding $[Cu^{I}(CH_3CN)_4](BArF)$ (410 mg, 0.452 mmol) to either N3 (114 mg, 0.230 mmol) or N5 (120 mg, 0.230 mmol) and in dry, air-free tetrahydrofuran (THF) (15 mL) and the resulting solution was allowed to stir for 30 minutes. The isolation of the compounds was afforded by precipitation, under argon atmosphere, by addition of dry, deoxygenated pentane (60 mL). The yellow powder obtained were made to re-precipitate from THF/pentane (10 mL / 60 mL) for three times, in both cases. Identity and purity of the compounds were verified by elemental analysis and/or ^{1}H-NMR spectroscopy as follows:

$[(N3)Cu^{I}_{2}(CH_3CN)_2](BArF)_2$

^{1}H-NMR (CD_3NO_2, Figure 1): δ 8.65-8.58 (4 H, py-6, d), 8.98-7.9 (4 H, py-4, t), 7.5-7.3 (8 H, py-3, py-5, br d). 3.3-3.0 (8 H, s), 3.0-2.6 (8 H, br s), 2.5-2.35 (4 H, t), 2.1-1.9 (6 H,

CH_3CN, s), 1.6-1.3 (2 H, s). Anal. Calcd for ($C_{83}H_{44}B_2Cu_2F_{40}N_8$): C, 48.35; H, 2.15; N, 5.43. Found: C, 47.41; H, 2.10; N, 4.41.

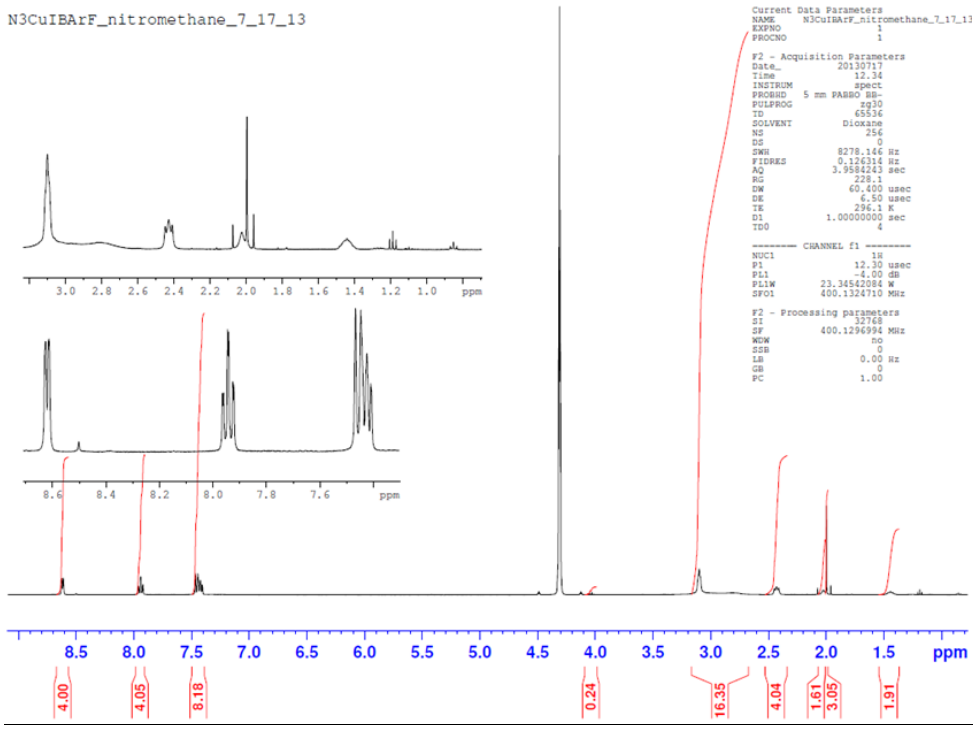

Figure 1. ^{1}H NMR (CD_3NO_2) of $[(N3)Cu^I_2(CH_3CN)_2](BArF)_2$.

$[(N5)Cu^I_2(CH_3CN)_2](BArF)_2$

^{1}H-NMR (CD_3NO_2, Figure 2): δ 8.71-8.63 (4 H, py-6, d), 8.0-7.92 (4 H, py-4, t), 7.53-7.4 (8 H, py-3, py-5, m). 3.3-3.0 (8 H, s), 3.0-2.6 (8 H, br s), 2.45-2.3 (4 H, s), 2.0 (6 H, CH_3CN,

s), 1.3-1.1 (4 H, s) , 1.1-1.0 (2 H, s). Anal. Calcd for ($C_{85}H_{48}B_2Cu_2F_{40}N_8$): C, 48.85; H, 2.31; N, 5.36. Found: C, 47.67; H, 2.48; N, 4.42.

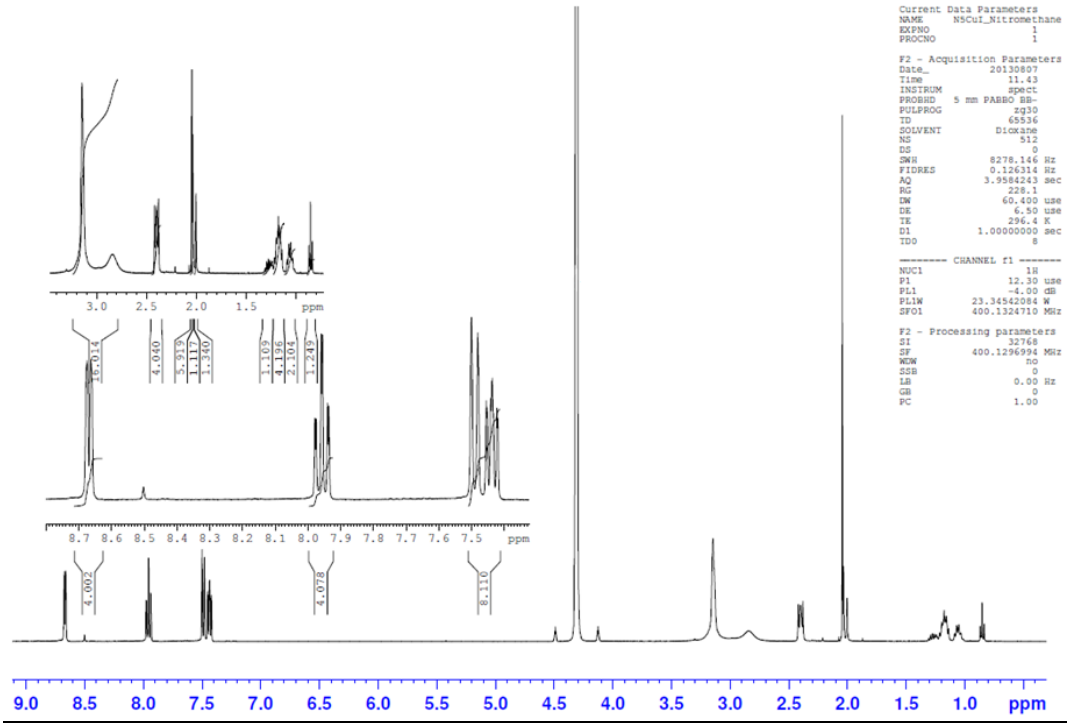

Figure 2. ^{1}H NMR (CD_3NO_2) of $[(N5)Cu^I_2(CH_3CN)_2](BArF)_2$.

$[Cu^I(CH_3CN)_4](BArF)$ was synthesized according with previous procedures.[19] Synthesis and manipulations of copper salts were performed according to standard Schlenk techniques or in an MBraun glovebox (with O_2 and H_2O levels below 1 ppm). UV-Vis spectra were recorded with a Cary 50 Bio spectrophotometer equipped with a liquid nitrogen chilled Unisoku USP-203-A cryostat. NMR spectroscopy was performed on Bruker 300 and 400

MHz instruments with spectra calibrated to either internal tetramethylsilane (TMS) standard or to residual protio solvent.

2.3 Determination of O_2 solubility in Acetone

Both the solubility of O_2 in acetone at 25 °C (0.01134 mol/L) and the solubility at different temperatures were determined using data from previously carried out temperature-dependent studies.[20,21] The formula used for the temperature dependence of the molar fraction solubility of O_2 in acetone is the following:

$$\ln \chi = -24.3100 + (649.40 / T) + [2.6414 (\ln T)]$$

where χ is the molar fraction solubility of O_2 in acetone and T is the temperature, in Kelvin.

2.4 Gas Mixing

Dioxygen (O_2; Air Gas East, grade 4.4) was dried by passing the gas through a short column of supported P4010 (Aquasorb, Mallinkrodt). Red rubber tubing (Fisher Scientific; inner diameter: 1/4 in.; thickness: 3/16 in.) was used to attach the gas cylinders fitted with appropriate regulators to two MKS Instruments Mass-Flo Controllers (MKS Type 1179A) regulated by an MKS Instruments Multi Channel Flow Ratio/Pressure Controller (MKS Type 647C). The gas mixtures, N_2/O_2, were determined by the set flow rates of the two gases. For example, a 10% O_2 mixture would be made by mixing O_2 at a rate of 10 standard cubic centimeters per minute (sccm) with N_2 at 90 sccm for a total flow of 100 sccm. By varying the ratio of O_2 and N_2 with the gas mixer, the concentration of the gases were

determined by taking the percentage of the gas added and multiplying by the solubility of the corresponding gas in acetone.

2.5 Transient Absorption Experimental Details

Experimental information for the setup of the Nd:YAG flash-photolysis apparatus has been previously reported.[22] The apparatus was equipped with liquid nitrogen chilled Unisoku USP-203-A cryostat. The samples, $[(N3)Cu^{II}_2(O_2)](BArF)_2$ and $[(N5)Cu^{II}_2(O_2)](BArF)_2$, were irradiated with λ_{ex} = 532 nm pulsed light (10 mJ/pulse) and data were collected at the monitored wavelengths from averages of 30 laser pulses. Samples (about 70 μM) were prepared under an inert atmosphere (drybox) in 1 cm quartz cuvettes with four polished windows made custom by Quark glass. The cuvettes were equipped with a 14/20 joint and Schlenk stopcock. Gas mixtures were added to sample solutions through direct bubbling through a 24-inch needle (19-gauge) for 5 seconds for 10 times with intervals of 10 seconds between each time. During data collection the gas flowed through the headspace of the sample solution into the cuvette.

2.6 Determination of k_{O2} and Eyring Plots for the reactions of O_2 with N3 and N5 Ligand-Copper Compounds

Samples of **1** and **2** were prepared for the laser experiments bubbling O_2 gas into acetone solutions of $[(N3)Cu^{I}_2(CH_3CN)_2](BArF)_2$ (~ 35 μM) and $[(N5)Cu^{I}_2(CH_3CN)_2](BArF)_2$ (~ 75 μM), respectively, at low temperature. In order to determine the second-order rate constants for dioxygen binding to the dicopper(I) centers (occurring after laser excitation of **1** and **2**) O_2 concentration (pseudo-first-order-conditions: excess of O_2) was varied using the gas mixer apparatus (see Section 2.4) and values of k_{obs} were determined at each O_2

concentration. Second-order rate constants were, then, determined from the slope of the pseudo-first-order plots ($[O_2]$ vs. k_{obs}). Laser measurements were performed in a temperature range from -80^{0}C to -92^{0}C and data were fitted with the Eyring equation $\ln (k\, h / k_B T) = -(\Delta H^{\ddagger} / RT) + (\Delta S^{\ddagger} / R)$ (where h = Planck constant, k_B = Boltzmann constant, T = temperature, and k = second order rate constant) for k_{O2}. Temperature dependence studies have been performed in this work using 532 nm excitation wavelength.

2.7 Quantum Efficiency Measurements

Quantum yields were determined in acetone solvent at -80^0 C for the 532 nm excitation wavelength. Samples of **1** were prepared bubbling $O_{2(g)}$ in solutions of $[(N3)Cu^{I}_2(CH_3CN)_2](BArF)_2$ in dried and distilled acetone at -80^{0}C. The absorbance of the samples at 532 nm (i.e. 0.14 at 532 nm) were monitored using a Cary 50 Bio spectrophotometer equipped with a liquid nitrogen chilled Unisoku USP-203-A cryostat. $[Ru(bpy)_3]Cl_2$ in CH_3CN at room temperature (RT) was used as actinometer and its solutions were prepared to ensure to match the optical density of **1** at 532 nm. Data collection for the change in absorbance (ΔA) at the correspondent λ_{max} values (365 nm) where the change in extinction coefficients ($\Delta\varepsilon$) are known was made. The quantum yield at 532 nm was calculated with equation **(1)**:

$$\Phi(LCu^{II}_2O_2) = (\Delta A_{450}{}^{Cu} / \Delta A_{450}{}^{Actin})\,(\Delta\varepsilon_{450}{}^{Actin} / \Delta\varepsilon_{450}{}^{Cu})\,(n_{acetone}{}^2 / n_{CH3CN}{}^2) \qquad \textbf{(1)}$$

where 'Actin' is $[Ru(bpy)_3]Cl_2$ in CH_3CN at RT. The values $\Delta\varepsilon_{450}{}^{[Ru(bpy)_3]Cl_2} = -10600\ M^{-1}cm^{-1}$ [23] and $\Delta\varepsilon_{365}{}^{[(N3)Cu(II)_2(O_2)](BArF)_2} = -7264\ M^{-1}cm^{-1}$ (determined in this work) were used. For the

refractive index, the value 1.34163 for CH_3CN (n_{CH_3CN}) at 298.15 K has been used[24] whereas a temperature correction of 0.00045 per Kelvin has been added to the refractive index of acetone at 293.15 K (1.359)[25] to obtain the refractive index which has been used for acetone at 193.15 K in equation **(1)** ($n_{acetone}$): 1.359 + [0.00045·(293.15-193.15)] = 1.404.

3. Results and Discussion

The dicopper(I) compounds based on dinucleating ligands N3 and N5 that possess bis[(2-(2-pyridyl)ethyl]amine (PY2) tridentate moieties (having one tertiary amine and two pyridyl groups each) linked through a methylene chain of variable length (-$(CH_2)_n$-, n = 3,5, Chart 1), have been previously described in the literature.[26-28] Reaction with excess O_2 at low temperatures afforded quantitative formation of $[(N3)Cu^{II}_2(O_2)]^{2+}$ (**1**) and $[(N5)Cu^{II}_2(O_2)]^{2+}$ (**2**). Species **1** and **2** were stable below –80 °C, even when excess O_2 was removed in vacuo.[29] The peroxo formulation of **1** and **2** is, in part, based on previous findings from resonance Raman spectroscopy: N3, ν_{O-O} = 765 cm^{-1}; N5, ν_{O-O} = 741 cm^{-1}.[30]

Chart 1. Structure of the compounds studied in this work.

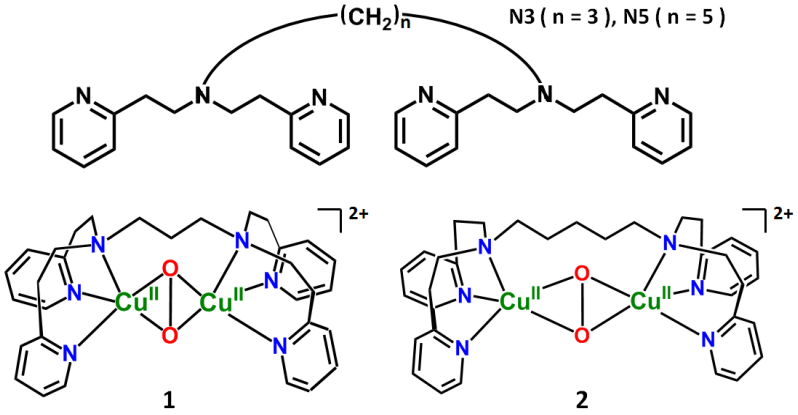

Representative absorption spectra for the reaction of $[(N3)Cu^{I}_{2}(CH_3CN)_2]^{2+}$ with O_2 to yield $[(N3)Cu^{II}_{2}(O_2)]^{2+}$ (**1**), at 193 K in acetone are shown in Figure 3a.

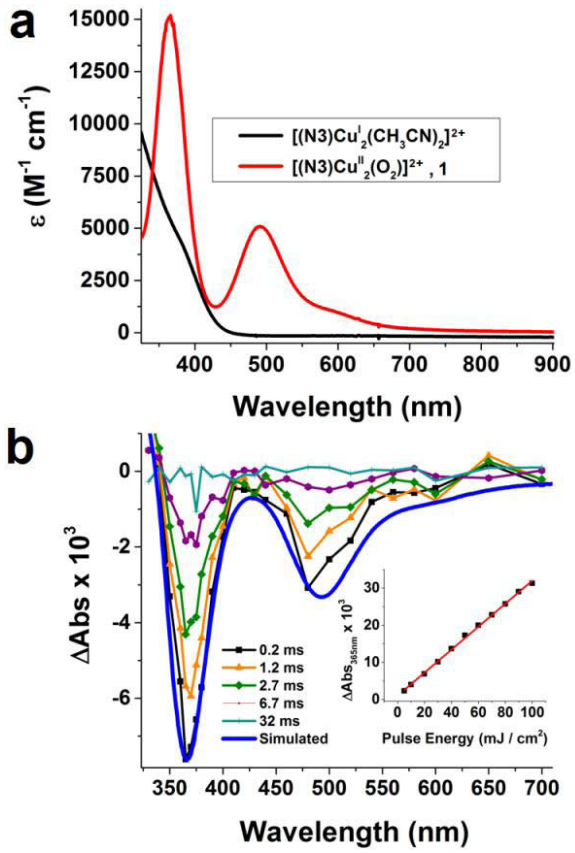

Figure 3. Benchtop and laser absorption spectra of $[(N3)Cu^{I}_{2}(CH_3CN)_2]^{2+}$ and $[(N3)Cu^{II}_{2}(O_2)]^{2+}$ (**1**). (a) Absorption spectrum of **1** (red line) obtained from oxygenation of $[(N3)Cu^{I}_{2}]^{2+}$ (black line) at 193 K in acetone. (b) Transient absorption difference spectra collected at the indicated delay times after 532 nm laser excitation (10 mJ/pulse, 8-10 ns fwhm) of **1** in acetone at 193 K. Overlaid in blue is a simulated spectrum based on subtraction of the red spectrum from the black in 1a. The inset shows the magnitude of the absorption change as a function of the incident irradiance.

An intense color change from yellow to purple/brown accompanied this reaction consistent with previous studies that established a 2:1 Cu to O_2 binding stoichiometry.[27,28] The intense electronic absorption bands centered at 365 nm (15100 M^{-1} cm^{-1}) and 490 nm (5100 M^{-1} cm^{-1}),

as well as those observed at 360 nm (21800 M^{-1} cm^{-1}) and 430 nm (5200 M^{-1} cm^{-1}) for $[(N5)Cu^{II}_2(O_2)]^{2+}$(**2**) (Figure 4), have been previously assigned as peroxide-to-copper(II) ligand-to-metal charge-transfer (LMCT) transitions.

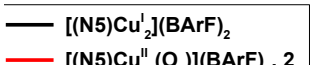

Figure 4. Absorption spectrum of **2** (red line) obtained from oxygenation of $[(N5)Cu^{I}_2(CH_3CN)_2]^{2+}$ (black line) at 193 K in acetone.

Resonance Raman and DFT calculations have provided compelling evidence that peroxide is coordinated to the two copper centers in a μ-η^2-η^2-(side-on) mode in both $[(N3)Cu^{II}_2(O_2)]^{2+}$ (**1**) and $[(N5)Cu^{II}_2(O_2)]^{2+}$ (**2**).[30]

In our new studies described here, we observed that pulsed green light excitation of **1** resulted in absorption difference spectra such as that shown in Figure 3b. The data were fully consistent with those expected for the loss of dioxygen from **1**. Indeed, simulations of the transient spectra with the presently determined bench-top absorption spectrum of **1** (Figure 3a) were in excellent agreement with that measured transiently (Figure 3b, in blue). Similar behavior was observed after photoexcitation of **2** under the same experimental conditions (Figure 5).

Figure 5. Transient absorption difference spectra collected at the indicated delay times after 532 nm laser excitation (10 mJ/pulse, 8-10 ns fwhm) of **2** in acetone at 193 K. Overlaid in red on the experimental data is a simulated spectrum (Abs($[(N5)Cu^{I}_{2}(CH_3CN)_2]^{2+}$)- Abs(**2**)).

Significantly different absorption profiles would have been observed if, for example, a copper-oxygen-containing compound with differing structure, a superoxo or a μ-oxo compound (such as a now well known bis-μ-oxo dicopper(III) complex) formed upon photolysis.[31-35] The quantum yield for O_2 release measured 30 ns after laser excitation of **1** was determined to be 0.14 $\pm$ 0.01. The absorption change was found to be linear with respect to the laser fluence over a 5-100 mJ cm^{-2} range indicating that a monophotonic process was involved (Figure 3b, inset, for **1**, and Figure 6 for **2**).

Figure 6. Difference in absorbance observed at 360 nm as a function of the applied laser energy for **2**.

Therefore, the observed 2-electron transfer photochemistry was initiated by absorption of a single green photon (Scheme 1).

Scheme 1. One-photon two-electron oxidation of peroxide to dioxygen.

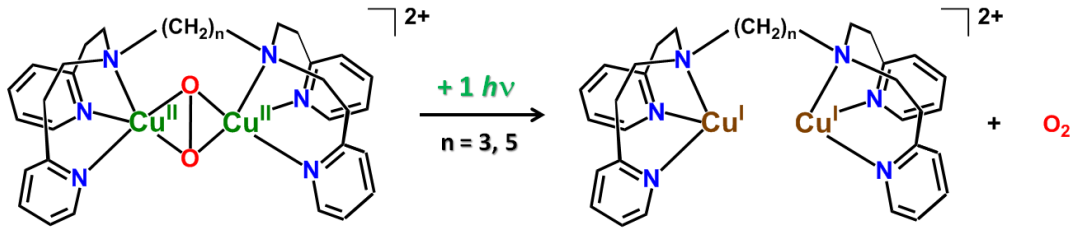

In contrast, the photolysis of compounds $[(TMPA)Cu^{II}_2(O_2)]^{2+}$ (**3**) and $[(PV\text{-}TMPA)Cu^{II}_2(O_2)]^{2+}$ (**4**) did <u>not</u> lead to O_2 release under conditions identical to those used for

1 and **2**. These compounds also possess strong peroxide-to-copper absorption bands, i.e., λ_{max} = 524 nm (ε = 11300 M^{-1} cm^{-1}) and λ_{max} = 615 nm (ε = 5800 M^{-1} cm^{-1}) for **3**[36,37] and λ_{max} = 517 nm (ε = 5600 M^{-1} cm^{-1}) and λ_{max} = 600 nm (ε = 1500 M^{-1} cm^{-1}) for **4**,[38] but the peroxide ligand is coordinated to the two copper(II) ions with a μ-1,2-(end-on) mode (Chart 2).[36,38,39]

Chart 2. Structure of dicopper(II) μ-1,2-(end-on) compounds studied in this work.

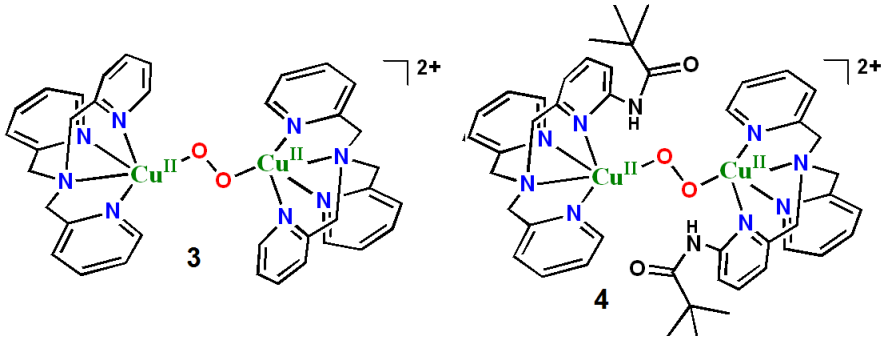

Thus, the photochemistry reported herein is consistent with the mechanisms shown in Scheme 2. For all four compounds, visible light excitation formally promotes an electron from peroxide to copper to yield a transient non-detectable, mixed-valent, copper(II)-superoxide species $[Cu^{I}\text{-}Cu^{II}(O_2)]^{2+}$. In the case of **1** and **2**, the putative formally mixed-valent intermediate rapidly accepts a second electron and releases O_2 with a rate constant k > 10^8 s^{-1}, $[(N3)Cu^{I}Cu^{II}O_2]^{2+}$ → $[(N3)Cu^{I}Cu^{I}]^{2+}$ + O_2 (Scheme 2, top, right-to-left for **1**). In contrast, for **3** and **4**, geminate back electron transfer from Cu(I) to superoxide is proposed

to generate the initially excited dicopper peroxo compound, $[(TMPA)Cu^{I}Cu^{II}O_2]^{2+}$ → $[(TMPA)Cu_2^{II}O_2]^{2+}$ (Scheme 2, bottom, illustrative of the chemistry for **3**).

This mechanism is supported by the fact that Cu^{II}-superoxo compounds based on the bis-(2-pyridylethyl)amine (PY2) tridentate chelate ligand-copper compounds, like **1** and **2**, have never been observed (Scheme 2, top). Extensive kinetic studies have shown that initial O_2 coordination to copper(I) in the PY2 tridentate ligand environment is highly unfavorable.[40-43] The formation of binuclear peroxo dicopper(II) compounds is driven by interaction/reaction with the second ligand-copper(I) species.[18,42,44,45] On the other hand, cupric-superoxide compounds based on tetradentate N-donor ligands, i.e. $[(TMPA)Cu^{II}(O_2)]^{+}$ (precursor to formation of **3**) and $[(PV\text{-}TMPA)Cu^{II}(O_2)]^{+}$ (precursor to formation of **4**), have, in fact, been stabilized and characterized at low temperatures.[32,35,46,47]

Scheme 2. Reaction schemes for the photochemistry of side-on vs. end-on dicopper(II) compounds.

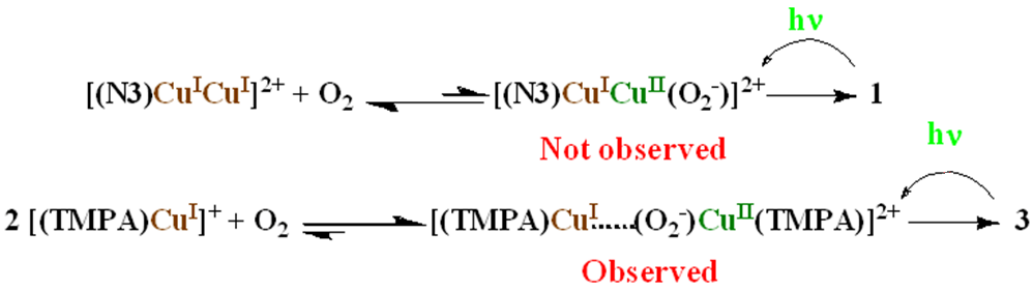

As expected and known for the redox chemistry of copper compounds, ligand-$Cu^{II/I}$ reduction potentials are about 200 mV more negative for compounds with tetradentate TMPA type ligands than for those possessing the tridentate moieties in the N3 and N5 copper compounds[33,40,41,48] (Table 1).

Table 1. Comparison of reduction potentials for some copper complexes. ΔG is the estimated free Gibbs energy variation for the dissociation reaction of O_2 from the relative copper(II)-superoxide species.

	Ligand	$E_{1/2}$ (V)	ΔG (kJ mol^{-1})
Tetradentate Ligands	Im-TMPA	-0.44 [a]	-79
	NMe_2-TMPA	-0.44 [a]	-79
	TMPA	-0.41,[a]	-84
	Q-TMPA	-0.32 [a]	-92
	TBP-TMPA	-0.32 [a]	-92
Tridentate Ligands	Mepy2	-0.32 [b]	-92
	N3	-0.28 [b]	-96
	Bzpy1	-0.22 [a]	-100
	N5	-0.16 [b]	-105

Potentials are measured in DMF (ref a) and in acetonitrile (ref b) and are reported vs. Fc/Fc^+.
[a] Lucas, H. R.; Meyer, G. J.; Karlin, K. D. *J. Am. Chem. Soc.* **2010,** *132*, 12927.
[b] Karlin, K. D.; Tyeklar, Z.; Farooq, A.; Haka, M. S.; Ghosh, P.; Cruse, R. W.; Gultneh, Y.; Hayes, J. C.; Toscano, P. J.; Zubieta. J. *Inorg. Chem.* **1992,** *31*, 1436.

$E(O_2/O_2^-)$ has been taken as -0.86 V in DMF and -0.87 V in acetonitrile versus Fc^+/Fc, from:
Sawyer, D. T.; Chlerlcato, G. Jr.; Angells, C. T.; Nannl, E. J. Jr.; Tsuchlya, T. *Anal. Chem.* **1982**, *54*, 1720.

This difference in reduction potentials is due both to ligand denticity (N4 vs. N3 donors) and chelate ring size (5 vs. 6-membered ring).[49] Therefore, assuming the $E^o(O_2^{0/-})$ potential to be insensitive to the copper coordination environment, an ~ 200 mV (~ 20 kJ/mol) larger driving force for O_2 release from the putative mixed valent intermediates of **1** and **2** would explain the observed one-photon two-electron transfer chemistry and the lack of similar photochemistry for **3** and **4** (Scheme 2, top).

In previously studied oxo-bridged dinuclear metal complexes,[50-53] simultaneous d-d excitation of two metal centers by a single photon was observed spectroscopically. We postulate that this is <u>not</u> likely the origin of the 2-electron transfer photochemistry of $[(N3)Cu^{II}_2(O_2)]^{2+}$ (**1**) and $[(N5)Cu^{II}_2(O_2)]^{2+}$ (**2**) outlined in Schemes 1 and 2, as simultaneous excitations are rare to our knowledge, and unprecedented for metal peroxo compounds. Nevertheless, a simultaneous excitation mechanism cannot be ruled out based solely on the experimental finding disclosed herein.[30]

How unusual is the one-photon two-electron transfer photochemistry reported here? The answer is that such photochemistry is rare, yet three different reaction mechanisms have been proposed: 1) multiple exciton generation; 2) secondary thermal reactions; and 3) reductive elimination reactions.

'Multiple exciton generation' has been observed when the photon excitation energy exceeds twice the energy stored in the excitonic state. Hence it truly represents a means for forming multiple excited states from absorption of a single photon and not necessarily multiple electrons.[54,55] Recently, however multiple exciton generation in quantum dot solar cells has been shown to result in photocurrents in excess of 100% efficiency[56] that has renewed interest in this photochemistry as well as the molecular analogues singlet fission[57-60] and the aforementioned simultaneous d-d excitation.[50-53]

Secondary thermal electron transfer reactions that occur as a result of a primary photo-induced electron transfer reaction are also known. This has some relevance to the science reported here as the proposed mechanism in Scheme 2 implicates a second thermal electron transfer reaction from superoxide to Cu(II). In literature examples the secondary reaction may involve disproportionation chemistry,[61,62] but by far the most common involves reactions that result from irreversible oxidation of an organic compound that leads to the

well-known 'current doubling' in photoelectrochemical cells.[63,64] However, as these current-doubling reactions consume high energy organic reagents their practical utility is questionable.

'Photo-reductive elimination' reactions of transition metal compounds have previously been asserted to proceed by one-photon two-electron transfer mechanisms. These reports bear the most resemblance to the work described herein and therefore deserve some further discussion. It is known that thermal oxidation addition reactions of transition metal compounds can sometimes be reversed with steady-state light illumination.[65-77] A classic example is Vaska's compound, *trans*-$Ir^{I}(PPh_3)_2(CO)Cl$, which was the first synthetic compound shown to reversibly bind dioxygen.[78] Steady-state ultraviolet light excitation of $[Ir^{III}(PPh_3)_2(CO)(O_2)Cl]$ did, in fact, yield Vaska's compound but was accompanied by photochemical side reactions that made quantification of the photon stoichiometry difficult.[66] Unwanted photochemistry similarly hindered mechanistic studies of $Pt(PPh_3)_2O_2$ compounds.[67] Many diatomic molecules, in addition to O_2, undergo oxidative addition reactions, and our review of this broader 'photo-reductive elimination' reaction chemistry revealed no previous reports that clearly established the photon stoichiometry. Most often the difficulty in the older work resulted from very low quantum yield reactions with unwanted side reactions, experimental conditions that generally preclude characterization techniques that require pulsed light excitation. On the other hand, the present study clearly shows that a single photon drives O-O bond formation (i.e., the 2nd O-O bond for the double bond in dioxygen, starting with a single bonded peroxide moiety) *and* two electron transfer chemistry. Furthermore, the relatively high quantum yields and reversible binding of O_2, make the copper compounds ripe for fundamental studies where signal averaging is needed and for practical applications in photocatalysis.

The dicopper(I) compounds generated with light from $[(N3)Cu^{II}_2(O_2)]^{2+}$ (**1**) and $[(N5)Cu^{II}_2(O_2)]^{2+}$ (**2**) do indeed react cleanly with O_2, reverting back to the initial dicopper(II) peroxo species. This then provides a convenient method for characterizing rapid Cu^I/O_2 chemistry. Thus, the present report not only includes the first example of photochemical ejection of molecular oxygen from a synthetically derived dicopper-dioxygen adducts (here, peroxo dicopper(II) compounds **1** and **2**), but also provides for kinetics of fast Cu^I_n-O_2 reactivity. This approach is superior to the previously reported 'flash-and-trap' experiments that require the inclusion of CO gas and various lines of experimentation:[32,33,79] (a) fewer compounds and less handling is involved if only the O_2-adduct is studied, (b) as part of the overall analysis, it is additionally required to determine CO rebinding kinetics to corresponding ligand-metal-CO complexes subjected to CO-photo-ejection,[32,33] and (c) carbon monoxide may interfere or alter the kinetics of O_2-rebinding.[80]

Thus, variable dioxygen concentration studies were performed in pseudo-first-order conditions (excess of O_2) and second-order kinetic constants for dioxygen binding to both $[(N3)Cu^I_2(CH_3CN)_2]^{2+}$ and $[(N5)Cu^I_2(CH_3CN)_2]^{2+}$ were determined (Figure 7, Tables 1 and 2).

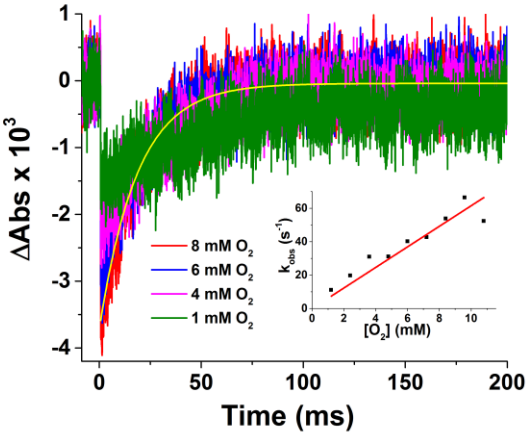

Figure 7. Representative kinetic traces observed at 365 nm obtained upon varying O_2 concentration at 193 K. The first-order exponential fit for the trace relative to $[O_2]$ = 8 mM is overlaid in yellow. The inset shows the pseudo-first-order plot for O_2 binding to $[(N3)Cu^{I}_2(CH_3CN)_2]^{2+}$ yielding a second-order rate constant of (5.0 ± 0.6)·10^3 M^{-1} s^{-1}.

Temperature-dependent kinetic studies performed here have also allowed determination of activation parameters for O_2 binding to $[(N3)Cu^{I}_2(CH_3CN)_2]^{2+}$ and $[(N5)Cu^{I}_2(CH_3CN)_2]^{2+}$ (Figure 8, Tables 2 and 3).

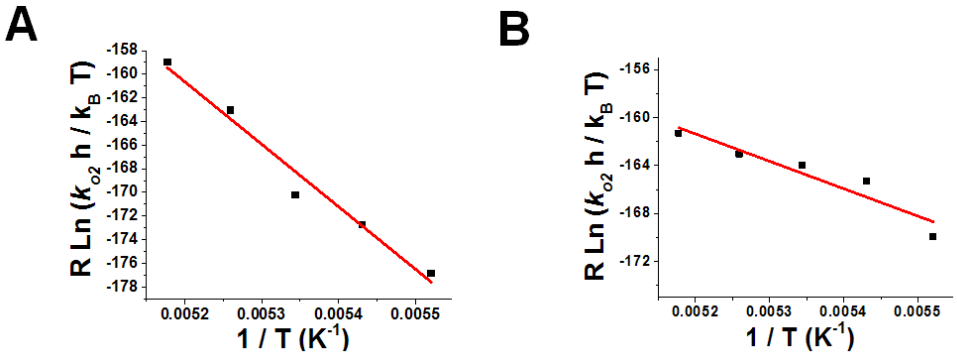

Figure 8. Eyring plots obtained for the determination of the activation parameters for the rate constants k_{O2} for (A) $[(N3)Cu^{I}_2(CH_3CN)_2](BArF)_2$ and for (B) $[(N5)Cu^{I}_2(CH_3CN)_2](BArF)_2$.

Table 2. Comparison of kinetic parameters for O_2 binding to $[(N3)Cu^{I}_2(CH_3CN)_2]^{2+}$ and $[(N5)Cu^{I}_2(CH_3CN)_2]^{2+}$.

	$(N3)Cu^{I}_2$	$(N5)Cu^{I}_2$
$\Delta H^{\ddagger,a}$	8 ± 1	23 ± 4
$\Delta S^{\ddagger,b}$	3 ± 6	-43 ± 23
k_{O2} (-90 °C)[c]	(3.8 ± 1.2) ·10³	(7.0 ± 1.9) ·10³
k_{O2} (21°C)[c]	(2.8 ± 1.2) ·10⁷	(3.2 ± 1.0) ·10⁶

[a]ΔH, kcal mol^{-1}. [b]ΔS, cal K^{-1} mol^{-1}. [c]k_{O2}, M^{-1} s^{-1}.

In fact, the k_{O2} values obtained here and trends observed in comparing $[(N3)Cu^{II}_2(O_2)]^{2+}$ (**1**) and $[(N5)Cu^{II}_2(O_2)]^{2+}$ (**2**) closely track those reported from previous stopped-flow kinetic studies performed in dichloromethane (DCM) solvent on the same dicopper(I) precursors studied here.[18] However, the activation enthalpies found in DCM were smaller (0.6 to 2.4 kcal mol^{-1}, Table 3). This might be due to a slightly more pronounced tendency for acetone as solvent to coordinate[81-83] to the three-coordinate copper(I) centers formed after flash photolysis.

Table 3. Comparison of second order rate constants for O_2 binding to copper(I): 'dTy' is 'deoxy tyrosinase' and 'dHc' is 'deoxy hemocyanin'.

T (^{0}C)	k_{O_2} (M^{-1} s^{-1})			
	This Work		Previous Works	
	$(N3)Cu^I_2$	$(N5)Cu^I_2$	dTy and dHc	
21	$(2.8 \pm 1.2)\cdot 10^7$ (extrapolated)	$(3.2 \pm 1.0)\cdot 10^6$ (extrapolated)	$1.9 \cdot 10^7$ [a] $2.3 \cdot 10^7$ [b] $(3.1 \text{ to } 15.4) \cdot 10^7$ [c]	
-80	$(1.50 \pm 0.05)\cdot 10^4$	$(1.50 \pm 0.5)\cdot 10^4$		
-83	$(7.3 \pm 0.8)\cdot 10^3$	$(1.2 \pm 0.1)\cdot 10^4$		
-86	$(6.1 \pm 0.3)\cdot 10^3$	$(1.1 \pm 0.1)\cdot 10^4$		
-89	$(4.7 \pm 0.4)\cdot 10^3$	$(8.9 \pm 0.5)\cdot 10^3$		
-90	$(3.8 \pm 1.2)\cdot 10^3$ (extrapolated)	$(7.0 \pm 1.9)\cdot 10^3$ (extrapolated)	$(N3)Cu^I_2$	$(N5)Cu^I_2$
			$(1.1 \pm 0.1)\cdot 10^3$ [d]	$(4.1 \pm 0.3)\cdot 10^3$ [d]
-92	$(3.0 \pm 0.3)\cdot 10^3$	$(5.0 \pm 0.4)\cdot 10^3$		

[a] Hirota, S.; Kawahara, T.; Lonardi, E.; de Waal, E.; Funasaki, N.; Canters, G. W., *J. Am. Chem. Soc.* **2005,** *127*, 17966. : Tyrosinase from *Streptomyces antibioticus* [b] Rodríguez-López, J. N.; Fenoll, L. G.; García-Ruiz, P. A.; Varón, R.; Tudela, J.; Thorneley, R. N. F.; García-Cánovas, F., *Biochem.* **2000,** *39*, 10497. : Tyrosinase from *Agaricus bisporus* .
[c] Andrew, C. R.; McKillop, K. P.; Sykes, A. G., *Biochim. Biophys. Acta, Protein Struct. M.* **1993,** *1162*, 105. : Hemocyanin from *Panulirus interruptus1*.
[d] Liang, H.-C.; Karlin, K. D.; Dyson, R.; Kaderli, S.; Jung, B.; Zuberbühler, A. D., *Inorg. Chem.* **2000,** *39*, 5884. : Synthetic N3 and N5 copper compounds in dichloromethane solvent.

The kinetics of O_2 coordination determined here also reveals noticeable similarities to that observed for the copper-containing proteins hemocyanin (Hc; O_2-carrier in mollusks and arthropods) and tyrosinase (Tyr; ubiquitous *o*-phenol monooxygenase).[84-86] These possess similar dicopper active sites where each copper ion binds three protein-derived N-ligands, with Cu···Cu = 4.6 Å ($Cu^I \cdots Cu^I$) and 3.6 Å for the oxygenated form with Cu^{II}-(μ-η^2:η^2-O_2^{2-}

)-Cu^{II} moiety, the same structure found in $[(N3)Cu^{II}_2(O_2)]^{2+}$ (**1**) and $[(N5)Cu^{II}_2(O_2)]^{2+}$ (**2**) (Chart 1). Interestingly, the rate constant for formation of **1**, when extrapolated to 21^0 C, is in very good agreement with the values previously reported for the Tyr[87] and Hc[88] (Table 3). In particular, we notice that the rate constant determined for O_2 binding to the Tyr active site was 1.9×10^7 $M^{-1}s^{-1}$ at 21 °C, essentially the same (Tables 2 and 3) as that observed here for the dicopper protein model compounds $[(N3)Cu^{I}_2(CH_3CN)_2]^{2+}$ and $[(N5)Cu^{I}_2(CH_3CN)_2]^{2+}$. The significantly larger activation enthalpy found for the reaction to yield **2**, compared to the reaction that yields **1**, can be explained by the higher flexibility due to the longer -$(CH_2)_5$- linker present in N5.[18] The higher degree of rotational freedom due to the longer poly-methylene bridge is also consistent with the more negative activation entropy found for the formation of **2**.

4. Conclusions

In summary, we report the first unambiguous example of one-photon two-electron transfer release of O_2 gas. Such photochemistry occurred when dicopper(II) compounds that possess a μ-η^2-η^2-(side-on) peroxide coordination were illuminated with visible light, while it was absent for those that had a μ-1,2-(end-on) peroxide binding mode. These results indicate that the coordination environment, as controlled by the polydentate ligands employed,[89] is important for photoactivity and may be further optimized for solar light harvesting and efficiency. Photo-release of dioxygen provides a convenient method for quantification of the subsequent coordination and activation of O_2. In addition, many copper-peroxo compounds display intense peroxide to copper charge transfer absorption

bands in the visible region that may be exploited for solar energy conversion. The present study does not address how the first O–O bond (to form peroxide from water molecules) might be formed yet clearly shows that the second O–O bond in the dioxygen molecule (O=O) can be generated by absorption of a single photon. It is noteworthy that high valent copper compounds have recently been shown to be competent of forming the initial O-O bond[15,16,90] and this provides optimism that water oxidation to O_2 gas may, one day, be sensitized to visible light by copper coordination compounds.

5. Acknowledgments

The following co-authors contributed to the work presented in this chapter:

H. Christopher Fry, Shunichi Fukuzumi, Kenneth D. Karlin, and Gerald J. Meyer

6. References

(1) Karlsson, S.; Boixel, J.; Pellegrin, Y.; Blart, E.; Becker, H. C.; Odobel, F.; Hammarstrom, L. *J. Am. Chem. Soc.* **2010**, *132*, 17977.

(2) Hammarströ̈m, L.; Hammes-Schiffer, S. *Acc. Chem. Res.* **2009**, *42*, 1859.

(3) Gust, D.; Moore, T. A.; Moore, A. L. *Acc. Chem. Res.* **2009**, *42*, 1890.

(4) Bard, A. J.; Fox, M. A. *Acc. Chem. Res.* **1995**, *28*, 141.

(5) Dismukes, G. C.; Brimblecombe, R.; Felton, G. A. N.; Pryadun, R. S.; Sheats, J. E.; Spiccia, L.; Swiegers, G. F. *Acc. Chem. Res.* **2009**, *42*, 1935.

(6) Norris, M. R.; Concepcion, J. J.; Harrison, D. P.; Binstead, R. A.; Ashford, D. L.; Fang, Z.; Templeton, J. L.; Meyer, T. J. *J. Am. Chem. Soc.* **2013**, *135*, 2080.

(7) Kaveevivitchai, N.; Chitta, R.; Zong, R.; El Ojaimi, M.; Thummel, R. P. *J. Am. Chem. Soc.* **2012**, *134*, 10721.

(8) Wasylenko, D. J.; Ganesamoorthy, C.; Henderson, M. A.; Koivisto, B. D.; Osthoff, H. D.; Berlinguette, C. P. *J. Am. Chem. Soc.* **2010**, *132*, 16094.

(9) Gerken, J. B.; McAlpin, J. G.; Chen, J. Y. C.; Rigsby, M. L.; Casey, W. H.; Britt, R. D.; Stahl, S. S. *J. Am. Chem. Soc.* **2011**, *133*, 14431.

(10) Bediako, D. K.; Costentin, C.; Jones, E. C.; Nocera, D. G.; Saveant, J.-M. *J. Am. Chem. Soc.* **2013**.

(11) Huang, Z.; Luo, Z.; Geletii, Y. V.; Vickers, J. W.; Yin, Q.; Wu, D.; Hou, Y.; Ding, Y.; Song, J.; Musaev, D. G.; Hill, C. L.; Lian, T. *J. Am. Chem. Soc.* **2011**, *133*, 2068.

(12) Ellis, W. C.; McDaniel, N. D.; Bernhard, S.; Collins, T. J. *J. Am. Chem. Soc.* **2010**, *132*, 10990.

(13) Schley, N. D.; Blakemore, J. D.; Subbaiyan, N. K.; Incarvito, C. D.; D'Souza, F.; Crabtree, R. H.; Brudvig, G. W. *J. Am. Chem. Soc.* **2011**, *133*, 10473.

(14) Winterbourn, C. C. *Nat. Chem. Biol.* **2008**, *4*, 278.

(15) Zhang, M. T.; Chen, Z.; Kang, P.; Meyer, T. J. *J. Am. Chem. Soc.* **2013**, *135*, 2048.

(16) Barnett, S. M.; Goldberg, K. I.; Mayer, J. M. *Nat. Chem.* **2012**, *4*, 498.

(17) Chen, Z.; Meyer, T. J. *Angew. Chem., Int. Ed.* **2013**, *52*, 700.

(18) Liang, H.-C.; Karlin, K. D.; Dyson, R.; Kaderli, S.; Jung, B.; Zuberbühler, A. D. *Inorg. Chem.* **2000**, *39*, 5884.

(19) Liang, H. C.; Kim, E.; Incarvito, C. D.; Rheingold, A. L.; Karlin, K. D. *Inorg. Chem.* **2002**, *41*, 2209.

(20) Fischer, K.; Wilken, M. *J. Chem. Thermodyn.* **2001**, *33*, 1285.

(21) Battino, R. *IUPAC Solubility Data Series: Oxygen and Ozone; Pergamon: Oxford, New York* **1981**.

(22) Argazzi, R.; Bignozzi, C. A.; Heimer, T. A.; Castellano, F. N.; Meyer, G. J. *J. Phys. Chem.* **1994**, *33*, 5741.

(23) Yoshimura, A.; Hoffman, M. Z.; Sun, H. *J. Photochem. Photobiol. A* **1993**, *70*, 29.

(24) Iloukhani, H.; Almasi, M. *Thermochim. Acta* **2009**, *495*, 139.

(25) Kurtz, S. S.; Wikingsson, A. E.; Camin, D. L.; Thompson, A. R. *J. Chem. Eng. Data* **1965**, *10*, 330.

(26) Karlin, K. D.; Tyekl; xe; r, Z.; Farooq, A.; Haka, M. S.; Ghosh, P.; Cruse, R. W.; Gultneh, Y.; Hayes, J. C.; Toscano, P. J.; Zubieta, J. *Inorg. Chem.* **1992**, *31*, 1436.

(27) Karlin, K. D.; Haka, M. S.; Cruse, R. W.; Gultneh, Y. *J. Am. Chem. Soc.* **1985**, *107*, 5828.

(28) Karlin, K. D.; Haka, M. S.; Cruse, R. W.; Meyer, G. J.; Farooq, A.; Gultneh, Y.; Hayes, J. C.; Zubieta, J. *J. Am. Chem. Soc.* **1988**, *110*, 1196.

(29) However, removal of dioxygen to give back the precursor copper(I) binuclear compounds occurs upon warming (with vacuum) or via addition of carbon monoxide or triphenylphosphine.

(30) Pidcock, E.; Obias, H. V.; Abe, M.; Liang, H.-C.; Karlin, K. D.; Solomon, E. I. *J. Am. Chem. Soc.* **1999**, *121*, 1299.

(31) Woertink, J. S.; Tian, L.; Maiti, D.; Lucas, H. R.; Himes, R. A.; Karlin, K. D.; Neese, F.; Wu¨rtele, C.; Holthausen, M. C.; Bill, E.; Sundermeyer, J. r.; Schindler, S.; Solomon, E. I. *Inorg. Chem.* **2010**, *49*, 9450.

(32) Fry, H. C.; Scaltrito, D. V.; Karlin, K. D.; Meyer, G. J. *J. Am. Chem. Soc.* **2003**, *125*, 11866.

(33) Lucas, H. R.; Meyer, G. J.; Karlin, K. D. *J. Am. Chem. Soc.* **2010**, *132*, 12927.

(34) Mirica, L. M.; Ottenwaelder, X.; Stack, T. D. P. *Chem. Rev.* **2004**, *104*, 1013.

(35) Peterson, R. L.; Himes, R. A.; Kotani, H.; Suenobu, T.; Tian, L.; Siegler, M. A.; Solomon, E. I.; Fukuzumi, S.; Karlin, K. D. *J. Am. Chem. Soc.* **2011**, *133*, 1702.

(36) Jacobson, R. R.; Tyeklar, Z.; Farooq, A.; Karlin, K. D.; Liu, S.; Zubieta, J. *J. Am. Chem. Soc.* **1988**, *110*, 3690.

(37) Baldwin, M. J.; Ross, P. K.; Pate, J. E.; Tyeklar, Z.; Karlin, K. D.; Solomon, E. I. *J. Am. Chem. Soc.* **1991**, *113*, 8671.

(38) Yamaguchi, S.; Wada, A.; Funahashi, Y.; Nagatomo, S.; Kitagawa, T.; Jitsukawa, K.; Masuda, H. *Eur. J. Inorg. Chem.* **2003**, *2003*, 4378.

(39) Tyeklar, Z.; Jacobson, R. R.; Wei, N.; Murthy, N. N.; Zubieta, J.; Karlin, K. D. *J. Am. Chem. Soc.* **1993**, *115*, 2677.

(40) Kunishita, A.; Osako, T.; Tachi, Y.; Teraoka, J.; Itoh, S. *Bull. Chem. Soc. Jpn.* **2006**, *79*, 1729.

(41) Itoh, S.; Tachi, Y. *Dalton Trans.* **2006**, 4531.

(42) Lewis, E. A.; Tolman, W. B. *Chem. Rev.* **2004**, *104*, 1047.

(43) Itoh, S.; Nakao, H.; Berreau, L. M.; Kondo, T.; Komatsu, M.; Fukuzumi, S. *J. Am. Chem. Soc.* **1998**, *120*, 2890.

(44) Zhang, C. X.; Kaderli, S.; Costas, M.; Kim, E.-i.; Neuhold, Y.-M.; Karlin, K. D.; Zuberbühler, A. D. *Inorg. Chem.* **2003**, *42*, 1807.

(45) It should be noted that bidentate and/or tridentate anionic N-donor ligand chelates can stabilize copper(II)-superoxide and copper(III)-peroxide compounds. See (a) Itoh, S.

Curr. Opin. Chem. Biol. **2006**, *10*, 115-122. (b) Cramer, C.; Tolman, W. *Acc. Chem. Res.* **2007**, *40*, 601-608.

(46) Mirica, L. M.; Ottenwaelder, X.; Stack, T. D. P. *Chem. Rev.* **2004**, *104*, 1013.

(47) Karlin, K. D.; Kaderli, S.; Zuberbuhler, A. D. *Acc. Chem. Res.* **1997**, *30*, 139.

(48) Karlin, K. D.; Tyeklar, Z.; Farooq, A.; Haka, M. S.; Ghosh, P.; Cruse, R. W.; Gultneh, Y.; Hayes, J. C.; Toscano, P. J.; Zubieta, J. *Inorg. Chem.* **1992**, *31*, 1436.

(49) Rorabacher, D. B. *Chem. Rev.* **2004**, *104*, 651.

(50) L. Lohr Jr, L. *Coord. Chem. Rev.* **1972**, *8*, 241.

(51) Güdel, H. U.; Dubicki, L. *Chem. Phys.* **1974**, *6*, 272.

(52) Schugar, H. J.; Rossman, G. R.; Thibeault, J.; Gray, H. B. *Chem. Phys. Lett.* **1970**, *6*, 26.

(53) Hansen, A. E.; Ballhausen, C. J. *Trans. Faraday Soc.* **1965**, *61*, 631.

(54) Midgett, A. G.; Luther, J. M.; Stewart, J. T.; Smith, D. K.; Padilha, L. A.; Klimov, V. I.; Nozik, A. J.; Beard, M. C. *Nano Letters* **2013**, *13*, 3078.

(55) Beard, M. C.; Luther, J. M.; Semonin, O. E.; Nozik, A. J. *Acc. Chem. Res.* **2012**, *46*, 1252.

(56) Semonin, O. E.; Luther, J. M.; Choi, S.; Chen, H.-Y.; Gao, J.; Nozik, A. J.; Beard, M. C. *Science* **2011**, *334*, 1530.

(57) Smith, M. B.; Michl, J. *Annu. Rev. Phys. Chem.* **2013**, *64*, 361.

(58) Greyson, E. C.; Stepp, B. R.; Chen, X.; Schwerin, A. F.; Paci, I.; Smith, M. B.; Akdag, A.; Johnson, J. C.; Nozik, A. J.; Michl, J.; Ratner, M. A. *J. Phys. Chem. B* **2009**, *114*, 14223.

(59) Johnson, J. C.; Akdag, A.; Zamadar, M.; Chen, X.; Schwerin, A. F.; Paci, I.; Smith, M. B.; Havlas, Z.; Miller, J. R.; Ratner, M. A.; Nozik, A. J.; Michl, J. *J. Phys. Chem. B* **2013**, *117*, 4680.

(60) Wang, C.; Schlamadinger, D. E.; Desai, V.; Tauber, M. J. *ChemPhysChem* **2011**, *12*, 2891.

(61) Rowley, J. G.; Farnum, B. H.; Ardo, S.; Meyer, G. J. *J. Phys. Chem. Lett.* **2010**, *1*, 3132.

(62) Fukuzumi, S.; Kobayashi, T.; Suenobu, T. *Angew. Chem. Int. Ed.* **2011**, *50*, 728.

(63) Peter, L. M. *Chem. Rev.* **1990**, *90*, 753.

(64) Pettinger, B.; Schöppel, H. R.; Yokoyama, T.; Gerischer, H. *Berichte der Bunsengesellschaft für physikalische Chemie* **1974**, *78*, 1024.

(65) Ibers, J. A.; La Placa, S. J. *Science* **1964**, *145*, 920.

(66) Geoffroy, G. L.; Hammond, G. S.; Gray, H. B. *J. Am. Chem. Soc.* **1975**, *97*, 3933.

(67) Paonessa, R. S.; Prignano, A. L.; Trogler, W. C. *Organometallics* **1985**, *4*, 647.

(68) Tuczek, F.; Solomon, E. I. *Inorg. Chem.* **1992**, *31*, 944.

(69) Yan, S. G.; Brunschwig, B. S.; Creutz, C.; Fujita, E.; Sutin, N. *J. Am. Chem. Soc.* **1998**, *120*, 10553.

(70) Ledon, H.; Bonnet, M.; Lallemand, J.-Y. *J. Chem. Soc., Chem. Commun.* **1979**, 702.

(71) Freyer, W.; Stiel, H.; Hild, M.; Teuchner, K.; Leupold, D. *Photochem. Photobiol.* **1997**, *66*, 596.

(72) Katscher, U.; Schmidt, R.; Brauer, H. D. *Chem. Phys. Lett.* **1993**, *205*, 75.

(73) Boreham, C. J.; Latour, J.-M.; Marchon, J.-C.; Boisselier-Cocolios, B.; Guilard, R. *Inorg. Chim. Acta* **1980**, *45*, L69.

(74) Bergamini, P.; Sostero, S.; Traverso, O.; Deplano, P.; Wilson, L. J. *J. Chem. Soc., Dalton Trans.* **1986**, 2311.

(75) Vogler, A.; Kunkely, H. *J. Am. Chem. Soc.* **1981**, *103*, 6222.

(76) Rihter, B. D.; Kenney, M. E.; Ford, W. E.; Rodgers, M. A. J. *J. Am. Chem. Soc.* **1993**, *115*, 8146.

(77) Freyer, W.; Leupold, D. *J. Photochem. Photobiol. A: Chem.* **1997**, *105*, 153.

(78) Ibers, J. A.; La Placa, S. J. *Science* **1964**, *145*, 920.

(79) Momenteau, M.; Reed, C. A. *Chem. Rev.* **1994**, *94*, 659.

(80) Einarsdottir, O.; Szundi, I. *Biochim. Biophys. Acta* **2004**, *1655*, 263.

(81) P.N askar, J.; Hati, S.; Datta, D.; A. Tocher, D. *Chem. Commun.* **1997**, 1319.

(82) Broclawik, E.; Kozyra, P.; Datka, J. *C. R. Chim.* **2005**, *8*, 491.

(83) Datka, J.; Kukulska-Zając, E.; Kobyzewa, W. *Catal. Today* **2006**, *114*, 169.

(84) Magnus, K. A.; Hazes, B.; Ton-That, H.; Bonaventura, C.; Bonaventura, J.; Hol, W. G. J. *Proteins: Struct. Funct. Bioinform.* **1994**, *19*, 302.

(85) Solomon, E. I.; Sundaram, U. M.; Machonkin, T. E. *Chem. Rev.* **1996**, *96*, 2563.

(86) Solomon, E. I.; Ginsbach, J. W.; Heppner, D. E.; Kieber-Emmons, M. T.; Kjaergaard, C. H.; Smeets, P. J.; Tian, L.; Woertink, J. S. *Faraday Discuss.* **2011**, *148*, 11.

(87) Hirota, S.; Kawahara, T.; Lonardi, E.; de Waal, E.; Funasaki, N.; Canters, G. W. *J. Am. Chem. Soc.* **2005**, *127*, 17966.

(88) Andrew, C. R.; McKillop, K. P.; Sykes, A. G. *Biochim. Biophys. Acta, Protein Struct. M.* **1993**, *1162*, 105.

(89) Quant Hatcher, L.; Karlin, K. D. *J. Biol. Inorg. Chem.* **2004**, *9*, 669.

(90) Halfen, J. A.; Mahapatra, S.; Wilkinson, E. C.; Kaderli, S.; Young, V. G.; Que, L.; Zuberbühler, A. D.; Tolman, W. B. *Science* **1996**, *271*, 1397.

Claudio **Saracini**
The Johns Hopkins University
3400 N. Charles Street, 21218, Baltimore, MD

EDUCATION

The Johns Hopkins University

- M. Sc., Chemistry (2012)

University of Rome, Tor Vergata

- M. Sc., Chemistry of Biological Systems (2007), conferred with *summa cum laude*
- B.Sc., Chemistry, conferred with *summa cum laude*

RESEARCH EXPERIENCE

The Johns Hopkins University, PhD (2008-*Current*)

Project: Examining reactivity, stability, and kinetic properties of transient copper/O_2 compounds relevant to the chemistry occurring in the active sites of copper-containing enzymes and to light-driven electron transfer processes

Results:

- Shown the first example of one-photon two-electron transfer chemistry occurring in synthetic dinuclear copper/O_2 adducts (manuscript in preparation)
- Discovered wavelength-dependent O_2 photo-release from mononuclear copper/O_2 compounds (manuscript under review)
- Determined the reorganization energy of peroxide-to-superoxide conversion for a metal-bound O-O moiety (manuscript in preparation)
- Elucidated the photo-initiated mechanism of CO and O_2 fast binding to tridentate

synthetic copper(I) complexes (manuscript in preparation)

Techniques employed: Laser transient absorption spectroscopy, stopped-flow, organic and inorganic synthetic and purification techniques, air-free Schlenk techniques, low temperature sample- and synthetic-handling, theoretical electronic/nuclear structure calculations (DFT)

The Johns Hopkins University, Fellowship (2008)

Project: Application of theoretical models for prediction of temperature-dependent electron transfer rate constants and kinetic isotopic effects (KIE) experimentally determined for a series of metal-based compounds

Results: Clarified the contributions of wavefunction overlaps and temperature to the KIE

University of Rome, Tor Vergata, Fellowship (2005-2008)

Project: Design of a new synthetic receptor for organochlorine pesticides based on calixarenes (European Union-Founded - BIOCOP Project). Investigation on thermodynamics and kinetics of the interactions between the polysaccharide guar and borax as a matrix for pharmaceuticals

Results: Design of a calixarene-based receptor capable of selectively "trapping" organochlorine pesticides through hydrophobic interactions. Analysis of the nature of the guar/borax interactions through molecular dynamics simulations

Techniques employed: Atomic force microscopy (AFM), molecular dynamics simulations, UV-Visible and fluorescence spectroscopy, electrochemistry (differential pulse voltammetry and cyclic voltammetry)

COLLABORATIONS AND ACTIVITIES

- Collaboration with Prof. Gerald Meyer (Johns Hopkins University, USA): kinetic and thermodynamic studies on photo-release and re-binding of carbon monoxide in copper(I)-CO complexes and of dioxygen in mononuclear 1:1 and dinuclear 2:1 Cu/O_2 complexes using low temperature laser flash-photolysis

- Collaboration with Prof. Lin X. Chen (Northwestern University, USA): low

temperature transient absorption X-ray spectroscopy. Proposal awarded with beam time at the Advanced Photon Source at the Argonne National Laboratories (USA). Title of the proposal: "*Transient Structural Dynamics of [TMG_3tren-Cu^{II}-O_2^-]$^+$ Excited States and of the [TMG_3tren-Cu^I]$^+$/O_2 Recombination Reaction*", June 5-11 (2013)

- Collaboration with Prof. Frank Neese (Max Planck Institute, Germany): theoretical (TD-DFT) investigation of the wavelength-dependent O_2 photo-ejection process occurring in [(TMG_3tren)Cu^{II}(O_2^-)]$^+$

- Collaboration with Prof. Shunichi Fukuzumi (Osaka University, Japan). Elucidation of the electron transfer dynamics of a peroxide-to-superoxide oxidation for an O-O metal-bound fragment using stopped-flow techniques

AWARDS AND HONOURS

- Ernest M. Marks Award, Johns Hopkins University

- Shepard Memorial Award, Johns Hopkins University

TEACHING EXPERIENCE

- Teaching Assistantship, Johns Hopkins University (2009 and 2011). Course: General Chemistry. Responsibilities included holding help sessions, grading, and proctoring exams

- Teaching Assistantship, Johns Hopkins University (2010). Course: Physical Chemistry III for Chemical Engineers. Responsibilities included training students for experiments in the laboratory and grading their individual reports

CONFERENCE POSTERS

- **Saracini C.**, Zapata Rivera J. E., Liakos D. G., Peterson, R. L., Neese F., Meyer J. G.,

and Karlin K. D. Copper-Oxygen Bond Breaking and O_2 Photo-Ejection Induced by Selected Wavelength Excitation of Copper(II)-Superoxo Complexes: Laser Flash-Photolysis Experiments and Theoretical Studies *Gordon Research Conference, Electron Donor-Acceptor Interactions, Newport, RI, United States*, August 4-5 (2012)

- **Saracini, C.,** Meyer, J. G., and Karlin, K. D. Copper(I)-Dioxygen Binding Induced by Photodissociation of N-Donor Tridentate Copper(I)-CO Complexes *Gordon Research Conference, Photochemistry, Easton, MA, United States*, July 10-15 (2011)

CONFERENCE PRESENTATIONS

- **Saracini, C.,** Karlin, K. D. Excitation Wavelength Dependent O_2 Release from Copper-O_2 Compounds: Laser Flash-Photolysis Experiments and Theoretical Studies *246th ACS National Meeting and Exposition, Indianapolis, IN, United States*, September 8-12 (2013)

MANUSCRIPTS IN PREPARATION

- **Saracini C.**, Fry H. C., Fukuzumi S., Karlin K. D., and Meyer J. G. One-Photon Two-Electron Transfer Reaction Chemistry: Photorelease of O_2 from Dicopper Peroxo Compounds

- **Saracini C.**, Karlin K. D., and Meyer J. G. Photo-Promoted Copper(I)/Carbon Monoxide and Dioxygen Binding in Tripodal Tridentate Copper(I) Compounds: Insights into the Dynamics of Coordination to Copper

- Cao R., **Saracini C.**, Fukuzumi S., and Karlin K. D. Electron-Transfer Equilibrium between Dinuclear Copper Peroxo- and Superoxo Complexes with a Small Reorganization Energy

MANUSCRIPTS UNDER REVIEW

- Rolle III, C. L., **Saracini, C.**; Karlin, K. D. "Copper: Hemocyanin/Tyrosinase Models," (eibc0049.pub2) In *Encyclopedia of Inorganic and Bioinorganic Chemistry*; R.A. Scott, Editor-in-Chief and Section Editor (Bioinorganic Chemistry; Computational Methods: Physical Methods).; John Wiley & Sons, Ltd: Chichester (2014); in press

PUBLISHED ARTICLES

- **Saracini C.**, Liakos D. G., Zapata Rivera J. E., Neese F., Meyer J. G., and Karlin K. D. Excitation Wavelength Dependent O_2 Release from Copper(II)-Superoxide Compounds: Laser Flash-Photolysis Experiments and Theoretical Studies. *In Press*

- Sunghee K., **Saracini C.**, Siegler M. A., Drichko N., and Karlin K. D. Coordination Chemistry and Reactivity of a Cupric Hydroperoxide Species Featuring a Proximal H-Bonding Substituent, *Inorg. Chem.* (2012) *51*:12603–12605 Paper included in the Special Highlight "Virtual Issue" on Models for Metalloenzymes of *The American Chemical Society*

- Bocchinfuso G., Mazzuca C., **Saracini C.**, Venanzi C., Micheli L., Palleschi G., Palleschi A. Receptors for Organochlorine Pesticides based on Calixarenes, *Microchim. Acta* (2008) *163*:195–202